M. Tech (Power System) SHREYA CHAUDHARY 2020

DESIGN, DEVELOPMENT AND ANALYSIS OF GRID INTEGRATED PV SYSTEM

A DISSERTATION SUBMITTED IN PARTIAL FULFILLMENT OF THE REQUIREMENTS FOR THE AWARD OF THE DEGREE OF

MASTER OF TECHNOLOGY
IN
POWER SYSTEM

SUBMITTED BY:

SHREYA CHAUDHARY

(2K18/PSY/09)

UNDER THE SUPERVISION OF

Prof. Rachana Garg

and

Dr. M. Rizwan

DEPARTMENT OF ELECTRICAL ENGINEERING
DELHI TECHNOLOGICAL UNIVERSITY
(Formerly Delhi College of Engineering)
Bawana Road, Delhi-110042

2020

DEPARTMENT OF ELECTRICAL ENGINEERING

DELHI TECHNOLOGICAL UNIVERSITY

(Formerly Delhi College of Engineering)

Bawana Road, Delhi-110042

DECLARATION

I hereby certify that the work which is presented in the Major Project – II entitled "Design, Development and Analysis of Grid Integrated PV System" in fulfillment of the requirement for the award of the Degree of Master of Technology in Power System and submitted to the Department of Electrical Engineering, Delhi Technological University, Delhi is an authentic record of my own, carried out during a period from January to August 2020, under the supervision of Dr. Rachana Garg and Dr. M. Rizwan.

The matter presented in this report has not been submitted by me for the award of any other degree of this or any other Institute/University. The work has been accepted in peer reviewed Scopus indexed conference with the following details:

1	Title of the Paper:	An Adaptive Approach for Maximum Power Extraction from Grid Integrated Solar Photovoltaic System
	Author names:	Shreya Chaudhary, Rachana Garg and M. Rizwan
	Name of Conference:	1st International Conference on Energy, Material Sciences and Mechanical Engineering (EMSME), 2020
	Conference Dates with venue:	October 30 – November 01, 2020, NIT Delhi

	Have you registered for the Conference?	Yes
	Status of paper:	Accepted
	Date of communication:	15th July 2020
	Date of acceptance:	26th July 2020
	Date of publication:	In proceedings of the conference (Springer)
2	Title of the Paper:	Squared Error Autocorrelation based VSS-LMS Control Algorithm for Grid Integrated Solar Photovoltaic System.
	Author names:	Shreya Chaudhary, M. Rizwan and Rachana Garg
	Name of Conference:	2nd International Conference on Machine Learning Advances in computing, Renewable Energy and Communication (MARC), 2020
	Conference Dates with venue:	December 17 – December 18, 2020, KEC, Ghaziabad
	Have you registered for the Conference?	No
	Status of paper:	Accepted
	Date of communication:	27th July 2020
	Date of acceptance:	9th August 2020
	Date of publication:	In proceedings of the conference (Springer)

SHREYA CHAUDHARY

2K18/PSY/09

DEPARTMENT OF ELECTRICAL ENGINEERING

DELHI TECHNOLOGICAL UNIVERSITY

(Formerly Delhi College of Engineering)

Bawana Road, Delhi-110042

SUPERVISOR'S CERTIFICATE

To the best of our knowledge this work has not been submitted in part or full for any Degree or Diploma to this University or elsewhere. We further certify that the publication and indexing information given by the student is correct.

Dr. Rachana Garg
SUPERVISOR
(Professor, EED)

Dr. M. Rizwan
SUPERVISOR
(Associate Professor)

Place: Delhi

Date: 10.08.2020

ACKNOWLEDGEMENT

I want to convey my deepest appreciation to Dr. Rachana Garg and Dr. M. Rizwan for their support in the dissertation. I am indebted to them for allowing me to work under them, and for providing all the necessary guidance and equipment required for my project. It would have not been possible to conclude my project in absence of their invaluable time and advice. I sincerely appreciate their readiness to address all my doubts and queries regarding the project work and their consistent encouragement to carry my work forward. Working under them has been a great experience and it aided me in gaining a lot of personal as well as professional insight.

I am thankful to Prof. Uma Nangia, Head of Department, Electrical Engineering Department faculties in Electrical Department, DTU for their kind help, encouragement and knowledge throughout this course which helped me in completing my project work.

I am also indebted to my colleagues Ms. Manvi Mishra, Ms.Aparna Lal, my seniors Mr. Shirish Raizada, Mrs. Pallavi Verma, Mr. Avdhesh Kumar and all other colleagues and senior research scholars of Electrical Engineering Departments of DTU for helping me in all possible ways to finalize my project .

Finally, I am appreciative of my family for their love and encouragement. They have always provided me with all the needful resources and guidance to excel in life. I am fortunate to have them. All my capabilities are because of them and all my achievements truly belongs to them.

Date: 10.08.2020 (SHREYA CHAUDHARY)

ABSTRACT

Electricity is extremely important to any country for its growth and development. Thermal power plants based on coal and other fossil fuels have been a major source for electrical energy till date. But with the rise in requirement for electricity it is essential to look at other renewable sources like Solar, Wind, Geothermal Hydro etc. to meet this growing demand. In recent years power generation through Solar Photovoltaic (SPV) system has grown rapidly all over the world. The grid connected PV system has become popular all over the globe and can cater to the increasing demand of electrical energy in future.

The present work deals with the design, analysis and modeling of a 25 kW grid connected PV system. The system comprises of PV array, DC-DC boost converter and three-phase voltage source inverter which is synchronized with the utility grid. The load is connected at PCC. The characterization study photovoltaic module has been carried out under various load circumstances with varying environmental conditions. Incremental Conductance algorithm (IC) is applied for generating peak power from the PV array. VSC is designed using various control algorithms operating on unity power factor mode. VSC consists of DC bus capacitor which is supplied through the solar photovoltaic (SPV) module. PI controller is placed to contain the voltage level of DC bus at a fixed reference voltage for VSI control.

Conventional control techniques like SRFT, IRPT, PBT and Unit Template are applied to the system along with Adaptive techniques such as LMS and VSS-LMS. Parallel is drawn between all these techniques for changing meteorological and load conditions to assess their behavior, stability, reliability, and speed. An innovative adaptive algorithm is also presented, and the outcome is compared with the established controlling techniques. this algorithm is less sensitive to uncorrelated noise. It offers early settlement and faster and smoother convergence as with respect to LMS and VSS-LMS during non-stationary conditions.

TABLE OF CONTENTS

LIST OF TABLES

LIST OF FIGURES

LIST OF ABBREVIATIONS

AC	Alternating Current
DC	Direct Current
IC	Incremental Conductance
IGBT	Insulated Gate Bipolar Transistor
IRPT	Instantaneous Reactive Power Theory
LMS	Least Mean Square
MPPT	Maximum Power Point Tracking
P&O	Perturb and Observe
PBT	Power Balance Theory
PCC	Point of Common Coupling
PLL	Phase Locked Loop
PV	Photovoltaic
PWM	Pulse Width Modulation
SRFT	Synchronous Reference Frame Theory
THD	Total Harmonic Distortions
VSS-LMS	Variable Step Size Least Mean Square
VSS-SEA	Variable Step Size-Squared Error Autocorrelation
VSC	Voltage Source Converter
VSI	Voltage Source Inverter
UPF	Unity Power Factor
ZVR	Zero Voltage Regulation

LIST OF SYMBOLS

a	Diode Ideality Factor
C_{dc}	DC-link Capacitor
D	Duty Cycle
e	Prediction Error
f_{sw}	Switching Frequency
I_L	Load current
I_s	Sensed grid current
I_s^*	Reference grid current
k	Boltzmann's Constant
L_b	Boost Inductor
L_r	Interfacing Inductor
L_s	Source Inductor
Q	Charge
R_s	Series Resistance
R_{sh}	Shunt Resistance
V_{dc}	DC-link Voltage
V_s	AC grid voltage
V_t	Voltage Template
u	Unit Template
λ	Weight

CHAPTER 1

INTRODUCTION

1.1 GENERAL

The inspiration behind this dissertation is mentioned in this chapter. It provides an explanation for the requirement of the research done in this work. Energy can be classified into two categories:

- Renewable sources of energy
- Conventional sources of energy

Conventional energy constitutes those naturally occurring resources which are present in limited quantity and take millions of years to replenish. They can be majorly classified as:

1. Coal
2. Natural gas
3. Oil
4. Nuclear etc.

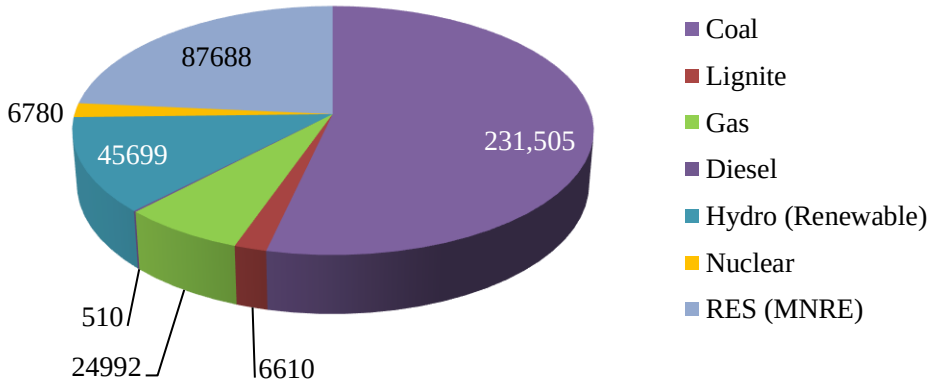

Fig. 1.1 Overview of India's power sector (in MW) as on 30.06.2020

Source: http://powermin.nic.in

An overview of India's energy sector is given in Fig. 1.1. It is visible from Fig. 1.1 that India depends heavily on coal for power generation.

Renewable or Non-conventional energy can be classified into:

1. Wind
2. Solar
3. Geothermal
4. Hydro
5. Biomass
6. Tidal etc.

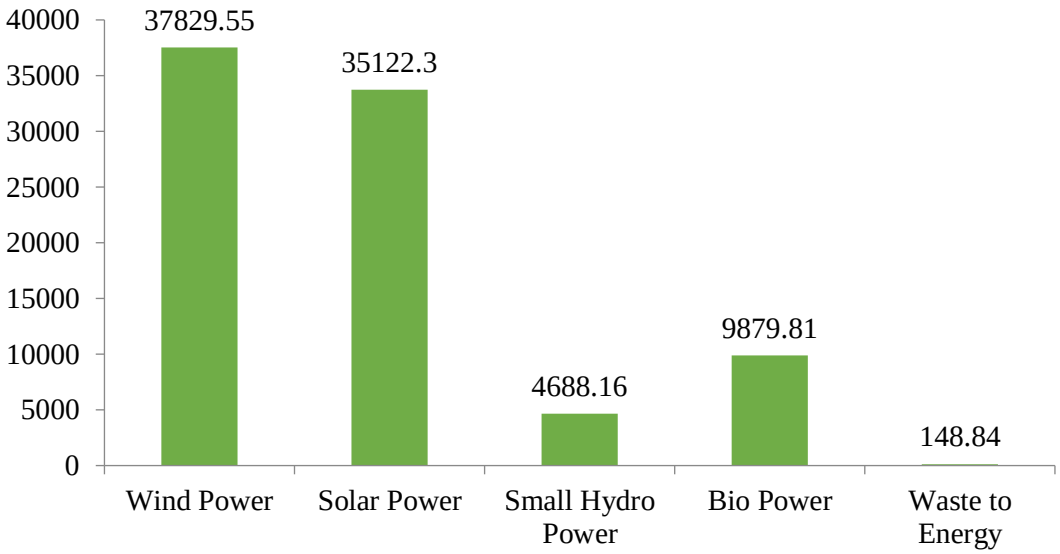

Fig. 1.2 Distribution of Renewable Energy in MW as on 30.06.2020

Source: MNRE website

In Fig. 1.2 sector wise data about the installed capacity of various Renewable Energy sources is given.

1.2 MOTIVATION

World is in a transient phase and energy is central for its present and future. India has contributed almost 10% in the increase in global demand for energy since 2000s, with its own demand for energy almost doubling up in this period. India's share in global demand has increased from 4.4% in the beginning of the century to 6% today and is expected to rise to 11% by 2040 [1]. Nearly 80% of this demand is met through coal-based power plants. With increase in environmental awareness and knowledge about the harmful effects of CO_2, SO_2, NOx, PM 2.5 and other greenhouse gases released as a result of burning of fossil fuels, it is the call of the hour to shift towards more environment friendly,

sustainable and renewable branch of energy generation like solar, hydro, wind, geothermal etc.

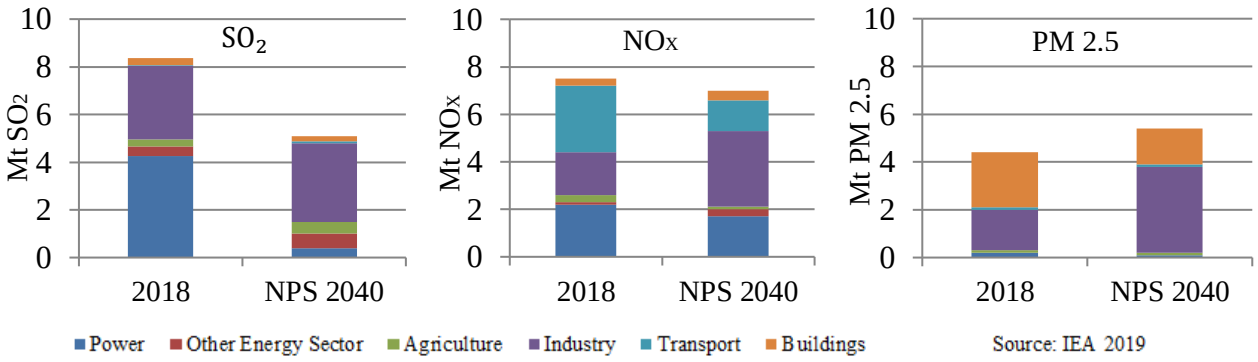

Fig 1.3 Air pollutants emissions in 2018 and 2040 (NPS)

Source: IEA (2019), *World Energy Balances*

Fig 1.3 shows the emissions of SO_2, NOx and PM 2.5 from various sectors in 2018 and in 2040 depending on the new policies scenario (NPS). Power sector is a major contributor of all three gases in 2018 but is expected to reduce drastically by 2040 due to the gradual shift towards renewable power generation.

Energy from renewable resources is energy which is obtained through those resources which can be replenished naturally on a human timescale. Power generated from renewable energy can be consumed directly or can be integrated to the grid. Table 1.1 gives the data of total renewable energy that has been integrated with the grid in India till date.

Table 1.1 Total grid connected Renewable Power (in MW) in India

Sector	**Achievement (April – June 2020)**	**Cumulative Achievements (on 30.06.2020)**
Wind Power	85.80	37829.55
Solar Power – Ground Mounted	192.66	32305.15
Solar Power – Roof Top	301.85	2817.15
Small Hydropower	5.00	4688.16
Biomass Power	5.00	9879.81
Waste to Power	1.20	148.84
Total	**591.46**	**87669.16**

1.3 SCOPE OF WORK

Thanks to the geographical location of India, near the equator, it receives good insolation, making the generation of solar energy possible and economical. Solar energy harnesses the energy from sun and converts it into electrical energy. It is done mainly in two ways. Photovoltaic or solar cells are electrical equipment which transform light energy straight to electricity via photovoltaic effect. These cells are fabricated from single junction silicon and can produce open circuit voltage of 0.5-0.6V [2]. Several solar cells when linked in series and/or parallel can attain the voltage and power levels as expected. Second method uses mirrors to concentrate solar rays and is called concentrated solar power [3].

The power delivered by solar photovoltaic is DC in nature. It can be used directly for DC appliances or can be transformed into AC through an inverter. A grid connected two stage SPV system includes a SPV module, DC-DC boost converter, MPPT (maximum power point tracker) for maintaining the peak power of SPV module, a voltage source converter (VSC), filter, AC grid and parallel loads. First stage consists of MPPT for controlling the SPV module such that it operates around its maximum power point. This is aided by a DC-DC boost converter whose power electronic device (MOSFET/IGBT) is controlled using a MPPT algorithm which varies the duty cycle (D) of MOSFET/IGBT with the intention of extracting maximum power from SPV array under the given ats conditions. There are conventional MPPT algorithms like Incremental Conductance (IC), Perturb and Observe (P&O), fractional current, fractional voltage etc., adaptive MPPT based on LMS filter and intelligent MPPT algorithms using fuzzy logic, neural network (NN) and other artificial intelligence (AI) based algorithms [7]. The second stage controls the current and voltage at the point of common coupling (PCC) of grid interconnected SPV system. Various current controlling algorithms are presented in literature which helps in proper synchronization of the grid and SPV system. They are classified into conventional like SRFT [21-25], IRPT [28], Power Balance Theory [29-30], Unit Template etc. adaptive control based on LMS [32], LMF, Normalized LMS, Sign-sign LMS, VSS-LMS, VSSMLMS[34], Robust VSS-LMS [35] etc. and intelligent control using fuzzy logic and artificial intelligence. The voltage source inverter (VSI) is linked at PCC which acts as current controlled device to inject PV power inside the grid and inject current in the grid to tackle load reactive power, harmonics mitigation and unbalance.

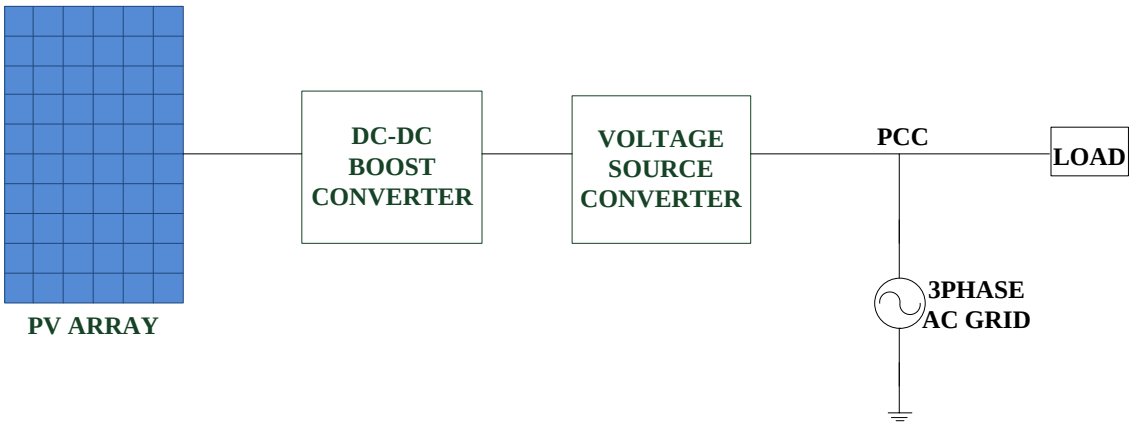

Fig. 1.4 Block diagram of grid interfaced PV system

Fig. 1.4 shows the block diagram of different parts of a Grid connected PV system [9].In this work various inverter current controlling algorithms are meticulously studied and developed using MATLAB/Simulink and comparison is drawn between them, also a new algorithm is proposed, and results are obtained for various loads for unbalancing under varying atmospheric state.

1.4 OUTLINE OF DISSERTATION

The thesis consists of following chapters-

Chapter 1- The chapter gives a brief review on current energy scenario, solar energy and grid connected PV system.

Chapter 2- It includes the literature review done in relation with the work presented in the thesis. The literature review is done to understand the generation of solar energy, designing of PV system, MPPT algorithms in SPV system, designing of grid integrated two-stage systems, power quality standards and mitigation of power quality problem.

Chapter 3- It explains designing of all the components of grid interfaced PV system which covers the design specification of a 25 kW PV system, DC-DC Boost converter, DC link capacitor and LC filter. It also explains the MPPT control algorithm used in this project.

Chapter 4- Different inverter current control techniques studied in literature are explained and implemented on the designed grid connected PV system. The different techniques include Synchronous Reference Frame Theory (SRFT), Instantaneous Reactive Power Theory (IRPT), Power Balance Theory (PBT), Unit Template theory, Least Mean Square (LMS) and Variable Step Size LMS (VSS-LMS). Results for all these algorithms for

changing loads under balance and unbalance circumstances are obtained with fluctuating irradiance using MATLAB/Simulink.

Chapter 5- The novel inverter current control algorithm proposed in this work is elaborated here. Its results are also plotted for parallel loads under balance and unbalance instants with fluctuating irradiance.

Chapter 6- Conclusion and the reach of the future scope of this work is discussed in this chapter.

CHAPTER 2

LITERATURE REVIEW

2.1 INTRODUCTION

In this chapter, many research papers and work related to PV module connected to micro grid are reviewed. The review work is done for the areas mentioned below-

i. Renewable energy sources

ii. Solar Photovoltaic system

iii. MPPT techniques and boost converter

iv. Inverter control techniques

2.2 LITERATURE SURVEY

2.2.1 Renewable energy sources

India 2020 [1] report by IEA, Paris gives the state of India's achievements in the energy sector. It states that due to major reforms and policies supporting cleaner, greener and cheaper sources of energy more than 750 million people have gained access to electricity which include power from offshore and onshore wind power plants, solar power plants, Rooftop Solar etc. It also predicts the improvement in India's energy sector in terms or reduction in release of atmospheric pollutants by 2040 depending on the new policy framework.

2.2.2 Solar PV System

Electricity is one of the most fundamental resource required for survival in today's world. With the demand for energy constantly increasing other sources of generating are becoming more popular, solar energy being one such form. Solar energy obtained from the sun is transformed into electrical energy for either direct use in DC form to supply loads or by converting it into AC form. For the conversion of solar to electrical form of energy Photovoltaic panels are used. PV panels are made up of numerous PV cells. [2]-[4] talks about the design and simulation of PV array. Mathematical equations revolving around the dependence of PV cell on its saturation current (I_o) are used to design a PV module to give

expected I-V and P-V plots of a PV array. [2] utilizes a ZVT-interleaved boost converter to boost the low PV voltage to high dc bus voltage. Theoretical system is cross verified with a 2 kW prototype. In [4] M. E. Elnagi Mahmoud et.al. design a two-diode model of PV module for fast results. SUNSET PX 1506 panel is studied under different aerial conditions. In [5] a solar panel like Mitsubishi PV-MLE255HD is developed to operate under varying atmospheric conditions. [6] provides an alternative to Total Cross Tied configuration called Tom-Tom configuration of PV under partial shaded conditions to increase the output power by relocating the shaded panels.

2.2.3 MPPT techniques and boost converter

For a PV system to operate at its peak capacity, under fluctuating atmospheric conditions, MPPT is used. MPPT maintains the operating point of I-V/P-V plot such that the output is maximum. [7] gives a comprehensive analysis of various MPPT control algorithms such as Hill Climbing, Fractional Open-Circuit Voltage, Incremental Conductance, Fractional Short-Circuit Current, Ripple Correlational Control (RCC), Fuzzy Logic Control, NN, etc. In [8] P&O, IC and FLC are compared.

In [9] implementation of MPPT in a grid interfaced system is given. In [10] and [11] a comparison is drawn between P&O and IC algorithms. Ascribed to the changing step size in IC it offers a faster response to the fluctuating environmental conditions. Less perturbation also leads to less power loss in IC in comparison to P&O control. Lu Xibin et.al in [12] propose a two stage MPPT algorithm with a computing stage and a regulating stage which offers a response which is 4.6 times faster than the conventional IC algorithm.

IC does not perform well when solar irradiance is increased. To overcome this a modified IC control is proposed in [13] which provides better steady state performance when solar irradiance is increased. [14] uses IC algorithm to maintain power at MPP.

MPPT is implemented with the help of a DC-DC Boost Converter. P. Sahu in [15] gives physical designing of a DC-DC boost converter. Simulation of a step-up converter for implementing MPPT in PV system is given by with fast boost and low cost [16].

2.2.4 Inverter control techniques

Power given by PV module is DC. A VSI is employed to covert DC to AC so that it can be integrated to the grid. A. Dhaneria in [17] designs a hardware prototype of 5 kW PV system connected to the grid and studies its behaviour under irradiance changing from 200 W/m^2 to 1000 w/m^2. PVsyst software is used in [18] to develop a 200 kW power plant in Dubai. Abundant inverter control techniques are described in literature [19]. A brief analysis of integration of grid, wind ad solar is given in [20].

They can be classified into conventional control, adaptive control, and intelligent control. N. Gupta in [21] simulates a characterisation study of a Grid interconnected PV system with a battery via SRF control. In [22] A.K. Singh et.al apply SRF in both UPF and ZVR mode of operation of a 25 kW grid interface PV system using SRF control for load imbalance and fluctuating solar intensity. A detailed analysis of a grid connected PV system is explained in [23]. SRF with indirect current control for power factor improvement is used in [24]. A. Khanna et.al in [25] use SRFT control to maintain a constant DC link voltage for different type of loads. [26] draws comparison between SRFT and an adaptive control known as Improved Second Order Generalized Integrator quadrature signal generator (ISOGI-QSG) where it is observed that ISOGI-QSG has better steady state and dynamic response than SRFT. [27] uses IRPT control to control a two-stage grid interfaced PV system of 50 kW rating for varying loads and irradiation. It is observed that IRPT gives a stable operation of the system developed. Comparison between SRF and IRPT is given in [28] which states that SRF offers a lower current THD than IRPT and offers less power loss due to better harmonic compensation. [29] uses PBT control on a 40 kW two stage grid linked PV system for power factor rectification and reactive power mitigation along with harmonics reduction. In [30] power balance theory is applied for controlling a current controlled voltage source inverter which is designed using TMS320C31 DSP.

A basic understanding of adaptive filter theory is obtained from the book “Adaptive Filter Theory” by S. O. Haykin [31]. Adaptive current control algorithms like LMS offer a better performance than conventional algorithms because it offers a faster response. LMS uses adaptive filter in which the future weight value is dependent on the present value as mentioned in [32] where it is applied to a grid tied PV with D-STATCOM for improved

power quality. R. H. Kwong and E. W. Johnston in [33] propose a VSS LMS algorithm. It states that the step size in LMS is fixed thus it can offer either high convergence rate or high accuracy. VSS-LMS has step size which can change to provide both fast convergence and high accuracy during fluctuation. Numerous variations of VSS-LMS are implemented to control the VSC of a Grid interfaced PV system like VSSMLMS [34] where square of error function acts as the cost function, RVSS-LMS [35] with early settlement and less affected by uncorrelated noise and performance at par with VSS-LMS in non-stationary circumstances. DNLMS [36] is applied to a grid connected PV system in UPF mode for harmonics free operations and the results are justified with a laboratory-based hardware model. Hyperbolic cosine based LMS is used in [37] to control a double stage grid integrated PV system for swift response and less oscillations. In [38] a VSS algorithm using squared error and error autocorrelation (VSS-SEAE) is presented. However, in abruptly changing environment, VSS-SEAE depicts weak performance. A gradient based VSS (GVSS-LMS) was presented recently in [39] with high convergent speed and low mis adjustment level, but high computational complexity.

The various inverter current control algorithms present in literature are designed keeping the speed of the algorithm in mind. It is essential for the grid current to remain as much undisturbed from external disturbances as possible. W. Loedwassana in [40] proposes an alteration to the existing VSS-LMS algorithm by changing the cost function from squared error to squared error autocorrelation function. This is done to get a smoother and faster performance than VSS-LMS. It also eliminates noise. Though the computational complexity is increased but performance of the filter is also improved.

The books “Power Electronics Circuit, Design and Implementation” by M. H. Rashid [41] and “Power Electronics Converters, application and Design” by Ned Mohan [42] helps in understanding the characteristics, working and designing of the various power electronics components and circuits involved.

In [43] the IEEE 519 standards are given which are elemental for harmonics control practices. According to the revised standards of 2014 permissible THD is below 5%.

2.3 CONCLUSION

Literature review is carried out for the present work “Design, Development and Analysis of a Grid Integrated PV System” is given in this chapter. Literature review is carried out to realize the scope of solar energy, PV modelling, MPPT control and designing of two-stage grid interfaced PV system. It also helped in understanding the problems encountered by the proposed systems like power quality, reactive power compensation, harmonics, load unbalancing and changing environmental conditions and ways to overcome them.

CHAPTER 3

DESIGN OF GRID INTERFACED PV SYSTEM

3.1 INTRODUCTION

Power generated from renewable energy sources can either be consumed directly for domestic and industrial purposes or can be sent to the grid after proper integration. Energy produced from PV depends on the rating of the PV array as well as on the external factors such as cloud cover, solar intensity, and temperature. This power, after being transformed to AC through a VSC, is fed to the grid. In this chapter all the parts of this system are designed, and their values are estimated for optimum operations.

3.2 PHOTOVOLTAIC ARRAY

Photovoltaic system is required to turn energy from solar to electrical. It consists of a PV cell which is a p-n semiconductor generating dc current when sunlight falls on it. The current generated is dependent on the sun's illumination. The smallest cell can generate a voltage of around 0.5-0.6 volts across its terminals and produce a small amount of power (0.1-3 Watts). These cells can be grouped together to form modules which are further arranged in series and parallel combinations to form a photovoltaic array [2].

Equation which mathematically explains the I-V profile of a photovoltaic cell as depicted in Fig. 3.1 is [2]

$$I = I_{pv,cell} - I_{0,cell}[\exp(\frac{qV}{akT}) - 1] \tag{3.1}$$

$$I_d = I_{0,cell}[\exp(\frac{qV}{akT}) - 1] \tag{3.2}$$

Where $I_{pv,cell}$ is the current due to incoming rays, I_d is Schottky diode current ,q is the electron charge, k is the Boltzmann constant, T (K) is temperature across p-n junction and a is the diode ideality factor. But equation 3.1 does not depict the I-V plot of a practical PV setup.

A practical system consists of numerous cells and thus calls for the inclusion of auxiliary parameters to equation 3.1 [3].

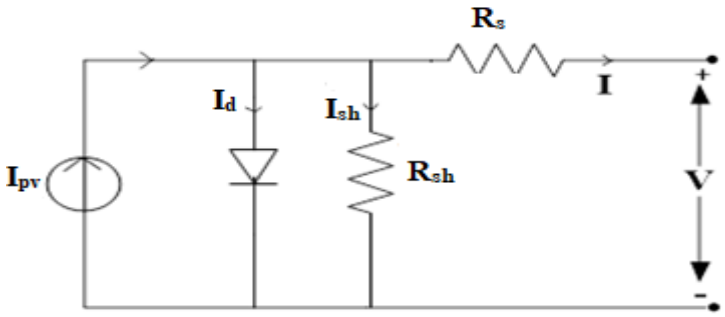

Fig. 3.1 Single-Diode circuit of a PV cell

$$I = I_{pv} - I_0[\exp(\frac{V + IR_s}{aV_t}) - 1] - \frac{V + IR_s}{R_{sh}} \tag{3.3}$$

Where I_0 indicates Saturation current,$V_t = N_s kT/q$ is the thermal voltage and Ns number of cells are in series. Cells in series impacts voltage and in parallel affects the current. R_s is the net series resistance and R_{sh} is net parallel resistance.

The characteristics of the PV cell can be plotted from equation 3.3. There are two main characteristics of PV, one is the I-V characteristics between the output current and output voltage and other is P-V characteristics between the power and output voltage.

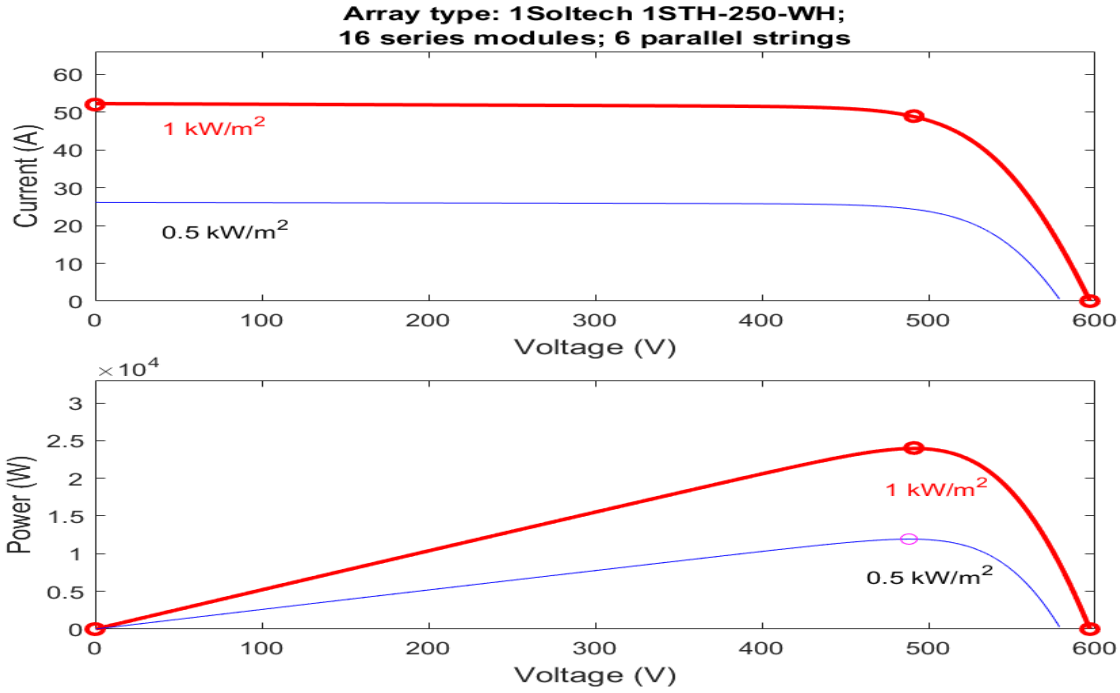

Fig. 3.2 I-V and P-V plots of PV module for different irradiance.

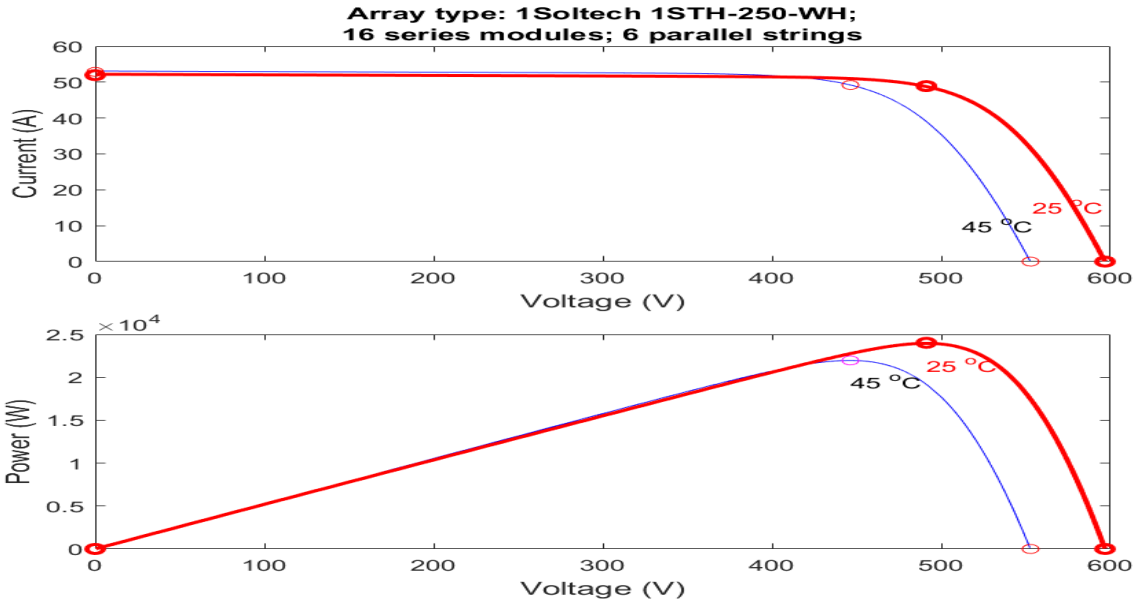

Fig. 3.3 I-V and P-V plots of PV module for different temperature.

Fig. 3.2 and Fig. 3.3 shows the I-V and P-V plots of a PV cell for three values of irradiance and two values temperature, respectively.

Table 3.1 PV module specifications

SPECIFICATIONS	**VALUE**
Maximum power of a single panel (W)	260
Cells per module (N_{cell})	60
Open-circuit voltage, V_{oc} (V)	38.6
Voltage on maximum power point, V_{mp} (V)	31.6
Short-circuit current, I_{sc} (A)	8.93
Current on maximum power point I_{mp} (A)	8.21
Temperature coefficient of V_{oc} (% ^{o}C)	-0.35601
Number of panels in series, N_s	16
Number of panels in parallel, N_p	6
Maximum power of the P-V array (kW)	24.910

3.3 SOLAR PV SYSTEM

In a two-stage grid interconnected PV system, first stage includes a solar PV system with a DC-DC Boost converter for MPPT. MPPT guarantees that the SPV system functions at its maximum power point during varying meteorological states. MPPT technique employed here is Incremental conductance (IC) due to its property of adjusting to fast shifting environmental conditions without much power loss. The first stage is linked to the second stage with a DC link capacitor. Power generated by SPV system is DC which is transformed to AC so that it can be fed to the grid. Thus, at the other stage VSC is used which is controlled by various current controlling algorithms. Fig 3.1 represents a two-stage grid interfaced PV system [21].

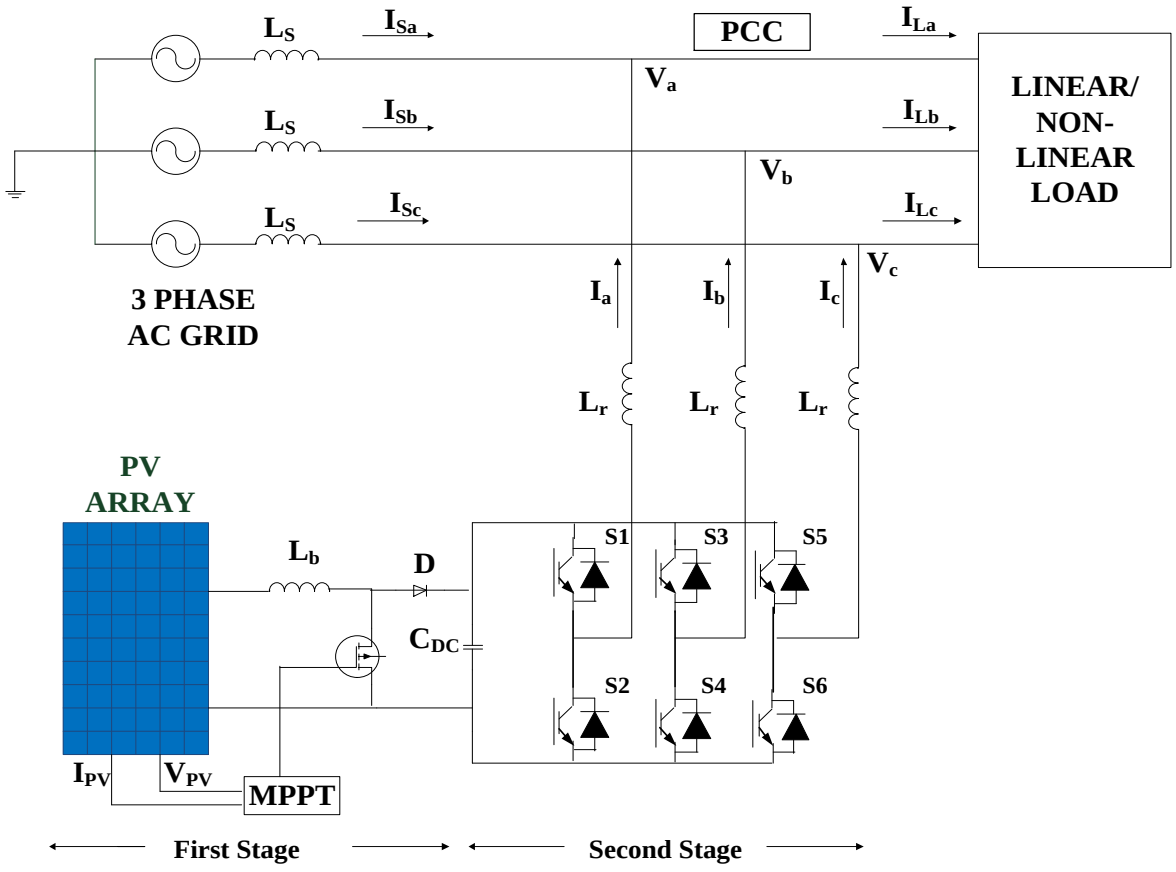

Fig. 3.4 Two- stage grid interfaced PV system

3.4 MAXIMUM POWER POINT TRACKING OF PV

Output of PV is maximum (P_m) when PV current is at I_{mp} and voltage is at V_{mp}.

$$P_m = V_{mp}.I_{mp} \tag{3.4}$$

As the I-V and P-V plots differ with temperature and solar irradiance , it is strenuous to support the voltage and current at V_{mp} and I_{mp} to generate maximum power ,P_m which leads to underutilization of PV capacity. MPPT techniques are thus developed to make sure that the produced V and I remain near the peak power point despite of fluctuation in temperature and solar intensity. In MPPT PV is interfaced to the load through a converter. Operating point of PV is managed by adjusting duty cycle of converter as given in the Fig. 3.5 [5].

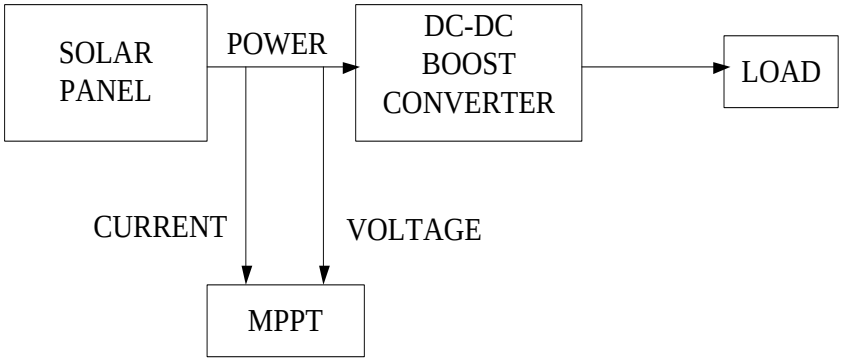

Fig. 3.5 Block diagram for MPPT in PV system using boost converter

There are various MPPT methods available for maintaining the point of operation of PV at mpp, for example P&O, IC, NN, Fuzzy logic control, etc. [7]. In [8] Fuzzy Logic Controller (FLC) is paralleled with P&O to track Global Maximum Power Point (GMPP) of SPV under partial shading. FLC offers a faster tracking with less oscillations. In [9] implementation of MPPT in a grid interfaced system is given. In [10] and [11] a comparison is drawn between P&O and IC algorithms. Ascribed to the changing step size in IC it offers a faster response to the fluctuating environmental conditions. Less perturbation also leads to less power loss in IC in comparison to P&O control. The MPPT technique used in this study is Incremental Conductance (IC).

3.4.1 Incremental Conductance Algorithm

Slope of PV array power curve at the MPP is zero, negative on the right and positive on the left of MPP [11]. The arithmetic equations are

$dP/dV=0$ at MPP (3.5)

$dP/dV>0$ left of MPP (3.6)

$dP/dV<0$ right of MPP (3.7)

Since

$$\frac{dP}{dV}=\frac{d(VI)}{dV}=I+V\frac{dI}{dV}\cong I+V\frac{\Delta I}{\Delta V} \tag{3.8}$$

So, equation (3.8) is rewritten as

At MPP,

$$\frac{\Delta I}{\Delta V}=-\frac{I}{V} \tag{3.9}$$

Left of MPP

$$\frac{\Delta I}{\Delta V}>-\frac{I}{V} \tag{3.10}$$

Right of MPP

$$\frac{\Delta I}{\Delta V}<-\frac{I}{V} \tag{3.11}$$

The MPP is obtained by comparing the instantaneous conductance term (I/V) with incremental conductance term. Fig 3.6 explains the flowchart of IC algorithm [8].

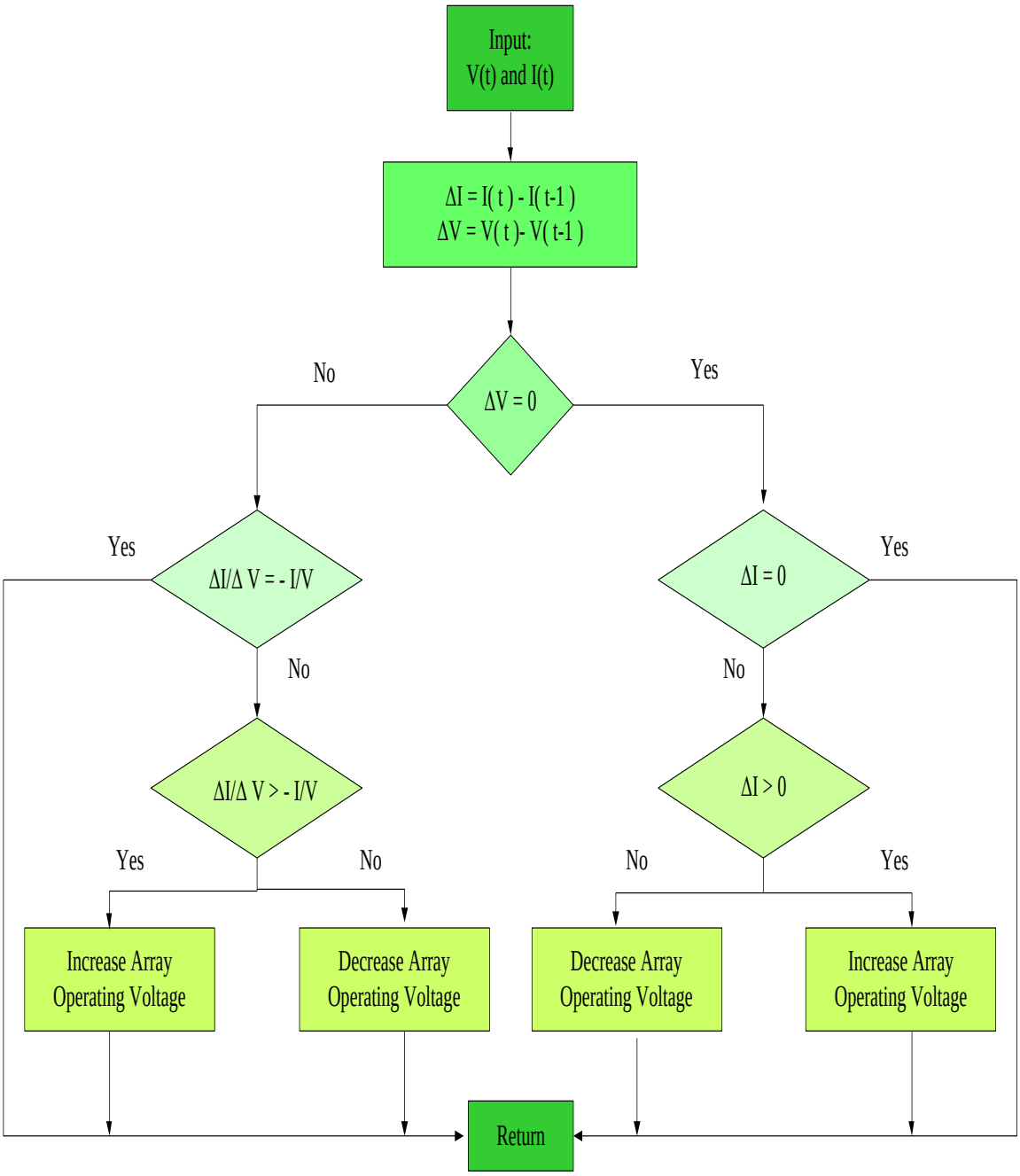

Fig. 3.6 Flowchart of incremental conductance technique

The MPPT in PV system can be implemented through DC-DC converters like Boost converter, Buck converter or Buck-Boost converter. Boost converter design depends on the ratings of PV panels, connected load, acceptable limits of ripple in input current and output voltage.

It includes an inductor, switch (MOSFET /IGBT), a power diode and capacitor as shown in Fig.3.7. The power electronics switch and diode are selected depending on the values of voltage, current and frequency of switching at which they must operate in the circuit. The value of L is estimated by [12]

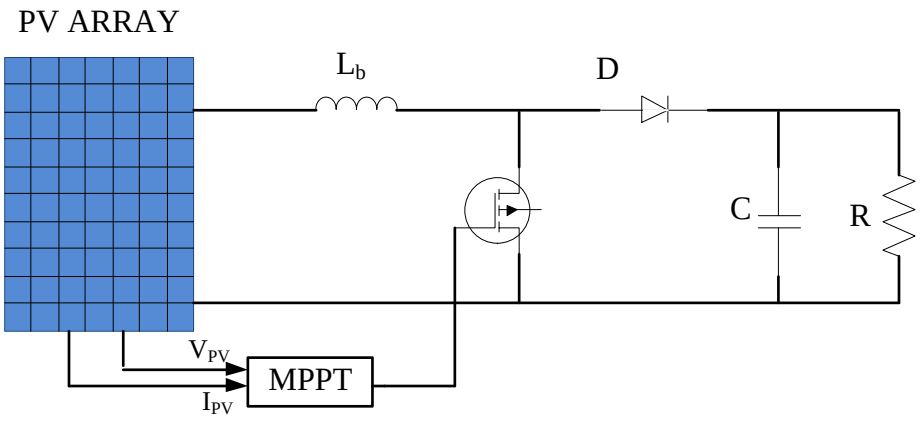

Fig. 3.7 Circuit diagram of DC-DC boost converter

$$L = \frac{V_{pv} D}{2\Delta i_{in} f_{sw}} \tag{3.12}$$

Where V_{pv}, the PV output voltage is 505V, D is the duty given by

$$D = 1 - \frac{V_{in}}{V_o} \tag{3.13}$$

Where $V_{in} = V_{pv} = 505V$ and Vo = 800, so D = 0.35. f_{sw} is the switching frequency (10kHz) and Δi_{in} is considered 20% of the input current i.e. 8.21A. The value of L from equation 3.12 comes out to be 0.5mH.

3.5 DESIGN OF DC LINK CAPACITOR

For proper functioning of VSI, DC-link voltage V_{dc} is required to be above two times the peak voltage on AC side [15].

$$V_{dc} = (2\sqrt{2}V_{LL})/\sqrt{3}m \tag{3.14}$$

Here, m is the modulation index with value 0.9, V_{LL} is ac side line-line voltage = 415 V. V_{dc} from equation is 754 V and is set at 800 V.

Dc-link capacitor is designed using principle of conservation of energy, boost converter feeds energy to the dc-link and VSI extracts this energy and feeds it to the grid. The capacitor sizing should ensure a stable DC-link voltage with lowest voltage ripple. DC-link capacitor value is found from equation 3.15 [15]

$$C_{dc} = I_{mpp}/2\omega V_{dcripple} \quad (3.15)$$

Here I_{mpp} is PV array current = 49 A, ω is grid frequency = 314rad/sec, $V_{dcripple}$ is ripple taken to be 16 V (2% of V_{dc}). C_{dc} from equation 3.15 comes to be 2.985 mF. It is rounded off to 3000μF.

3.5 AC INDUCTOR

AC inductance L_r is given by

$$L_r = \sqrt{3}mV_{dc}/12hf_{sw}\Delta i \quad (3.16)$$

Where Δi is the ripple current, 5%, f_{sw} 10kHz, Vdc is 800V, m is 0.9 and h (overload factor), 1.2. The value of L is calculated as 4.94mH. L_r used is 5mH.

Table 3.2 Parameter specifications of the proposed system

3-phase AC Source	415 V, R_s = 0.01 Ω, L_s = 1mH
Load	i)415 V, 20kVA,0.8 lagging pf (linear load). ii)3-phase diode rectifier, R_{dc} = 50 Ω, L = 50mH (nonlinear load).
Interfacing Inductor (L_r)	5 mH
Ref. DC-link Voltage (V_{dc})	800 V
DC-link Capacitor (C_{dc})	3000μF
Switching Frequency of Boost (f_{sw})	10 kHz
Inductor (L_b) for Boost Converter	0.5 mH
PV Array	P_{MPP} = 24.910 kW, V_{MPP} = 505 V, I_{MPP} = 8.21 A @ STC

3.6 CONCLUSION

A PV system of proper rating is required to get the desired power. All the parameters required for the development of a grid integrated PV system are calculated in this chapter. Boost

converter parameters are designed to ensure ripple free operation. C_{dc} is calculated to provide a fixed ripple free supply to the VSC. The values of various parameters are given in a tabular form in Table 3.2.

CHAPTER 4

CONTROL OF GRID CONNECTED PV SYSTEM

4.1 INTRODUCTION

A double stage grid interfaced system has two different controls, one for the boost converter stage and the other for VSC stage. The boost converter stage has MPPT control for maximum power, which is implemented using IC method. The VSC at PCC is shunt connected and is controlled as a current source to transfer the solar energy from DC-link to the grid and mitigate harmonics, compensate reactive power, and load imbalance at PCC. Control of VSC has two important aspects, first is to calculate 3-phase reference currents which VSC should supply to the grid and second is to create switching pulses for VSC ,so that its output current tracks the reference current in every phase.

Control algorithms can be classified as conventional control, adaptive control, and intelligent control techniques. Conventional control refers to the methods and theories developed to control dynamic systems with the help of differential or difference equation framework. It includes techniques like Synchronous Reference Frame Theory, Instantaneous Reactive Power Theory, Power Balance Theory, Unit Template Theory etc. In adaptive control change in system operating conditions changes the controller parameters. Some examples of adaptive control algorithm are Least Mean Square (LMS), Sign-Sign LMS, Normalized LMS etc. Intelligent control algorithms used fuzzy logic, neural networks etc.

4.2 CONVENTIONAL CONTROL ALGORITHMS

In this chapter various conventional control algorithms studied in this project are explained. The current control algorithms used in this work are –

- Synchronous Reference Frame Theory
- Instantaneous Reactive Power Theory
- Power Balance Theory
- Unit Template Theory

4.2.1 Synchronous Reference Frame Theory (SRFT)

Control given for evaluation of reference currents in SRFT is described below [16].

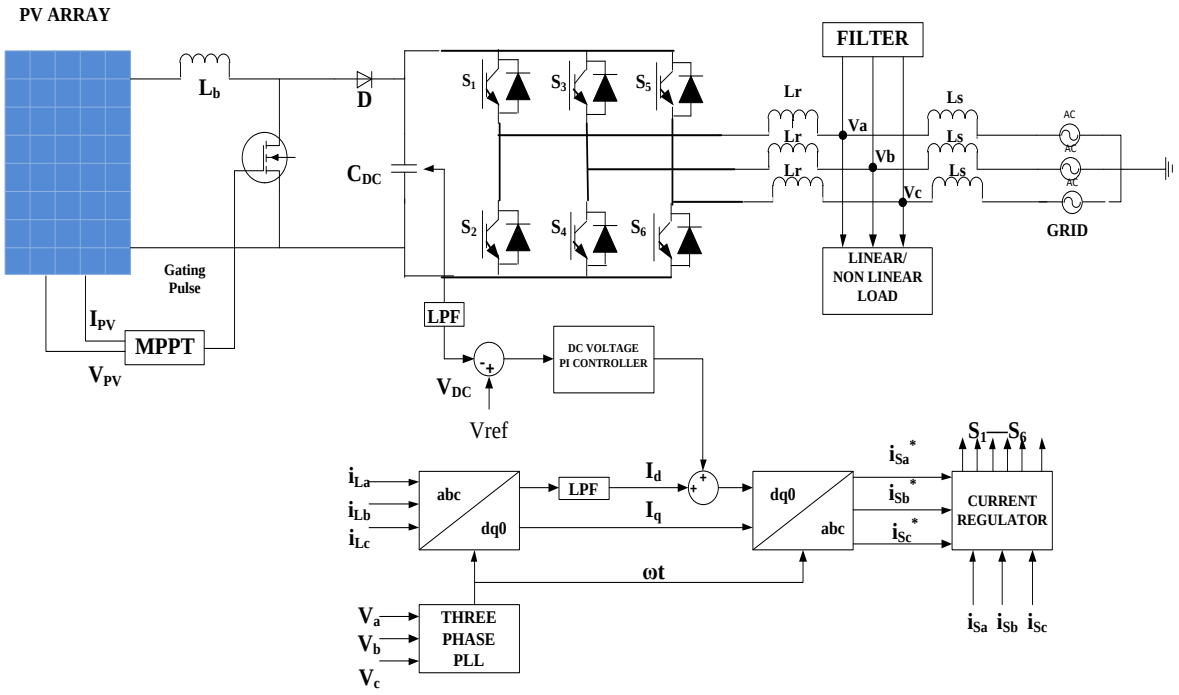

Fig. 4.1 Schematic layout of the proposed grid interfaced PV system using SRFT

It is based on the shift of the load currents (I_L) to d-q frame. It is shown in Fig. 4.1 where I_L, V_s and V_{dc} are feedback signals [16]. I_L are transformed to dq0,

$$\begin{bmatrix} i_{Ld} \\ i_{Lq} \\ i_{Lo} \end{bmatrix} = {}^{2}/_{3} \begin{bmatrix} cos\emptyset & -sin\emptyset & 0.5 \\ cos(\emptyset - 2\pi/3) & -sin(\emptyset - 2\pi/3) & 0.5 \\ cos(\emptyset + 2\pi/3) & -sin(\emptyset + 2\pi/3) & 0.5 \end{bmatrix} \begin{bmatrix} I_a \\ I_b \\ I_c \end{bmatrix} \quad (4.1)$$

Phase Locked Loop (PLL) is employed to synchronize them with the PCC voltage. These d-q currents are sent via an LPF to obtain DC component of i_{Ld} and il_q is terminated for unity power factor operation. d-q currents include fundamental and harmonic as

$$i_{Ld} = i_{dDc} + i_{dAC} \quad (4.2)$$

V_{dc} is fixed at a predetermined level through PI controller. This supports real power transfer from PV and calculation of VSC losses. A current signal is produced by PI controller,

$$i_{loss} = i_{loss}(k-1) + k_P[V_{DC}(k) - V_{DC}(k-1)] + k_I V_{DC}(k) \quad (4.3)$$

Where $V_{DC}(k) = V_{DC}^{*}(k) - V_{Dc}(K)$ and k_p and k_I are PI gain. Therefore, the reference d-axis current is

$$i_d^* = I_{dDC} + i_{loss} \tag{4.4}$$

The real power component of reference AC mains currents should be synchronized with PCC voltages. Reverse Park's transformation is used as given by

$$\begin{bmatrix} I_{sa}^* \\ I_{sb}^* \\ I_{sc}^* \end{bmatrix} = \begin{bmatrix} cos\emptyset & sin\emptyset & 1 \\ \cos(\emptyset - 2\pi/3) & \sin(\emptyset - 2\pi/3) & 1 \\ \cos(\emptyset + 2\pi/3) & \sin(\emptyset + 2\pi/3) & 1 \end{bmatrix} \begin{bmatrix} i_d^* \\ i_q^* \\ i_0^* \end{bmatrix} \tag{4.5}$$

In a PWM, the sensed grid currents (I_{sa}, I_{sb}, I_{sc}) and reference (I^*_{sa}, I^*_{sb}, I^*_{sc}) are equated to generate the gating pulse for six IGBT switches of VSC.

4.2.2 Instantaneous Reactive Power Theory

In IRPT the value of instantaneous reactive and real power is estimated by using Clarke's transform to convert PCC Voltage and I_L from a-b-c frame to α-β frame as shown in Fig. 4.2 [20].

$$\begin{bmatrix} v_\alpha \\ v_\beta \end{bmatrix} = \sqrt{\frac{2}{3}} \begin{bmatrix} 1 & -\frac{1}{2} & -\frac{1}{2} \\ 0 & \sqrt{\frac{3}{2}} & -\sqrt{\frac{3}{2}} \end{bmatrix} \begin{bmatrix} V_{La} \\ V_{Lb} \\ V_{Lc} \end{bmatrix} \tag{4.6}$$

$$\begin{bmatrix} i_\alpha \\ i_\beta \end{bmatrix} = \sqrt{\frac{2}{3}} \begin{bmatrix} 1 & -\frac{1}{2} & -\frac{1}{2} \\ 0 & -\sqrt{\frac{3}{2}} & -\sqrt{\frac{3}{2}} \end{bmatrix} \begin{bmatrix} i_{Lc} \\ i_{Lb} \\ i_{La} \end{bmatrix} \tag{4.7}$$

The instantaneous real (p_L) and reactive power (q_L) drawn by the load are given by

$$p_L = v_\alpha i_\alpha + v_\beta i_\beta = P_{LDC} + P_{LAC} \tag{4.8}$$

$$q_L = v_\alpha i_\beta - v_\beta i_\alpha = Q_{LDC} + Q_{LAC} \tag{4.9}$$

P_{LDC} and Q_{LDC} are the fundamental real and reactive powers of the load currents. P_{LAC} and Q_{LAC} represent the ripple in real and reactive power due to harmonics. LPF extracts the DC value (P_{LDC}) of the load power and reactive power component is zero for UPF mode of operation.

DC link voltage must be regulated, and losses caused in VSC must be supplied to get constant V_{dc}.

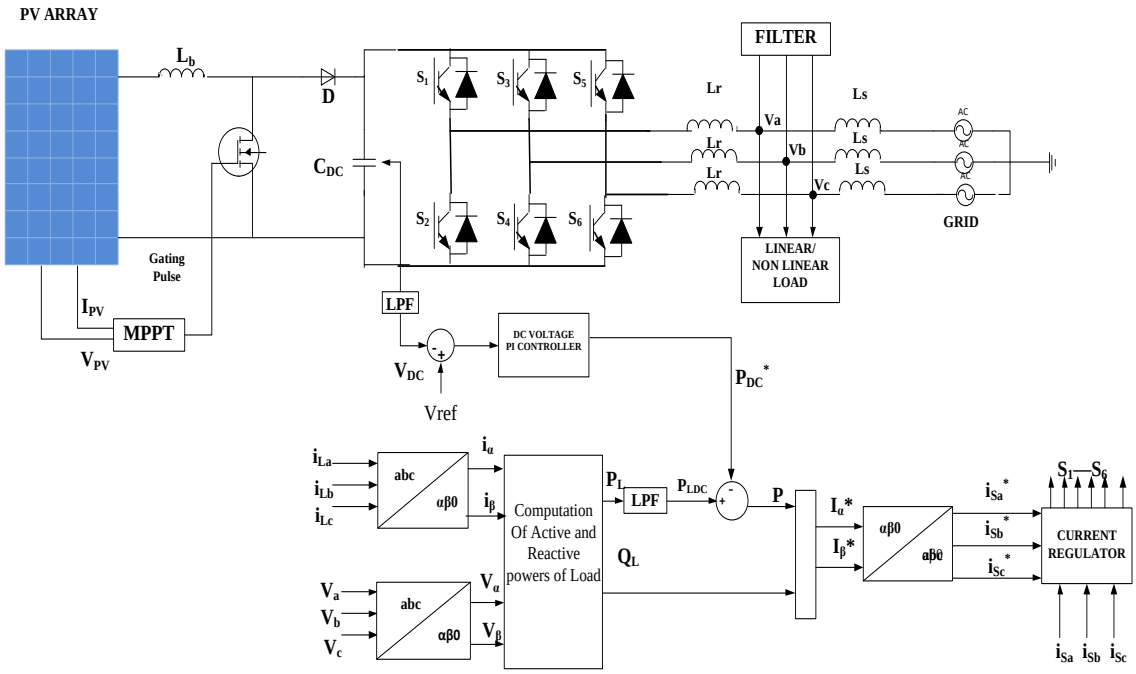

Fig. 4.2 Schematic layout of the proposed grid interfaced PV system using IRPT

The PI controller produces a signal corresponding to the real power essential to sustain the V_{dc} at the fixed value and to compensate for losses in the VSC. This is given by

$$P_{DC}^* = P_{DC}(k-1) + k_P\{V_{e(k)} - V_{e(k-1)}\} + k_I V_{e(k)} \quad (4.10)$$

where $V_e(k) = V^*_{dc}(k) - V_{dc}(k)$is voltage error between the ref. V^*_{dc} and the sensed V_{dc}, at the kth sample.

The amplitude of reference active power to AC mains while maintaining V_{dc} and compensating VSC losses is given as

$$P = P_{LDC} - P_{DC}^* \quad (4.11)$$

Corresponding to this P, the reference I^*_s along α and β axes are evaluated. Only active power portion is taken into consideration for UPF mode of operation. From IRPT for UPF mode of operation, the reference I^*_s in α, β are:

α-axis instantaneous current

$$i_{s\alpha}^{*} = \frac{v_{\alpha} P_T}{v_{\alpha}^2 + v_{\beta}^2} \tag{4.12}$$

β-axis instantaneous current

$$i_{s\beta}^{*} = \frac{v_{\beta} P_T}{v_{\beta}^2 + v_{\alpha}^2} \tag{4.13}$$

From Clarke's Transformation matrix, I_s^* achieved using

$$\begin{bmatrix} I_{sa}^{*} \\ I_{sb}^{*} \\ I_{sc}^{*} \end{bmatrix} = \frac{2}{3} \begin{bmatrix} 1 & 0 \\ -1/2 & -\sqrt{3}/2 \\ -1/2 & -\sqrt{3}/2 \end{bmatrix} \begin{bmatrix} i_{s\alpha}^{*} \\ i_{s\beta}^{*} \end{bmatrix} \tag{4.14}$$

I^*_s and I_s are compared using a PWM current controller. Current error after amplification is contrasted with a triangular carrier wave of 10kHz to create gate signals for VSC.

4.2.3 Power Balance Theory

The real power component of I_s is dependent on two components (V_{dc}) and real power of consumer loads). Its schematic layout is given in Fig. 4.3 The equations for calculating real power element of I_s are given below [23].

Amplitude of the three-phase voltage v_a, v_b, v_c is estimated by,

$$V_t = \sqrt{\left[\frac{2}{3}(v_a^2 + v_b^2 + v_c^2)\right]} \tag{4.15}$$

The unit vectors can be derived from,

$$u_a = \frac{v_a}{V_t},\ u_b = \frac{v_b}{V_t},\ u_c = \frac{v_c}{V_t} \tag{4.16}$$

The real power component dependent on consumer loads is estimated using,

$$P = v_a i_{La} + v_b i_{Lb} + v_c i_{Lc} \tag{4.17}$$

It contains AC as well as DC components where the AC component in the form of harmonics is filtered out using a LPF to achieve only the fundamental part.

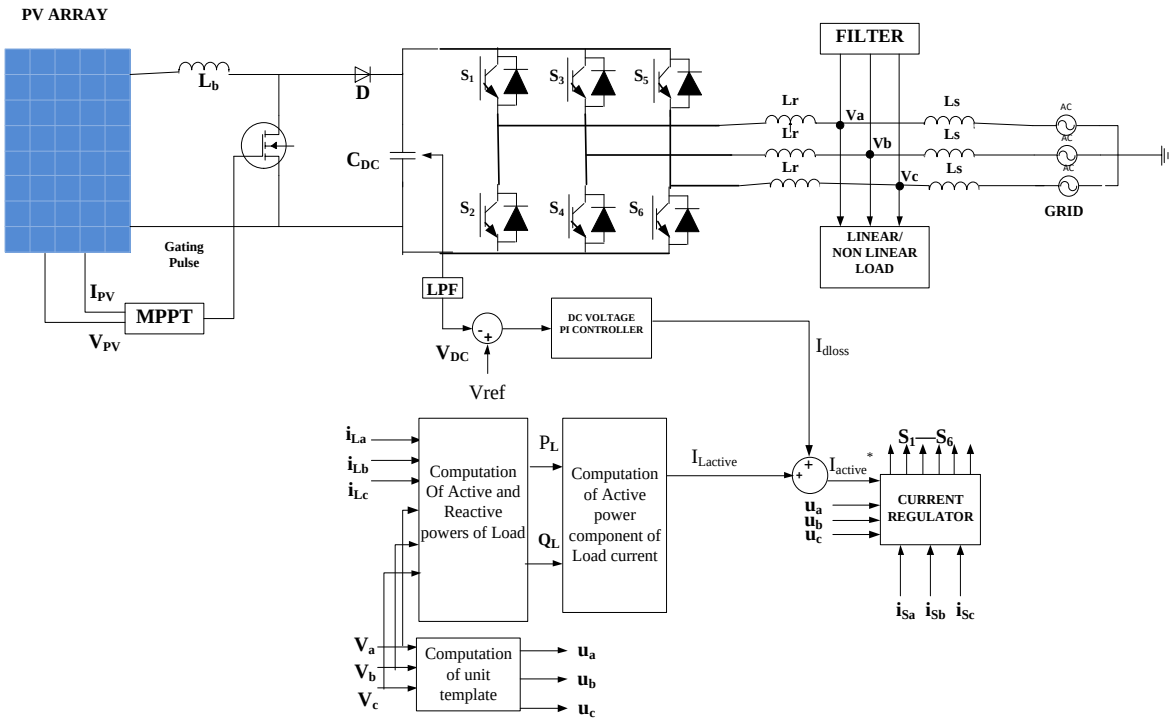

Fig. 4.3 Schematic layout of the proposed grid interfaced PV system using PBT

The load current $i_{Lactive}$ is given by,

$$i_{L\,active} = \frac{2P}{3V_t} \tag{4.18}$$

The real power of the grid is also used for regulating the V_{dc} of VSC using a PI controller.

$$I_{loss(n)} = I_{loss(n-1)} + k_p\left(V_{der(n)} - V_{dc(n)}\right) + k_i V_{dcer(n)} \tag{4.19}$$

Where, $V_{der(n)} = V^*_{dc(n)} - V_{dc(n)}$.

The total active power, I^*_{active} is given by,

$$I^*_{active} = I_{Lactive} + I_{loss} \tag{4.20}$$

Therefore, reference in phase grid current is calculated by,

$$I^*_{sa} = I^*_{active}u_a,\ I^*_{sb} = I^*_{active}u_{b,}\ I^*_{sc} = I^*_{active}u_c \tag{4.21}$$

I^*_s and I_s are equated using a PWM current controller. The current gap after amplification is paralleled with a triangular carrier wave of 10kHz frequency to get gate signals for IGBT's of VSC.

4.2.4 Unit Template Algorithm

The peak of amplitude of PCC voltage V_t is calculated by,

$$V_t = \sqrt{\left[\frac{2}{3}(v_a^2 + v_b^2 + v_c^2)\right]} \tag{4.22}$$

The unit vectors are derived using,

$$u_a = \frac{v_a}{V_t}, u_b = \frac{v_b}{V_t}, u_c = \frac{v_c}{V_t} \tag{4.23}$$

The reference grid current is achieved from the product of these unit templates (u_a, u_b, u_c) with dc-link PI controller output current I_s is given by

$$I_{sa}^* = I_s u_a \, , I_{sb}^* = I_s u_b \, , I_{sc}^* = I_s u_c \tag{4.24}$$

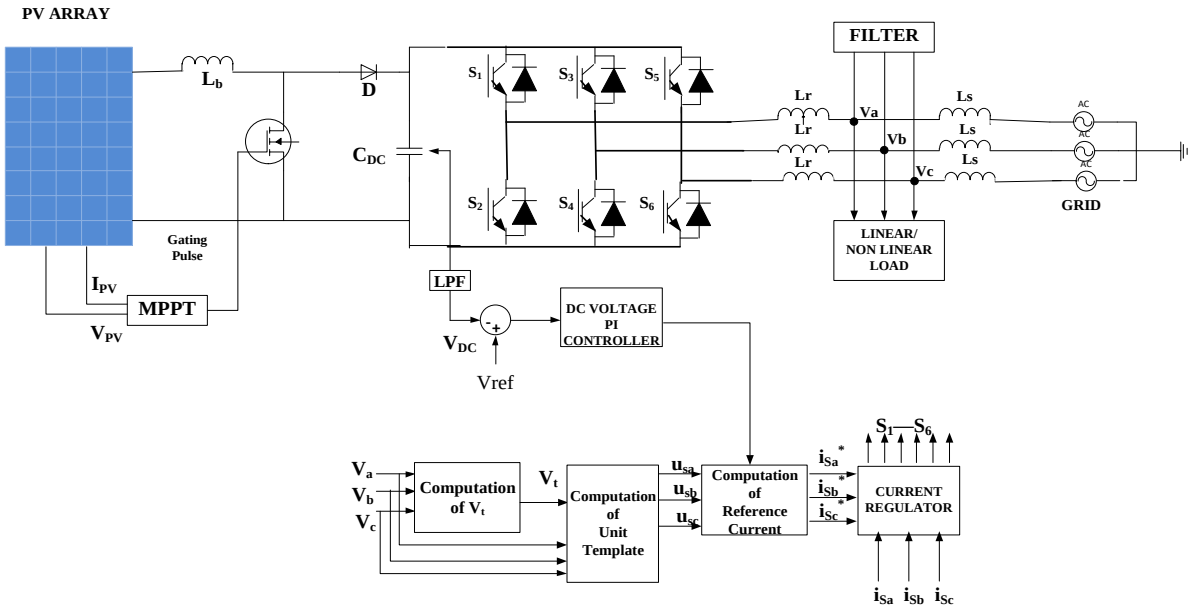

Fig. 4.4 Schematic layout of the proposed grid interfaced PV system using Unit Template

I^*_s and I_s are equated using a PWM current controller. The current gap after amplification is paralleled with a triangular carrier wave of 10kHz frequency to get gate signals for IGBTs of VSC.

4.3 ADAPTIVE CONTROL

Adaptive control studied in this work are-

- Least Mean Square (LMS)
- Variable Step Size- Least Mean Square (VSS-LMS)

4.3.1 Least Mean Square

The Least Mean Square method was given by Widrow and Hoff is an adaptive technique using a method based on gradient of steepest decent. It utilizes the gradient vector calculated from the data available to make successive corrections through iteration to weight vector to eventually get minimum squared error. It is represented in Fig. 4.5. The observed voltage v_{sa}, v_{sb}, vsc are utilized to calculate in-phase or active unit templates with the help of V_t as shown in the given equations [25].

$$V_t = \sqrt{\frac{2}{3}(v_{sa}^2 + v_{sb}^2 + v_{sc}^2)} \tag{4.25}$$

$$u_a = \frac{v_{sa}}{V_t}\ , u_b = \frac{v_{sb}}{V_t}\ , u_c = \frac{v_{sc}}{V_t} \tag{4.26}$$

Real weight component related to each phase is calculated in three blocks. Each block receives a load current ($i_L(t)$) component as input and the gap between input and output (y(t)) is termed as error signal (e(t)). For phase 'a',

$$e_a(t) = i_{La}(t) - y_a(t) \tag{4.27}$$

$$y_a(t) = \lambda_a(t) u_a(t) \tag{4.28}$$

Where $\lambda_a(t) = \int_0^t e_a(t) u_a(t) dt$ is the real weight for phase 'a'. Likewise, it is calculated for remaining two phases (λ_b and λ_c).

$$\lambda_{avg} = \frac{1}{3}(\lambda_a + \lambda_b + \lambda_c) \tag{4.29}$$

V_{dc} and V^*_{dc} are analyzed, and sent to the PI controller to get DC loss weight (λ_{cp})

$$\lambda_{cp}(m+1) = \lambda_{DC}(m) + k_P[V_e(m+1) - V_e(m)] + k_I V_e(m+1) \tag{4.30}$$

Where $V_e(m+1) = V^*_{dC}(m+1) - V_{dC}(m+1)$.

Resultant active weight component is obtained from

$$\lambda_r = \lambda_{avg} + \lambda_{cp} \tag{4.31}$$

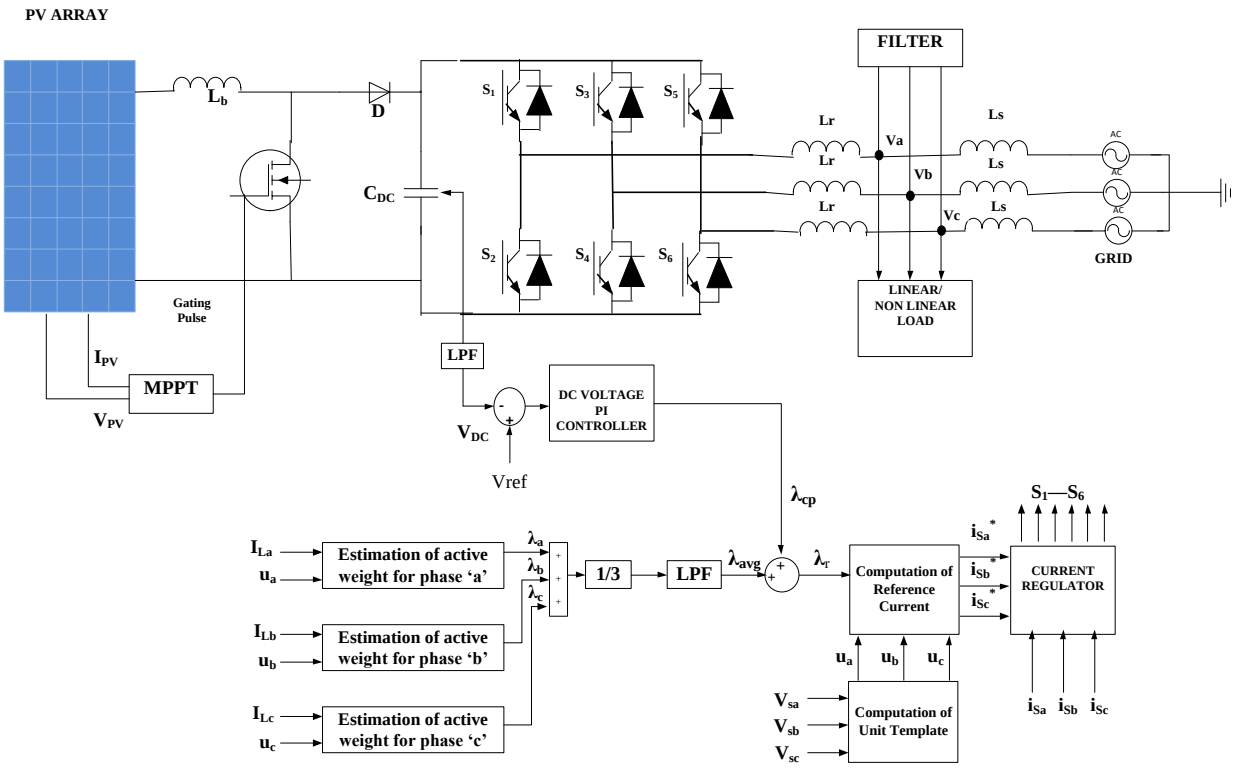

Fig. 4.5 Schematic layout of the proposed grid interfaced PV system using LMS

I^*_s is calculated from

$$I^*_{sa} = \lambda_r u_a \, , I^*_{sb} = \lambda_r u_b \, , I^*_{sc} = \lambda_r u_c \tag{4.32}$$

I^*_s is equated with I_s and the gap is paralleled with a carrier triangular signal of 10kHz using a PWM controller. The pulses from here are used as gate signal for VSC.

4.3.2 Variable Step Size Least Mean Square

Even though a simple LMS is has low complexity, its fixed step size leads to high mis adjustment level with high convergent speed and low mis adjustment level with low convergent speed. To control this issue a variable step size LMS (VSS-LMS) method is used, as shown in Fig. 4.6, where the cost function is a mean squared error function [26].

The line voltages V_{sab}, V_{sbc} at PCC are used to estimate V_s.

$$v_{sa} = \frac{2V_{sab}+V_{sbc}}{3}, v_{sb} = \frac{-V_{sab}+V_{sbc}}{3} \, , v_{sc} = \frac{-V_{sab}-2V_{sbc}}{3} \tag{4.33}$$

The terminal voltage V_t,

$$V_t = \sqrt{\frac{2}{3}(v_{sa}^2 + v_{sb}^2 + v_{sc}^2)} \tag{4.34}$$

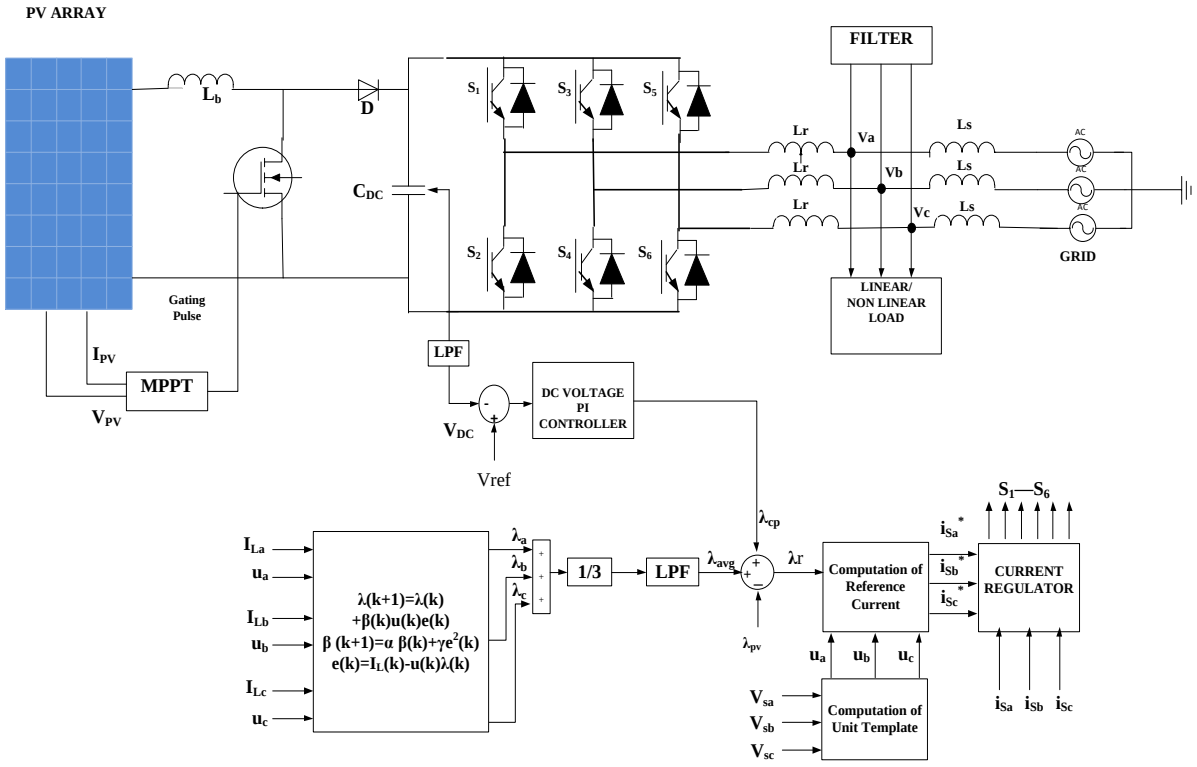

Fig. 4.6 Schematic layout of the proposed grid interfaced PV system using VSS-LMS

Unit templates are estimated from,

$$u_a = \frac{v_{sa}}{V_t}\ ,\ u_b = \frac{v_{sb}}{V_t}\ ,u_c = \frac{v_{sc}}{V_t} \tag{4.35}$$

The DC loss component, λ_{cp} is obtained using a PI controller from,

$$\lambda_{cp}(m+1) = \lambda_p(m) + k_p\{V_e(m+1) - V_e(m)\} + k_i V_e(m+1) \tag{4.36}$$

Where $V_e(m)$ is the error at m^{th} instant, given by

$$V_e(m) = V_{DCref}(m) - V_{DC}(m) \tag{4.37}$$

The feedforward SPV coefficient (λ_{pv}) is determined as,

$$\lambda_{pv} = \frac{2P_{pv}}{3V_t} \tag{4.38}$$

In VSS-LMS, evaluation of active component for phase a I_L for kth instant is revised by,

$$\lambda_a(m+1) = \lambda_a(m) + \beta_a(m)u_a(m)e_a(m) \quad (4.39)$$

Where λ_a (m)is the phase 'a' estimated active component at m^{th} instant, β_a (m) is used to calculate step size using,

$$\beta_a(m+1) = \alpha\beta_a(m) + \gamma e_a^2(m) \quad (4.40)$$

Where the convergence time of this algorithm is dependent on $0 < \alpha < 1$ and $\gamma > 0$. They are constant parameters for controlling exponential regress and fluctuations in step size parameters, respectively. e_a (m) is the prediction error estimated using,

$$e_a(m) = i_{La}(m) - u_a(m)\lambda_a(m) \quad (4.41)$$

Likewise, components are calculated for phase 'b & c' can be calculated utilizing (4.39) - (4.41).

The average active weight is calculated from

$$\lambda_{avg} = \frac{1}{3}(\lambda_a + \lambda_b + \lambda_c) \quad (4.42)$$

The resultant is given by

$$\lambda_r = \lambda_c + \lambda_{avg} - \lambda_{pv} \quad (4.43)$$

The active reference grid current i_{sa}^*, i_{sb}^*, i_{sc}^* is calculated as

$$i_{sa}^* = \lambda_r u_a \ , i_{sb}^* = \lambda_r u_b \ , i_{sc}^* = \lambda_r u_c \quad (4.44)$$

This reference current is then seen with the I_s and the resultant is then sent to a PWM controller which develops gating pulse for IGBTs of VSC.

4.4 RESULTS AND OBSERVATIONS

The model of a two-stage grid interconnected PV system is developed using MATLAB/Simulink. MPPT is controlled using IC algorithm. Results are obtained for different inverter control techniques under varying solar irradiance and unbalancing of linear and non-linear load. Waveforms are plotted for PV power (P_{pv},) voltage (V_{pv}) and Current (I_{pv}), V_{dc}, AC voltage at PCC (V_s), Grid current (I_s), Inverter current (I_{inv}), Load current (I_{load}), Inverter Real and Reactive Power (P and Q), Grid Real and Reactive Power (P_g and Q_g) and

Load Real and Reactive Power (P_{load} and Q_{load}). Plots for all these parameters are analyzed for different loads under two different circumstances-

i. Load Unbalancing- Unbalance is created by disconnecting one of three phases (b) from 0.3 to 0.4 sec. For linear load, a 20kVA load with 0.8 lagging pf is used and for non-linear load a three-phase diode rectifier with R_{dc}=50 Ω and L=50mH is used.

ii. Varying Irradiance- Solar irradiance is maintained at 1000 W/m^2 till 0.5 sec after which it is reduced to 500 W/m^2 as represented in Fig. 4.7.

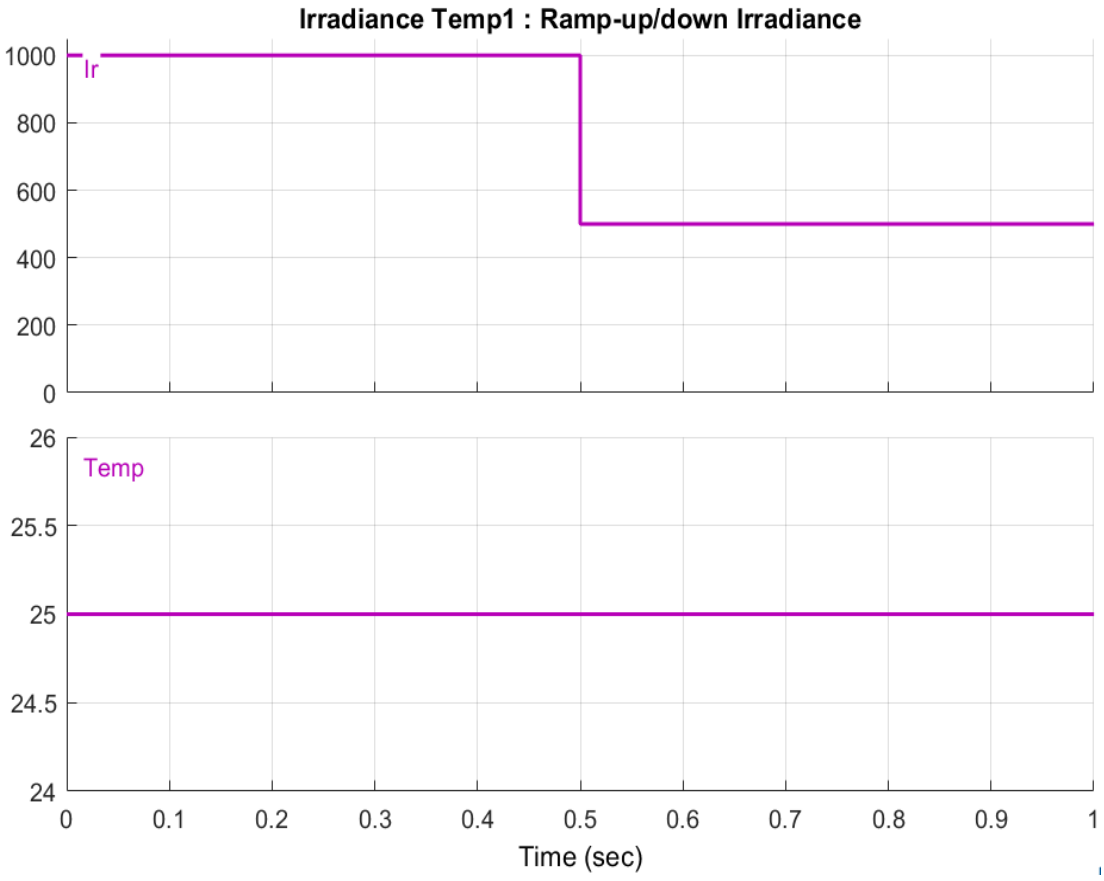

Fig. 4.7 Graph of changing irradiance and temperature

Results for conventional control algorithms-

1. **SRF Control**

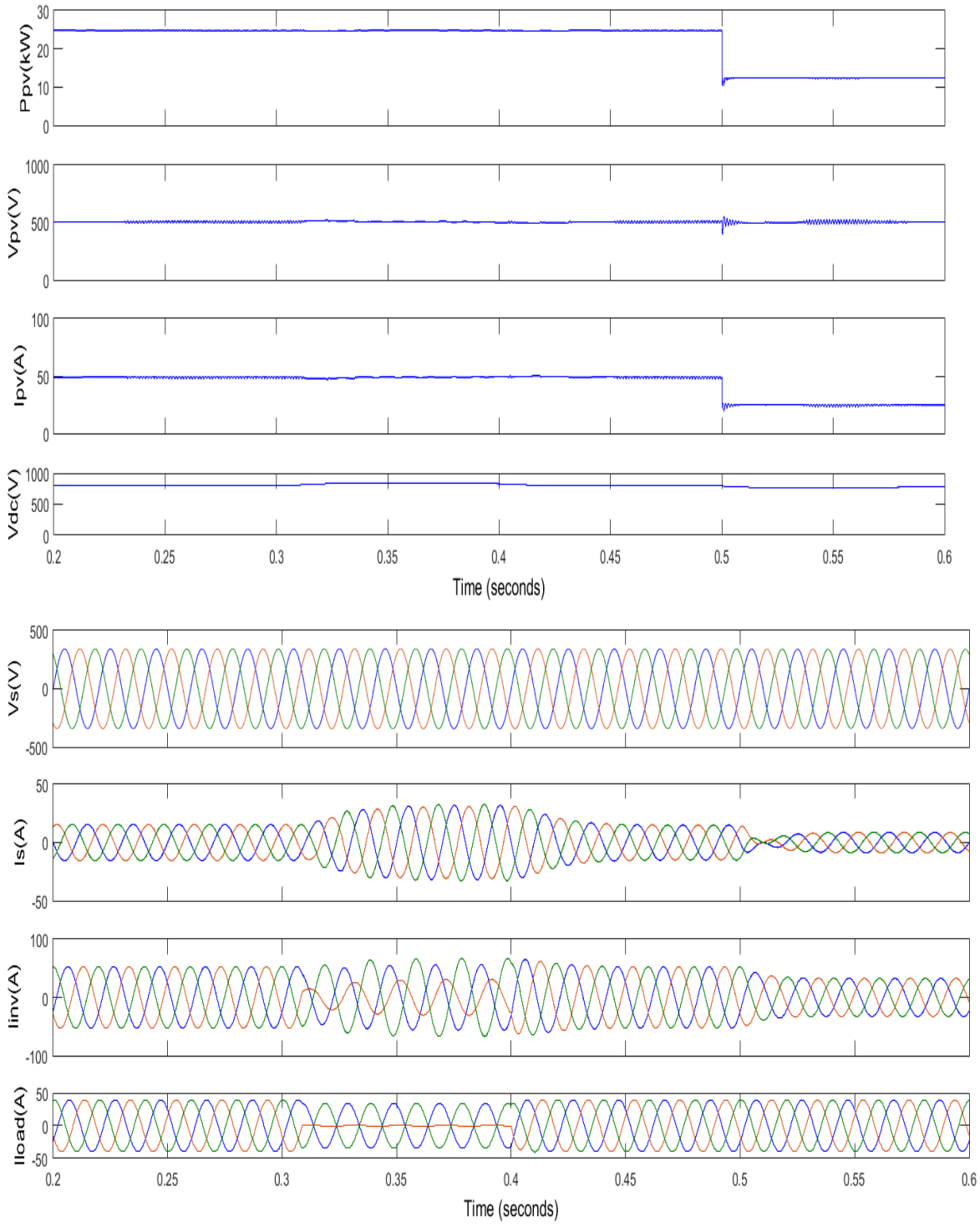

Fig. 4.8 Results for SRFT control under load imbalance and varying solar irradiance for linear load.

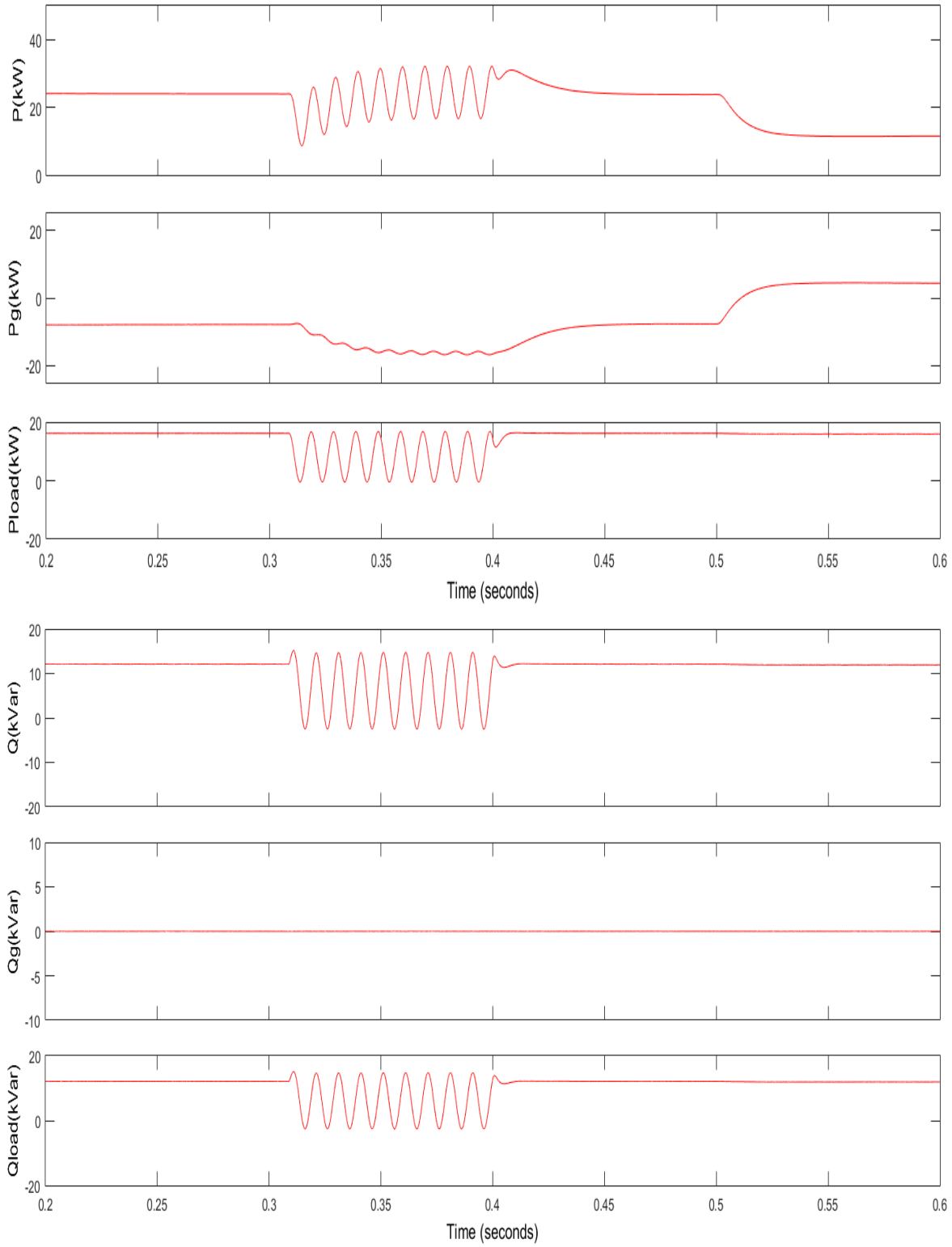

Fig. 4.9 Real and reactive power characteristics for SRFT control under load imbalance and varying solar irradiance for linear load.

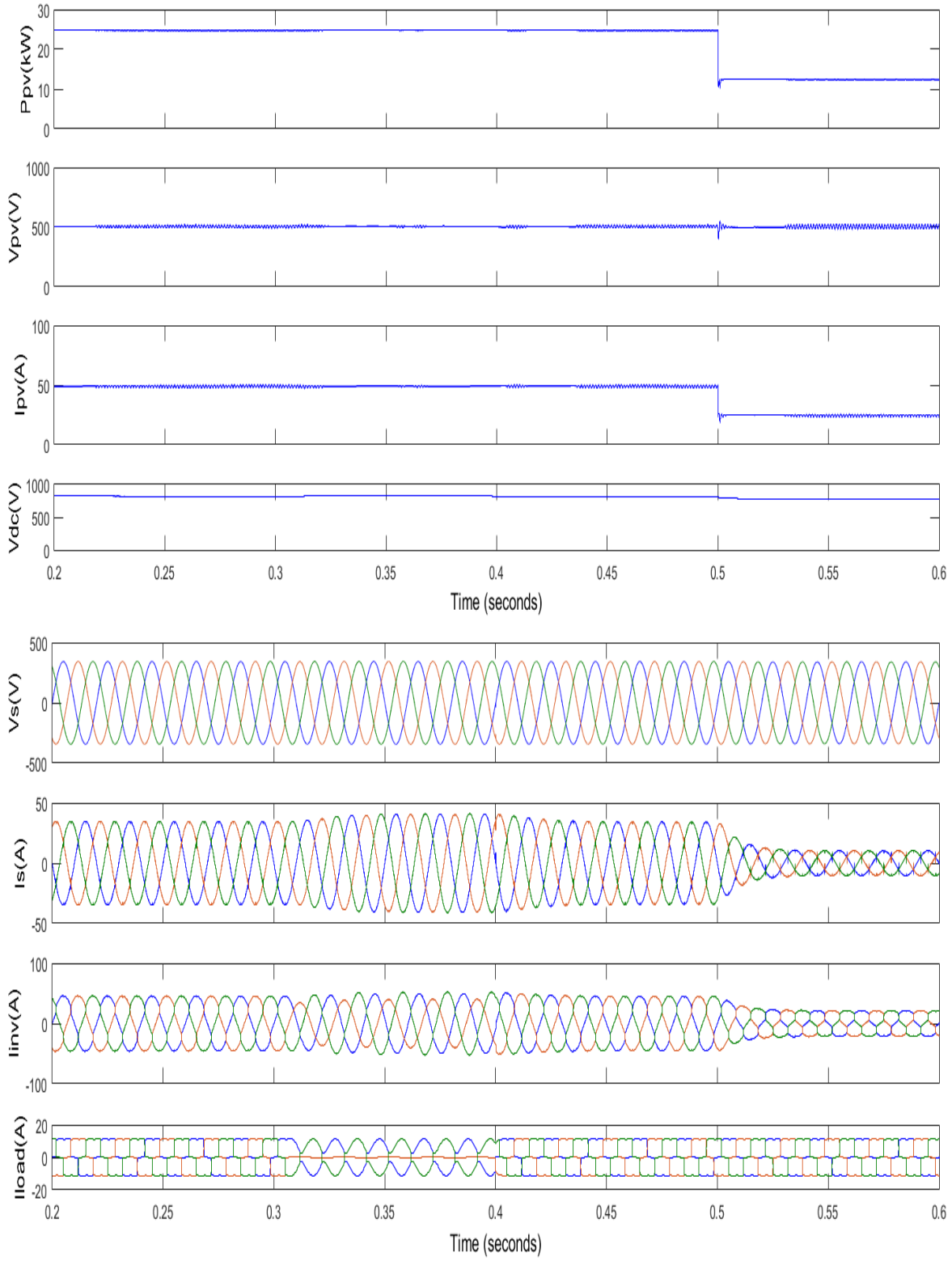

Fig. 4.10 Results for SRFT control under load imbalance and varying solar irradiance for non-linear load.

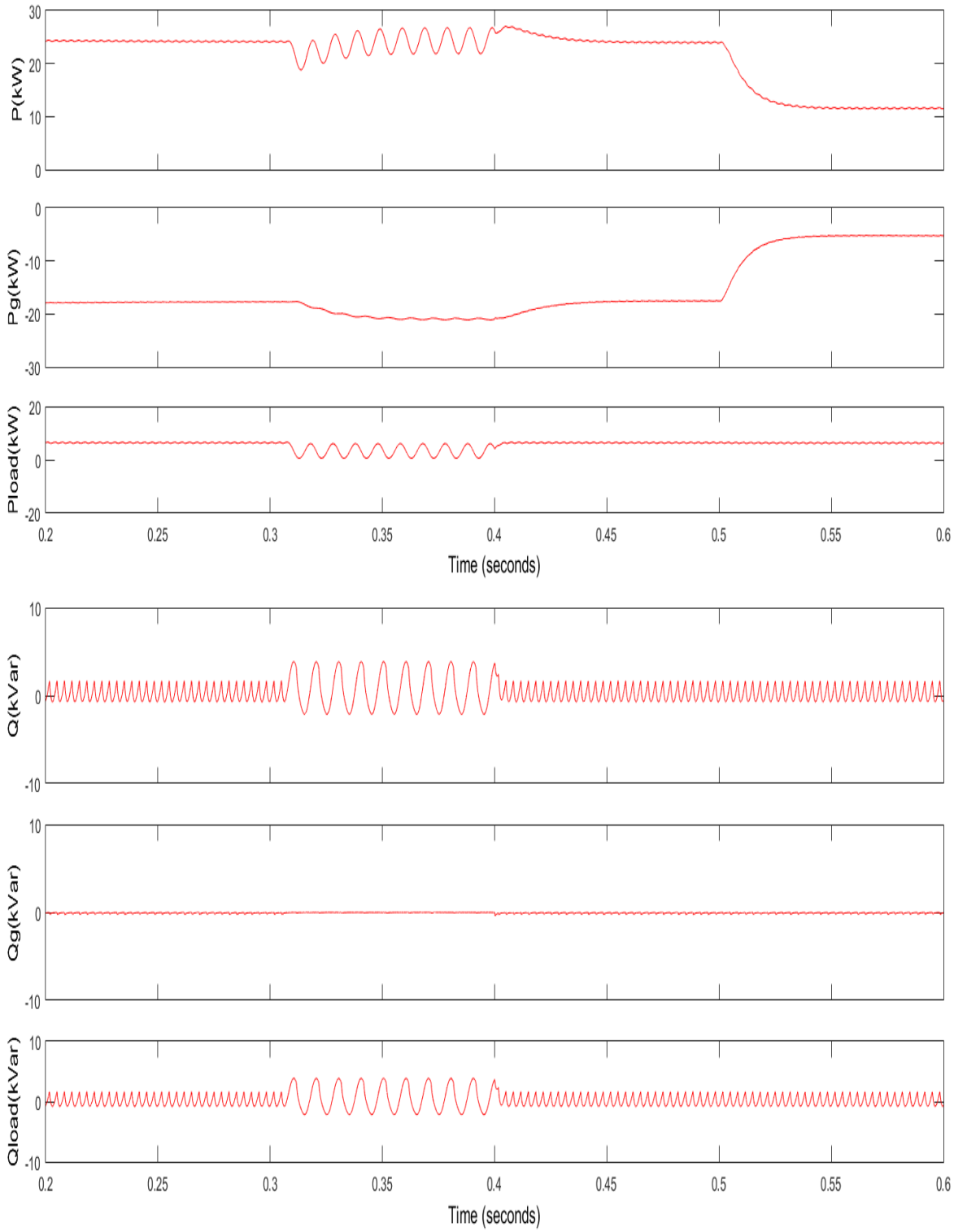

Fig. 4.11 Real and reactive power characteristics for SRFT control under load imbalance for non-linear load.

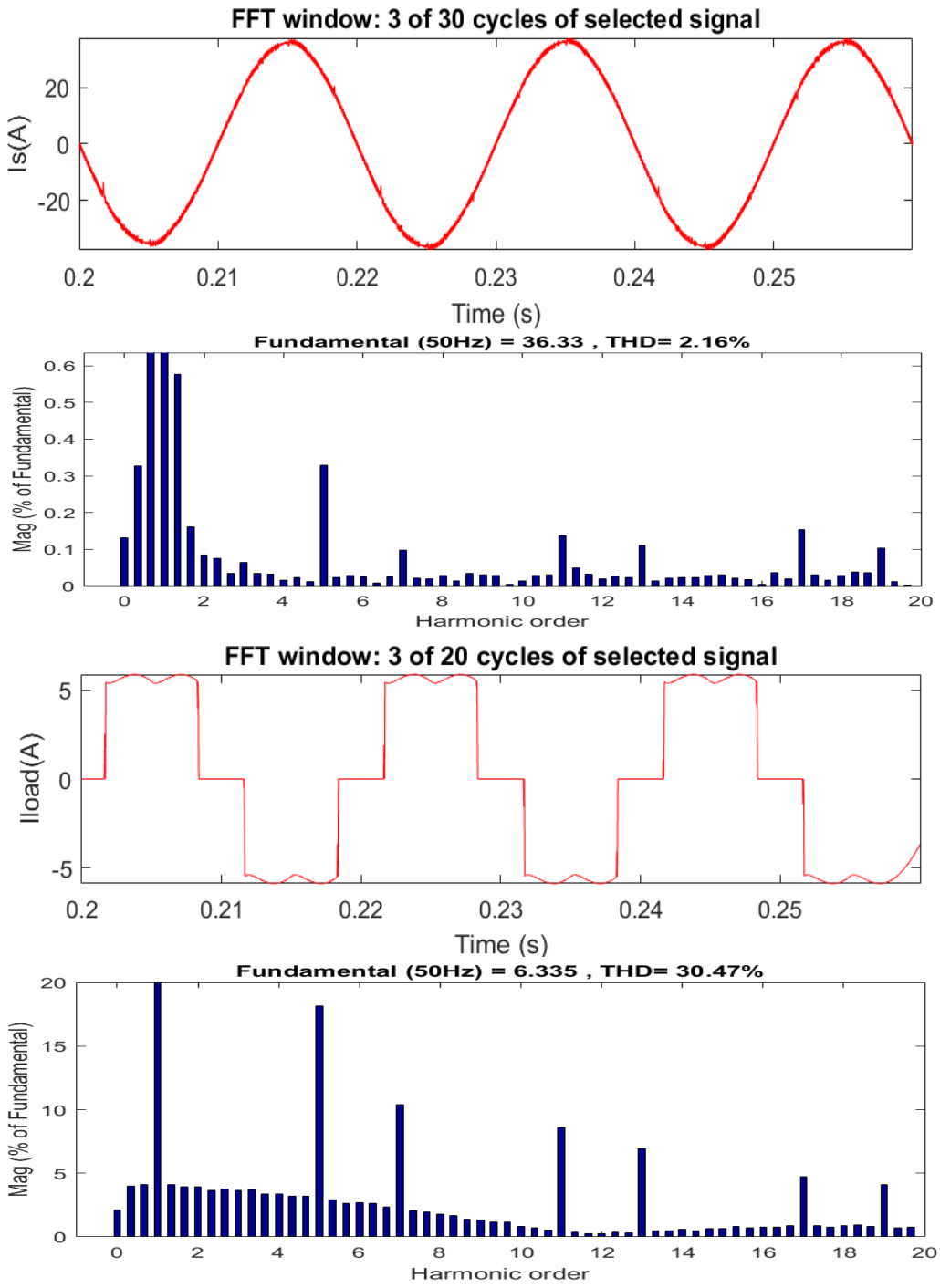

Fig. 4.12 FFT analysis of grid and load current using SRFT control, respectively.

Performance of the system is assesed from 0.2 sec to 0.6 sec. An imbalance is created from 0.3 sec to 0.4 sec by disconnecting phase b, following which there is a reduction in irradiance

from 0.5 sec and is reduced to 500 W/m^2. P_{pv}, V_{pv} and I_{pv} and V_s, I_{inv}, I_{load} , I_s and V_{dc} are plotted for a linear load of 20kVA, 0.8 lagging pf and three phase diode rectifier as non-linear with Rdc= 50 Ω and L=50mH.

At 0.3 sec there is a slight disturbance in power, voltage, and current of PV array due to load change as seen in Fig. 4.8. Distortion in I_s and I_{inv} are resolved at 0.4 sec and they remain sinusoidal. At 0.5 sec I_{pv} and P_{pv} decrease which requires P_g to increase to supply load.Vdc is also at 800 V. THD in I_s and I_{load} are 2.16% and 30.47%, resepctively.

Table 4.1 Comparison of different parameters for linear and nonlinear loads using SRFT.

PARAMETER	**LINEAR LOAD**		**NONLINEAR LOAD**	
	At 1000 W/m^2	**At 500 W/m^2**	**At 1000 W/m^2**	**At 500 W/m^2**
V_p (V)	505.6	500.82	504.86	500.09
I_p (A)	49.04	24.27	49.31	24.33
P_{pv} (kW)	24.91	12.44	24.91	12.44
V_{dc} (V)	800.81	793.81	800.22	793.37
V_s (V)	414.24	415.01	415.29	414.49
I_s (A)	-13.51	8.1	-29.45	-8.92
I_{inv} (A)	52.76	31.15	41.21	20.38
I_{load} (A)	39.25	39.25	11.46	11.46
P (kW)	24.13	11.92	24.13	11.92
Q (kVar)	12.2	12.2	-0.61	-0.61
P_g (kW)	-8.68	3.92	-18.42	5.82
Q_g (kVar)	-0.1	-0.1	-0.16	-0.16
P_l (kW)	16.1	16.1	6.36	6.36
Q_l (kVar)	12.1	12.1	-0.77	-0.77

2. IRPT Control

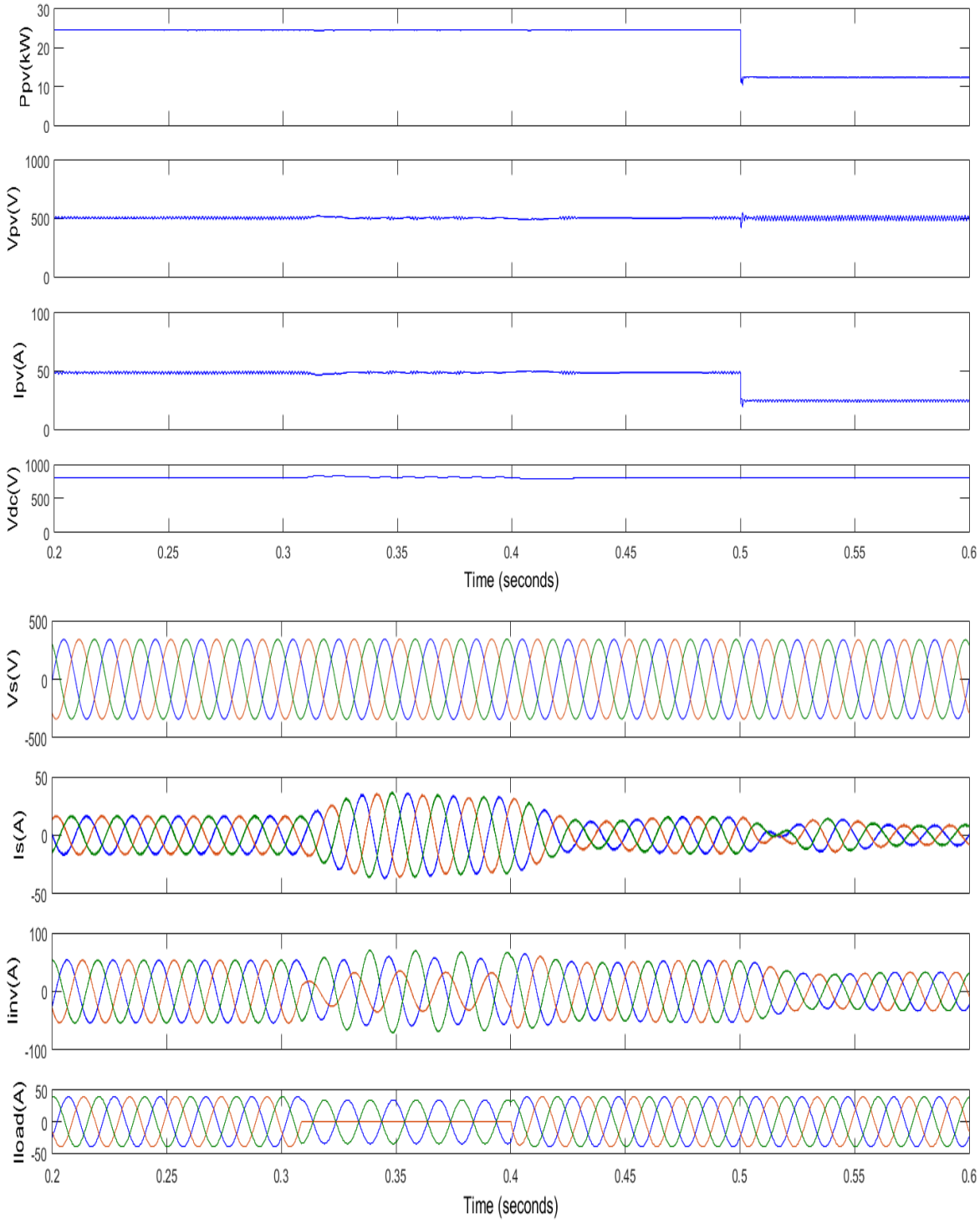

Fig. 4.13 Results for IRPT control under load imbalance and varying solar irradiance for linear load.

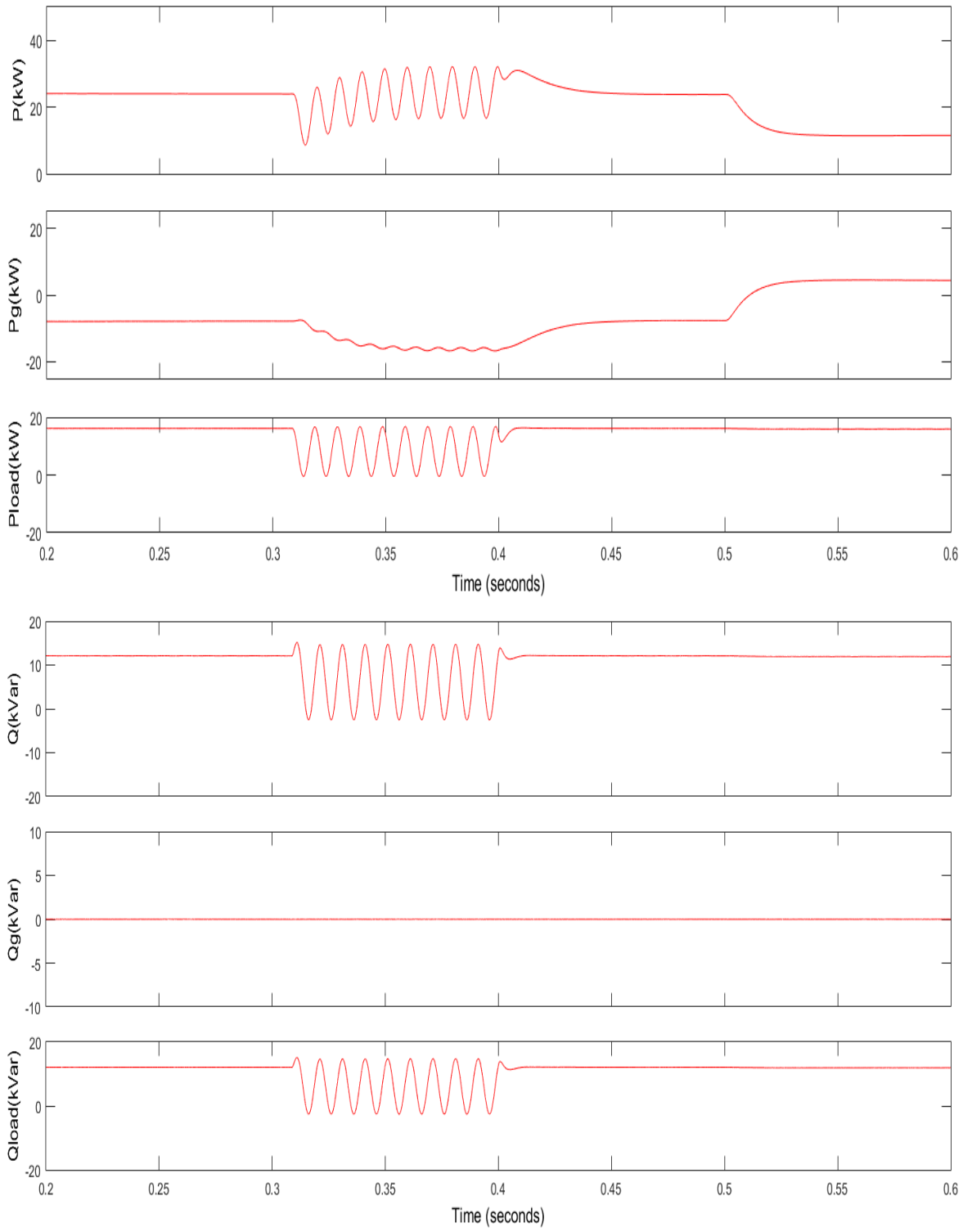

Fig. 4.14 Real and reactive power characteristics for IRPT control under load imbalance and varying solar irradiance for linear load.

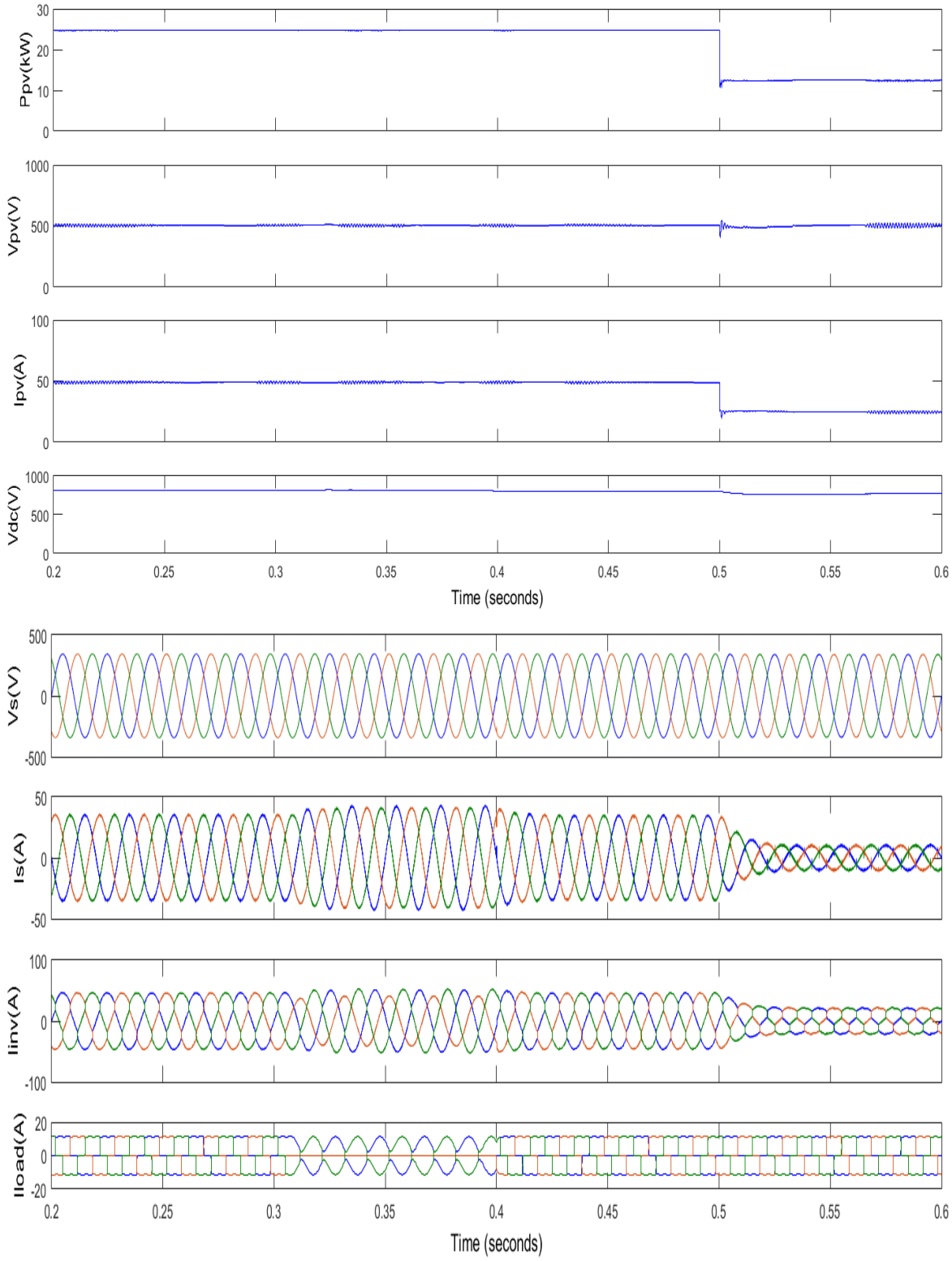

Fig. 4.15 Results for IRPT control under load imbalance and varying solar irradiance for non-linear load.

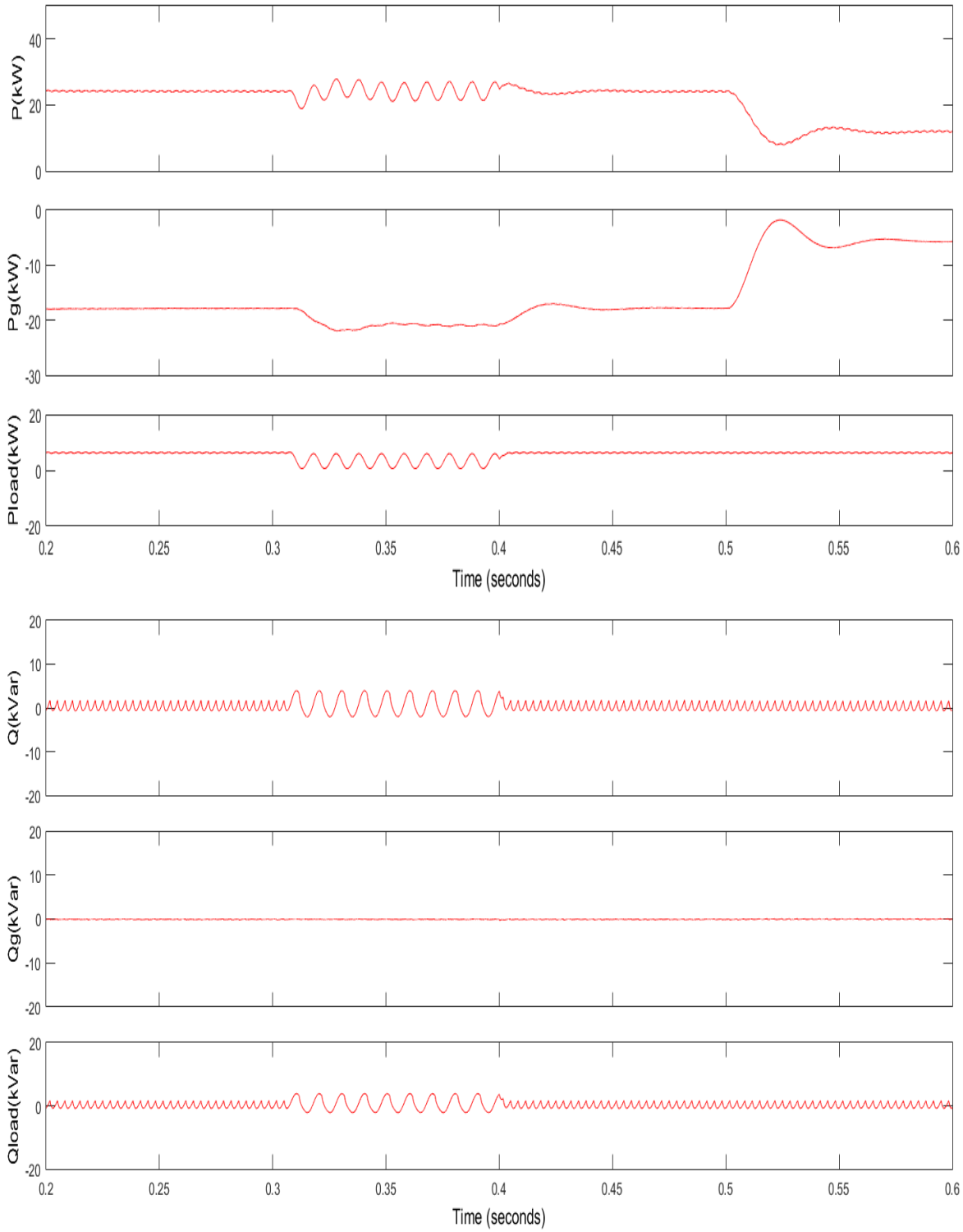

Fig. 4.16 Real and reactive power characteristics for IRPT control under load imbalance and varying solar irradiance for non-linear load.

Fig. 4.13 to Fig. 4.16 give the results for IRPT. V_{pv} is 505 V, I_{pv} is 49 A, P_{pv} is 24.9 kW, V_{dc} is 800 V. FFT analysis is done in Fig.4.17 and THD of I_s is 2.31% and I_{load} is 30.8%. Reactive power Q is at zero which is an indicator that there is reactive power compensation in UPF (unit power factor) mode. Q is almost same at zero due to UPF mode.Reactive power requirement of the load is met by PV system and grid reactive power Q_g remains zero. More complex than SRFT. THD is more in IRPT as compared to SRFT.

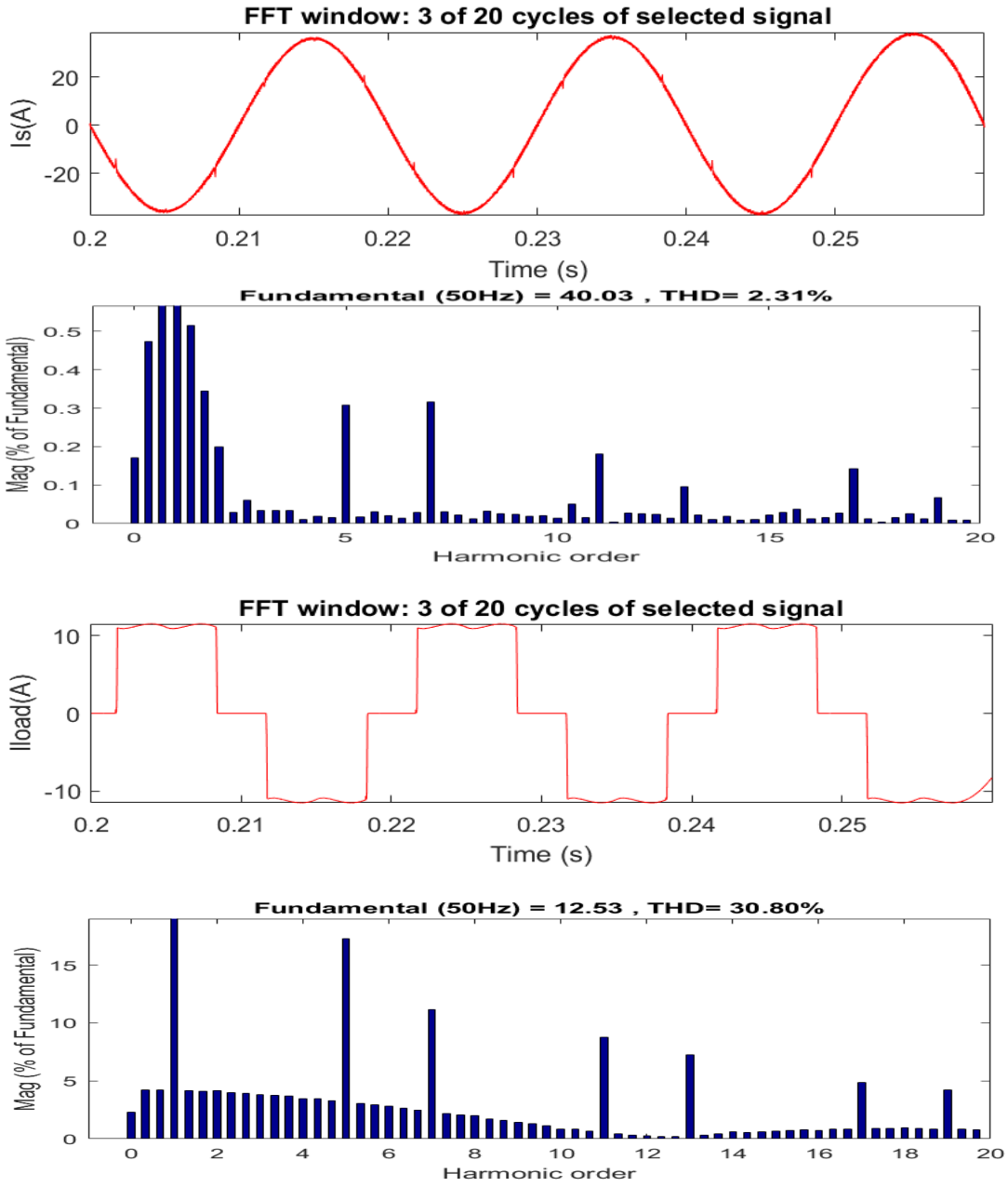

Fig. 4.17 FFT analysis of grid and load current using IRPT control, respectively.

Table 4.2 Comparison of different parameters for linear and nonlinear loads using IRPT.

PARAMETER	LINEAR LOAD		NONLINEAR LOAD	
	At 1000 W/m^2	At 500 W/m^2	At 1000 W/m^2	At 500 W/m^2
V_p (V)	503.9	501.47	504.26	499.98
I_p (A)	48.91	24.02	49.01	24.1
P_{pv} (kW)	24.91	12.44	24.91	12.44
V_{dc} (V)	799.91	793.25	800.07	793.84
V_s (V)	415.2	415.55	415.56	415.87
I_s (A)	-13.7	8.06	-29.45	-8.92
I_{inv} (A)	52.97	31.21	41.21	20.38
I_{load} (A)	39.27	39.27	11.45	11.45
P (kW)	24.16	11.99	24.16	11.99
Q (kVar)	12.2	12.2	-0.61	-0.61
P_g (kW)	-8.04	4.02	-18.45	5.63
Q_g (kVar)	-0.1	-0.1	-0.16	-0.16
P_l (kW)	16.1	16.1	6.36	6.36
Q_l (kVar)	12.1	12.1	-0.77	-0.77

3. Power Balance Theory (PBT) Control

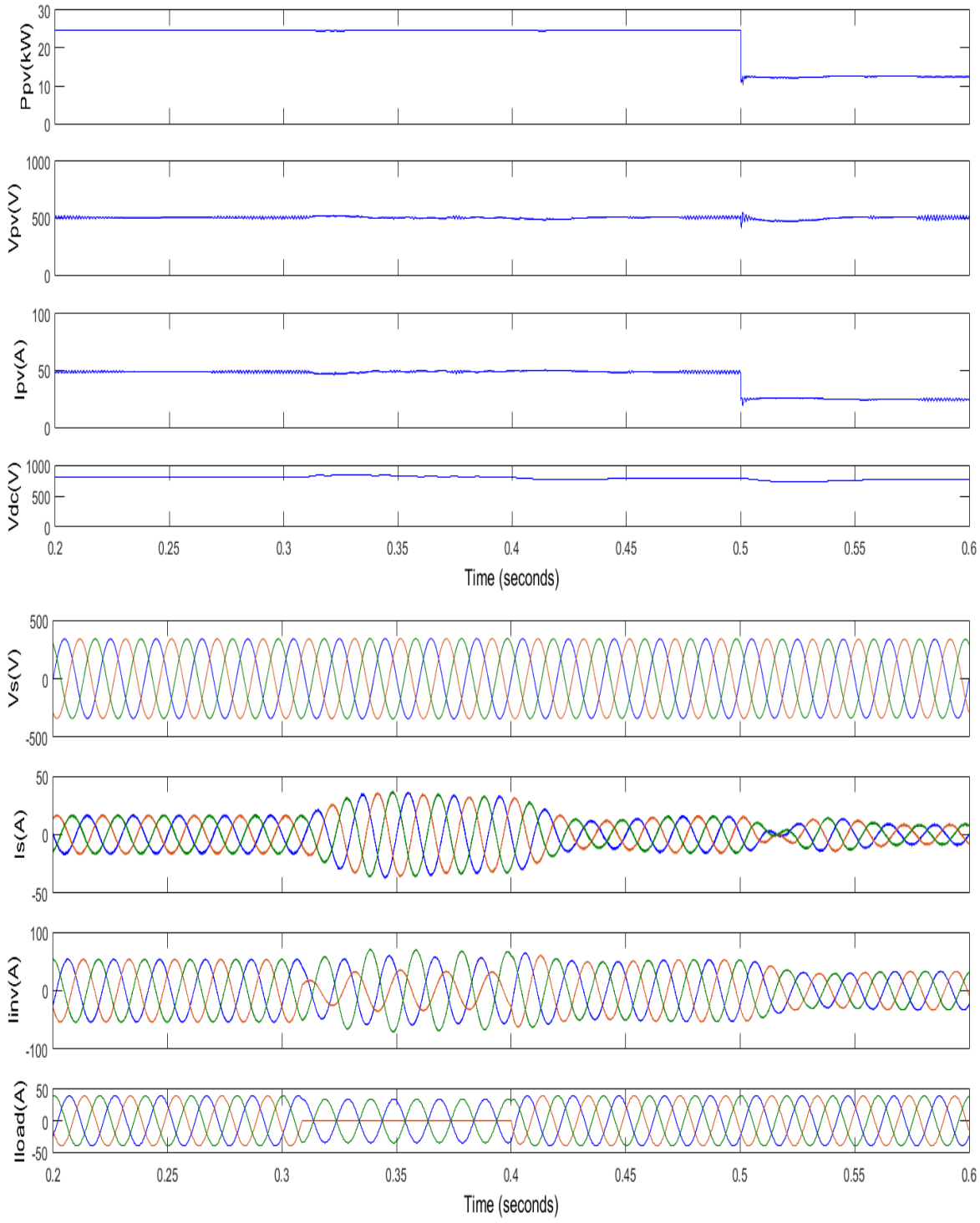

Fig. 4.18 Results for PBT control under load imbalance and varying solar irradiance for linear load.

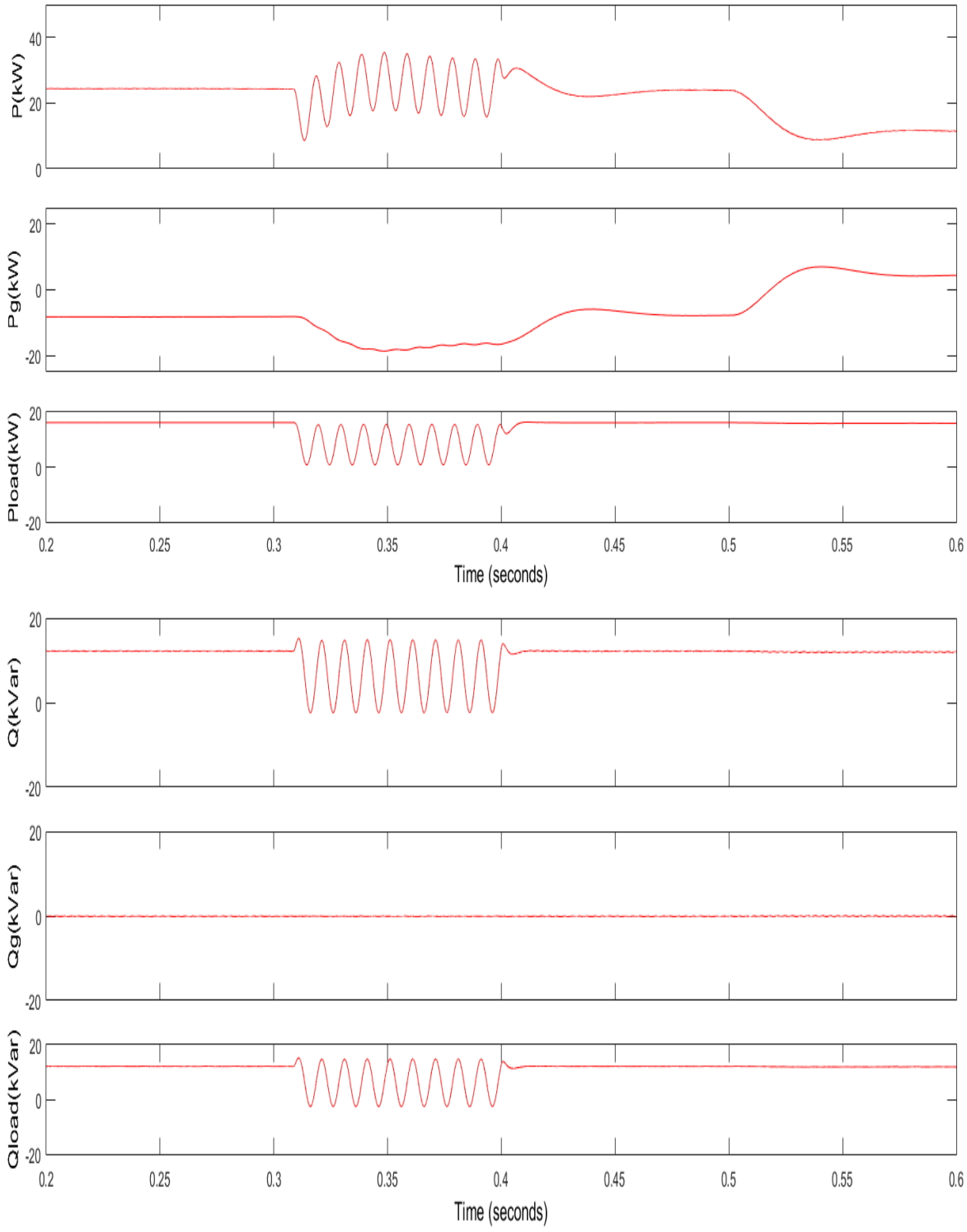

Fig. 4.19 Real and reactive power characteristics for PBT control under load imbalance and varying solar irradiance for linear load.

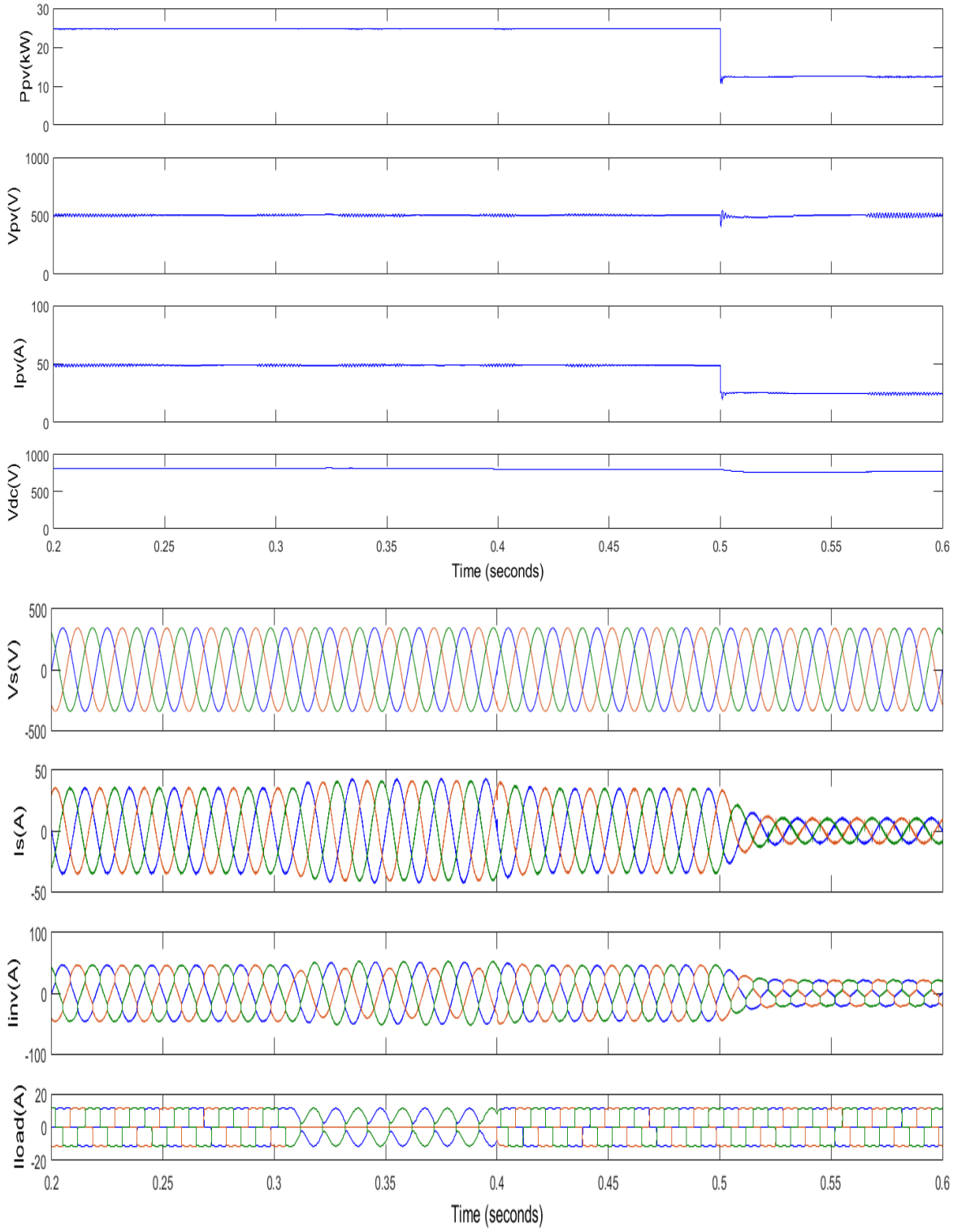

Fig. 4.20 Results for PBT control under load imbalance and varying solar irradiance for non-linear load.

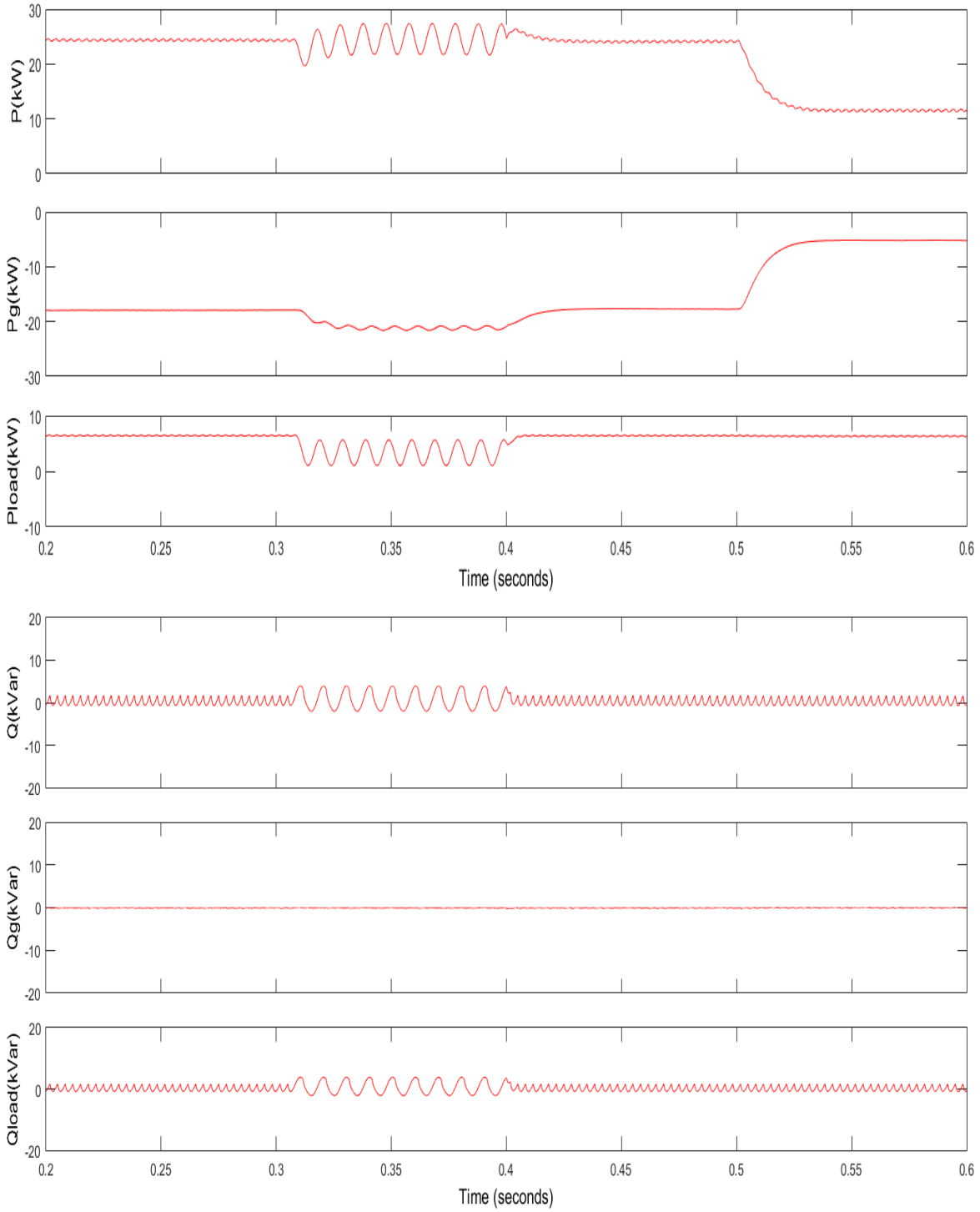

Fig. 4.21 Real and reactive power characteristics for PBT control under load imbalance and varying solar irradiance for non-linear load.

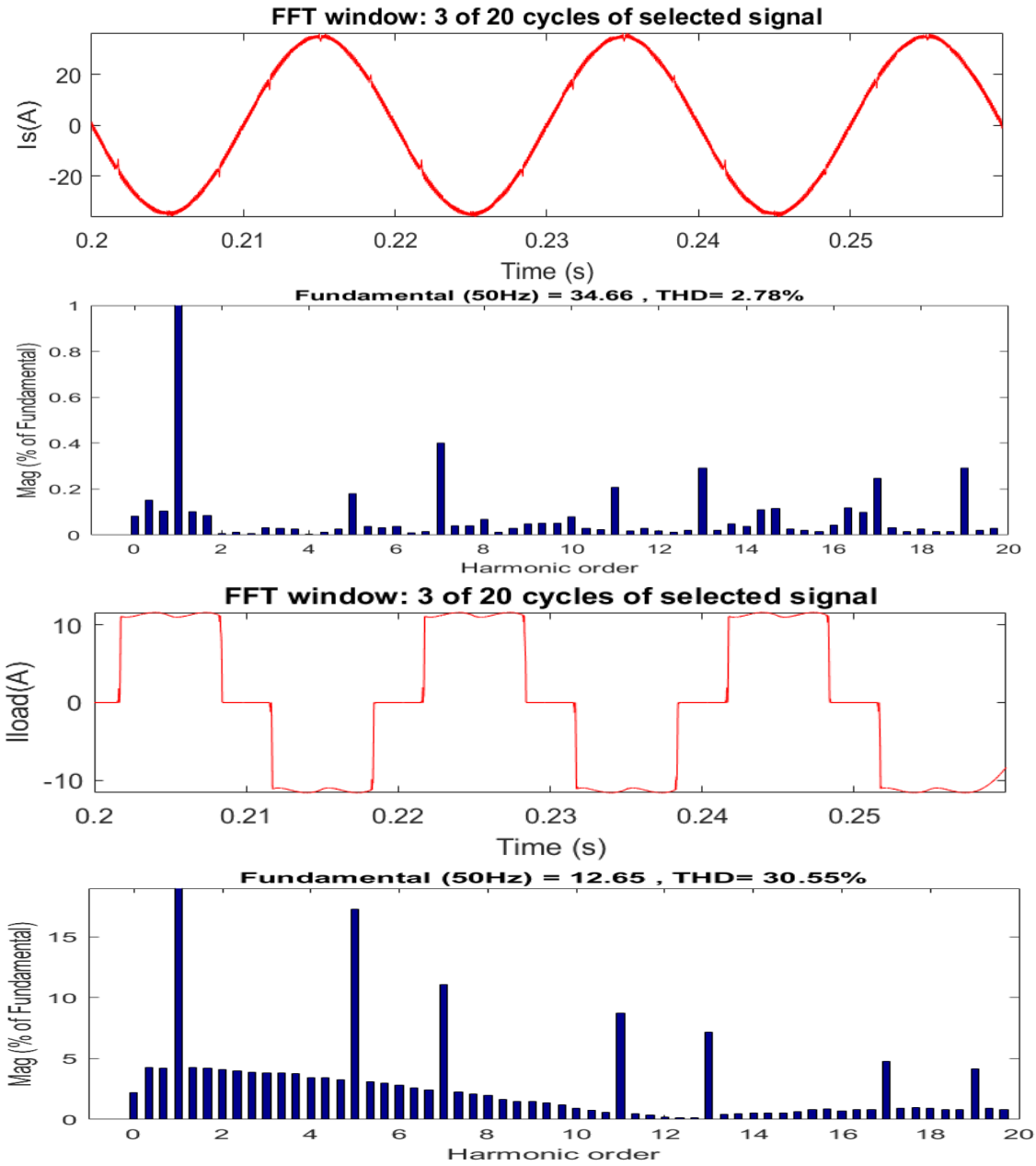

Fig. 4.22 FFT analysis of grid and load current using PBT control, respectively.

Fig 4.18 to Fig. 4.21 give results for PBT. The PV power generated at MPP is 24.910 kW, voltage is 505 V and current is 49 A, but the power extracted by the system is 24.21kW which is more than both SRFT and IRPT. V_{dc} is fixed at 800 V with the help of a PI controller. When the irradiance is 1000 W/m2 the rid absorbs 8.1 kW of power and when it is reduced to 500 w/m2 the grid starts supplying 4 kW power as the power extracted from PV is reduced to half for linear load.THD is 2.78% for I_s and 30.55% for I_{load}.

Table 4.3 Comparison of different parameters for linear and nonlinear loads using PBT.

PARAMETER	LINEAR LOAD		NONLINEAR LOAD	
	At 1000 W/m^2	At 500 W/m^2	At 1000 W/m^2	At 500 W/m^2
V_p (V)	505.2	502.21	505.26	501.98
I_p (A)	49.11	24.32	49.21	24.33
P_{pv} (kW)	24.91	12.44	24.91	12.44
V_{dc} (V)	800.96	794.45	800.47	793.99
V_s (V)	416.02	415.87	415.68	415.29
I_s (A)	-13.95	8.01	-29.45	-8.92
I_{inv} (A)	53.21	31.25	41.21	20.38
I_{load} (A)	39.26	39.26	11.45	11.45
P (kW)	24.21	12.05	24.21	12.05
Q (kVar)	12.2	12.2	-0.65	-0.65
P_g (kW)	-8.11	4.05	-17.85	5.69
Q_g (kVar)	-0.1	-0.1	-0.11	-0.11
P_l (kW)	16.1	16.1	6.36	6.36
Q_l (kVar)	12.1	12.1	-0.76	-0.76

4. Unit Template Control

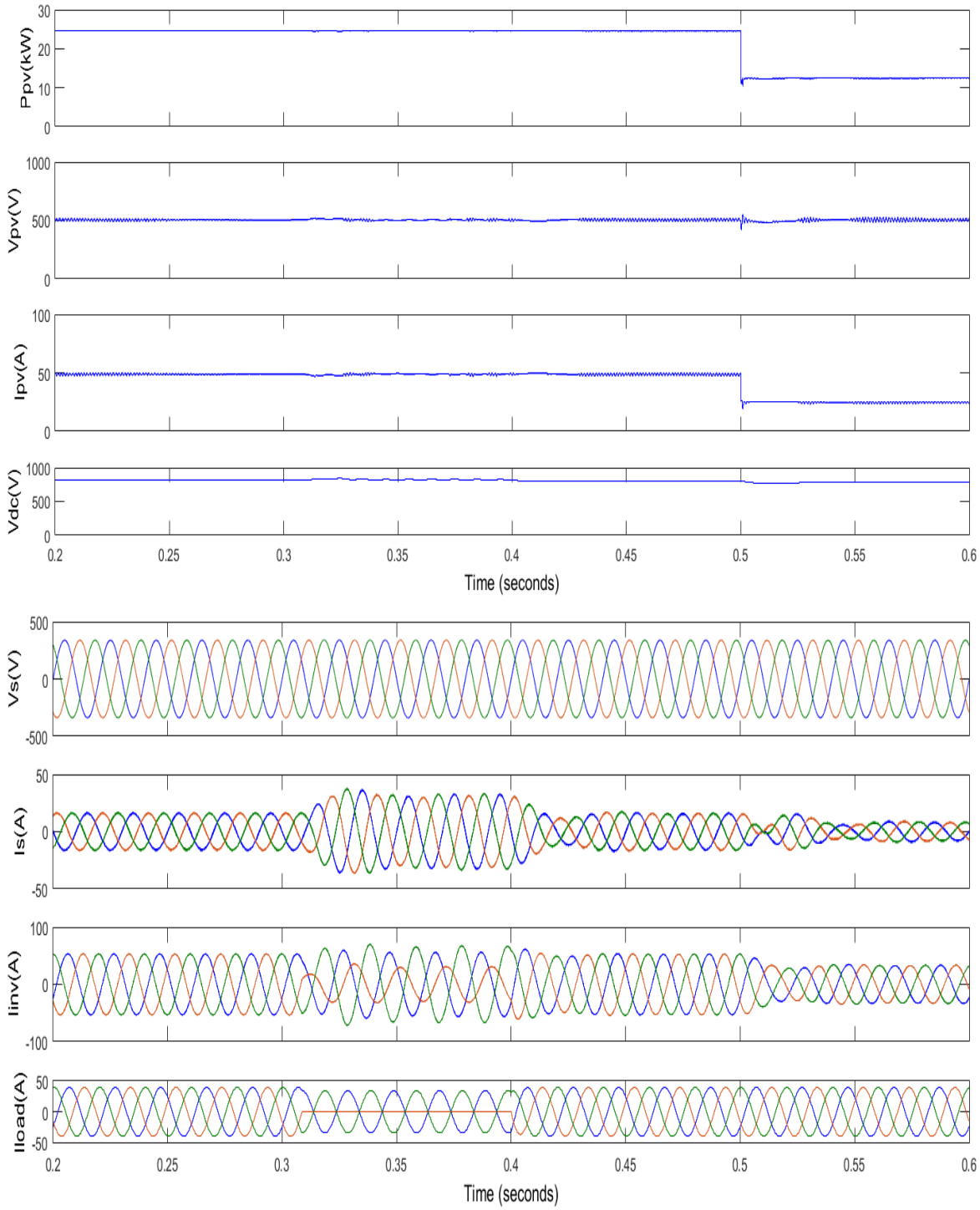

Fig. 4.23 Results for unit template control under load imbalance and varying solar irradiance for linear load.

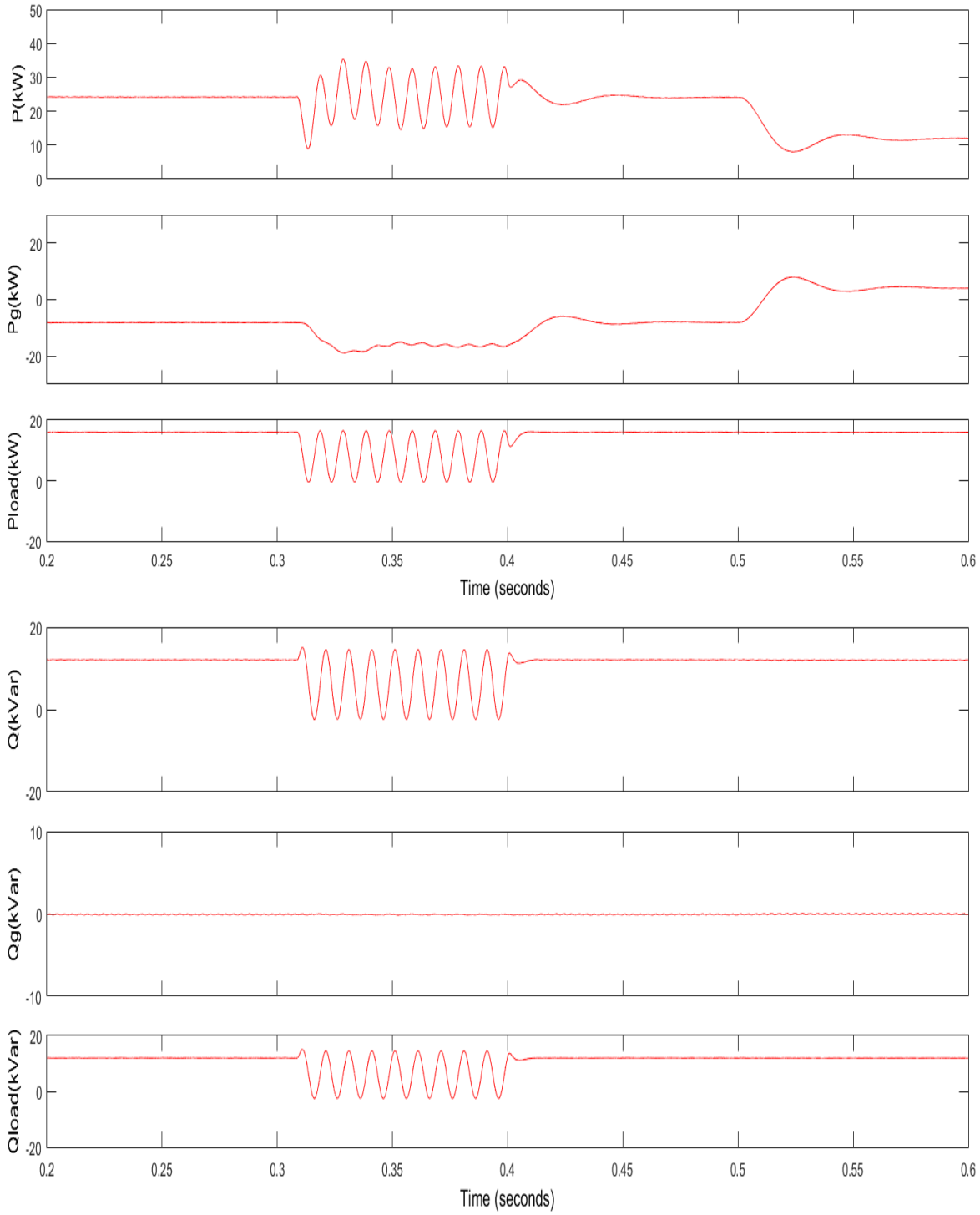

Fig. 4.24 Real and reactive power characteristics for unit template control under load imbalance and varying solar irradiance for linear load.

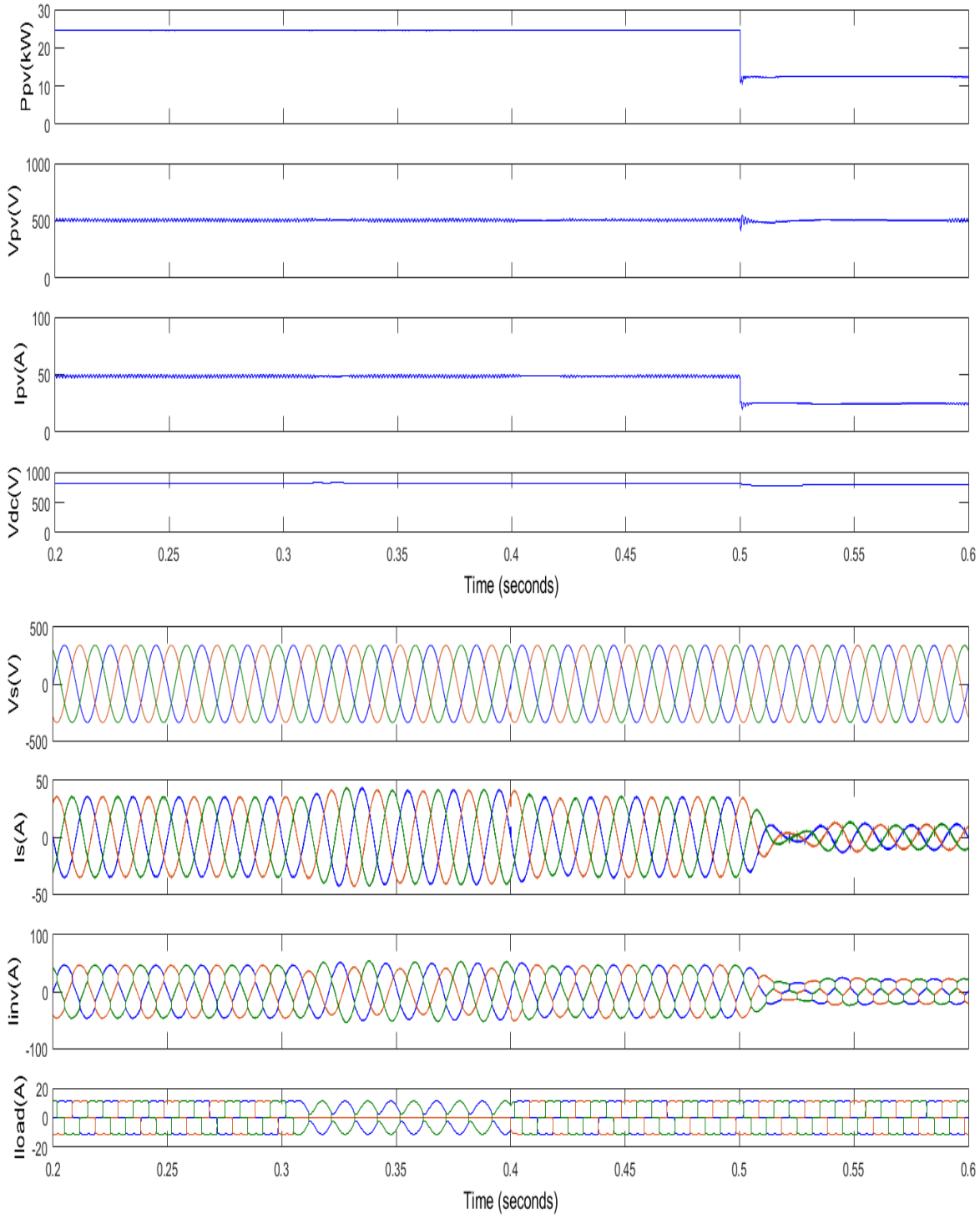

Fig. 4.25 Results for unit template control under load imbalance and varying solar irradiance for non-linear load.

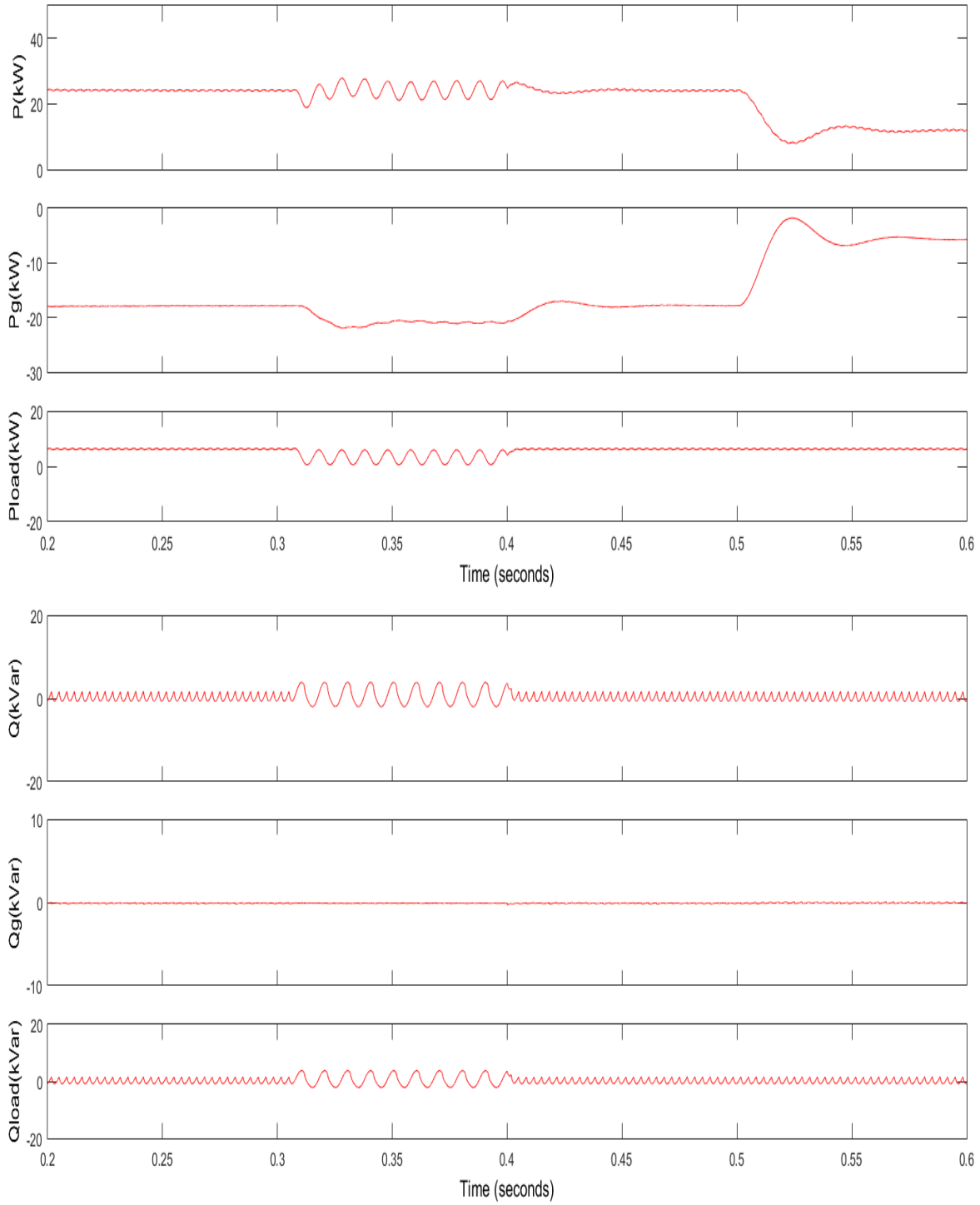

Fig. 4.26 Real and reactive power characteristics for unit template control under load imbalance and varying solar irradiance for non-linear load.

Fig. 4.23 to Fig. 4.27 are the results for the system using unit template. V_{dc} is also at 800 V and more stable during imbalance as compared to other algorithms. THD in I_s and I_{load} are 2.35% and 30.27%, resepctively. Computational complexity less than PBT. Performance is similar to PBT.

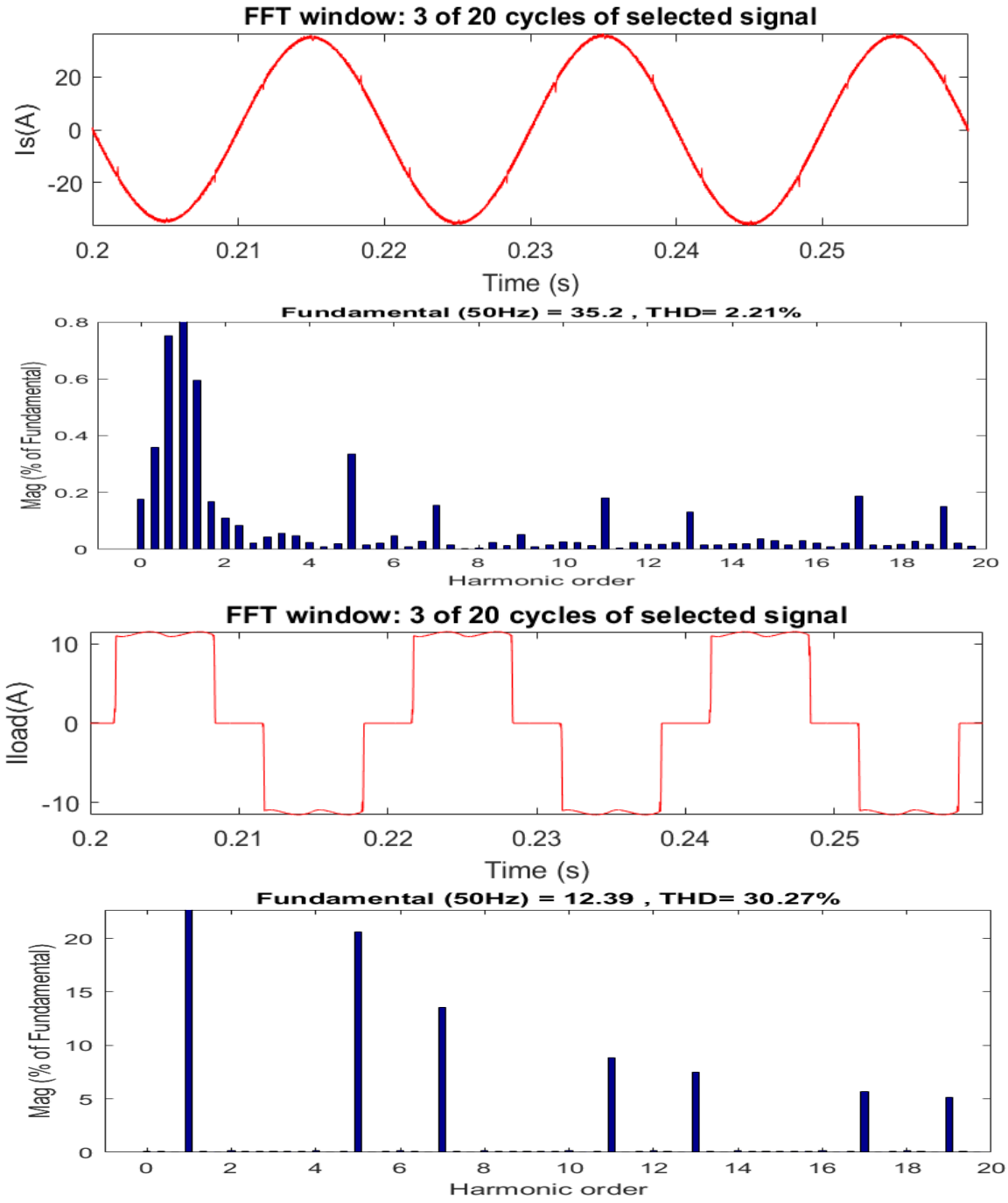

Fig. 4.27 FFT analysis of grid and load current using unit template control, respectively

Table 4.4 Comparison of different parameters for linear and nonlinear loads using unit template.

PARAMETER	LINEAR LOAD		NONLINEAR LOAD	
	At 1000 W/m^2	At 500 W/m^2	At 1000 W/m^2	At 500 W/m^2
V_p (V)	505.12	501.89	505.23	500.91
I_p (A)	49	24.52	49.01	24.23
P_{pv} (kW)	24.91	12.44	24.91	12.44
V_{dc} (V)	800.91	794.45	800.67	793.14
V_s (V)	416.2	416.15	416.16	415.98
I_s (A)	-13	8.26	-29.26	-9.35
I_{inv} (A)	53.27	31.41	41.71	20.8
I_{load} (A)	39.27	39.27	11.45	11.45
P (kW)	24.17	11.99	24.17	11.99
Q (kVar)	12.2	12.2	-0.61	-0.61
P_g (kW)	-8.07	4.02	-18.71	5.63
Q_g (kVar)	-0.1	-0.1	-0.16	-0.16
P_l (kW)	16.1	16.1	6.36	6.36
Q_l (kVar)	12.1	12.1	-0.77	-0.77

Among the various conventional inverter current control algorithms implemented it is observed that due to less calculations SRFT has less delay thus, offering faster convergence rate of inverter current. THD in grid current in SRFT is less as compared to IRPT indicating that it reduces more harmonics. SRFT is also faster than PBT and Unit Template due to less computational complexity. SRFT offers least THD among all conventional algorithms.

Results for adaptive control algorithm

1. **LMS**

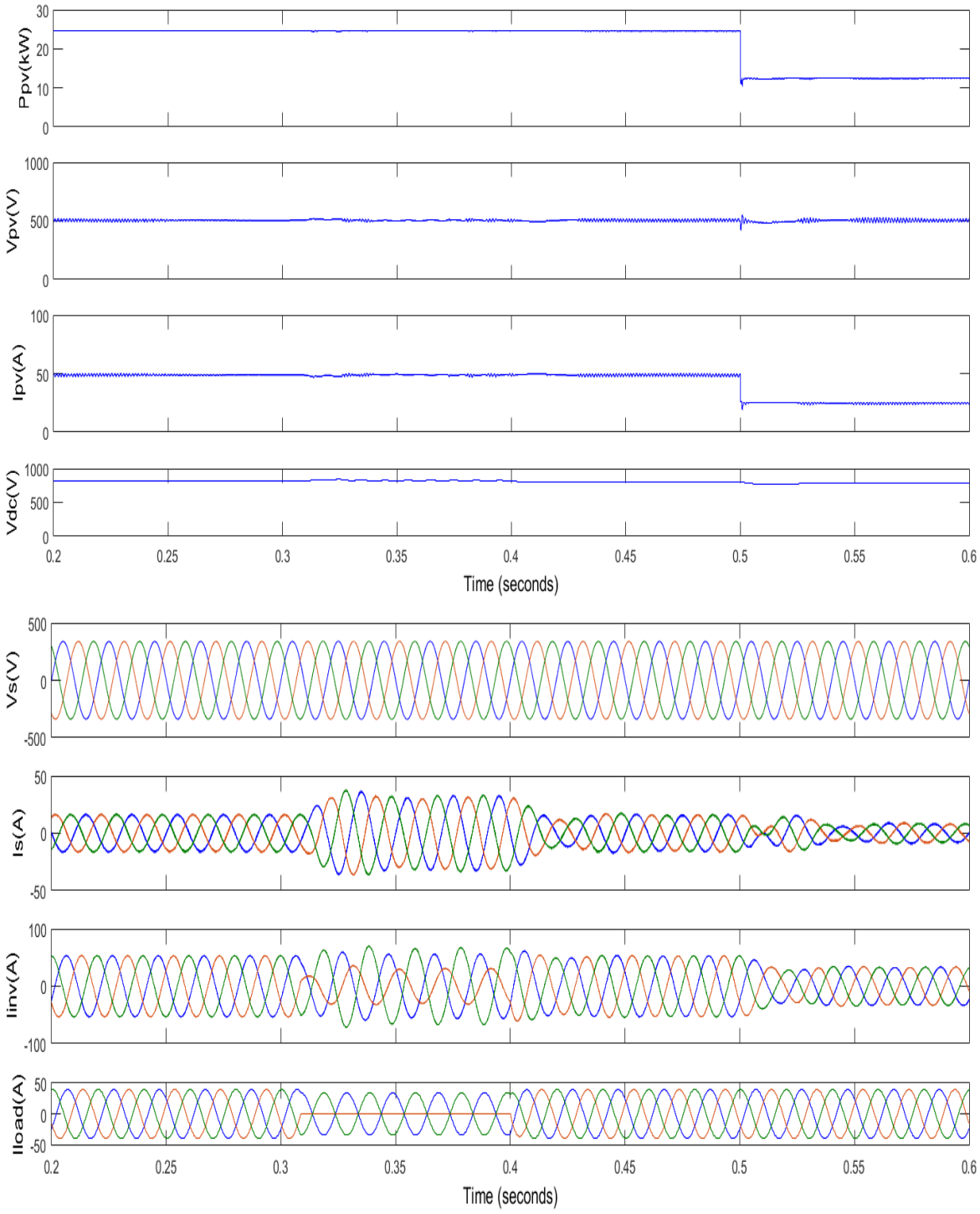

Fig. 4.28 Results for LMS control under load imbalance and varying solar irradiance for linear load.

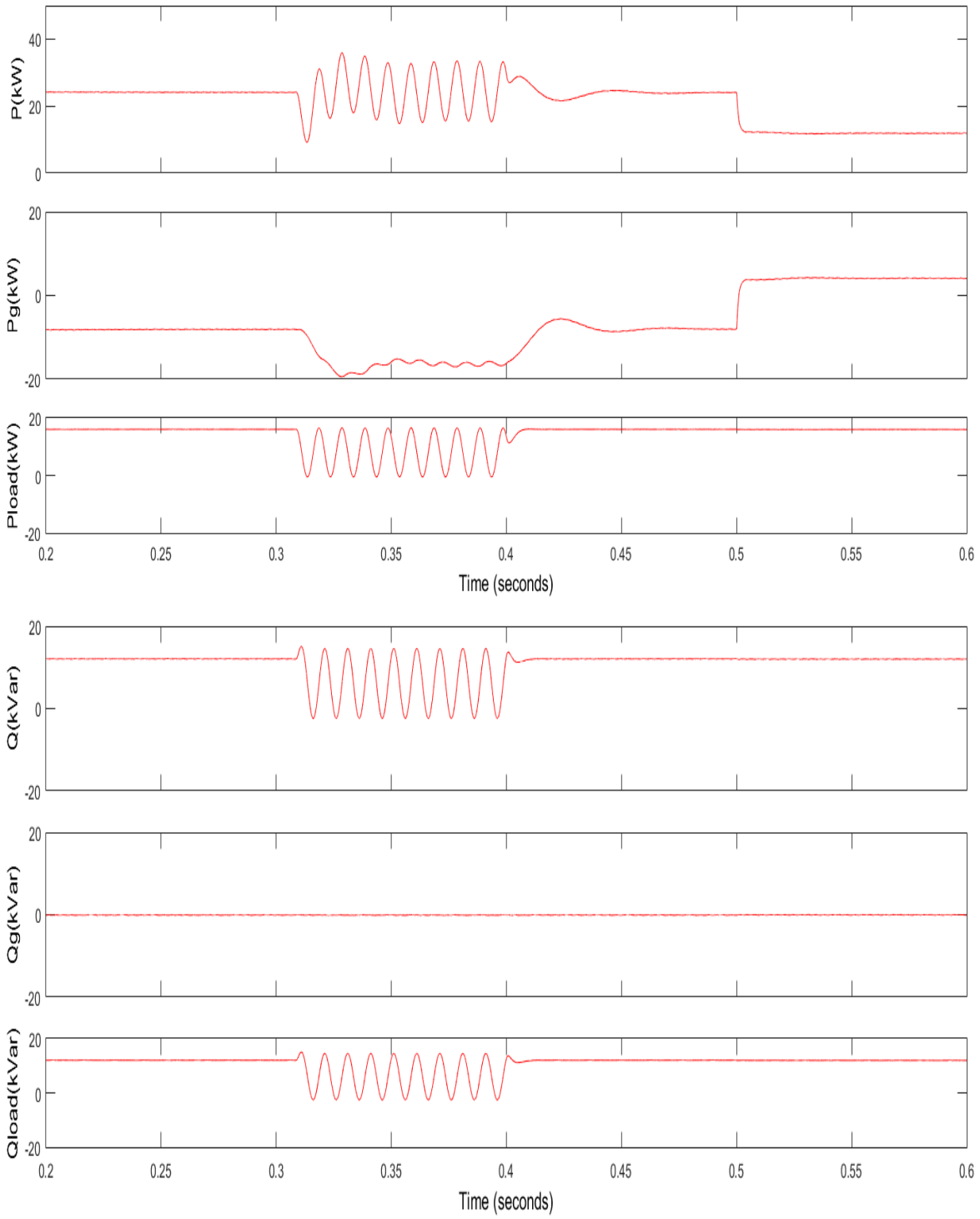

Fig. 4.29 Real and reactive power characteristics for LMS control under load imbalance and varying solar irradiance for linear load.

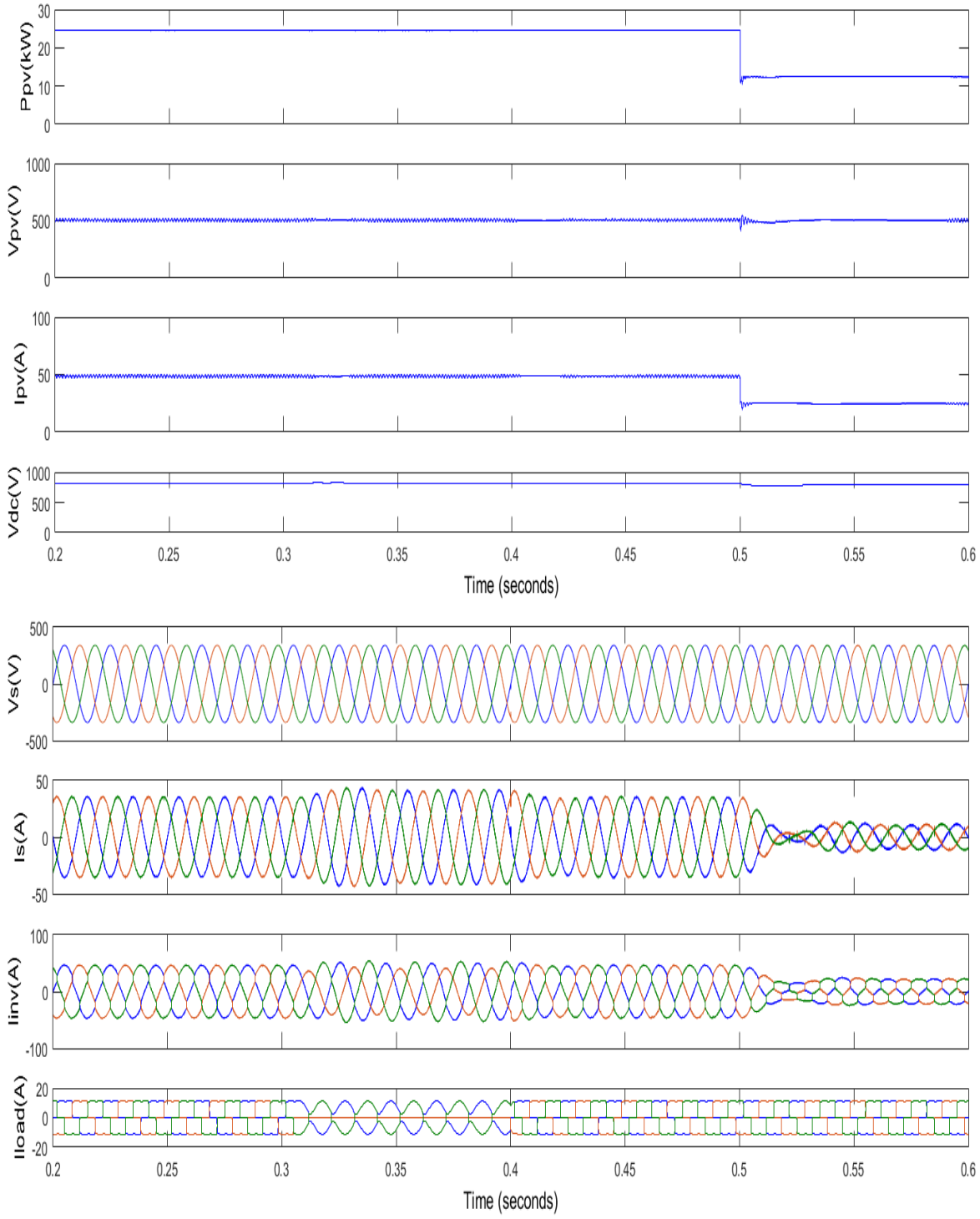

Fig. 4.30 Results for LMS control under load imbalance and varying solar irradiance for non-linear load.

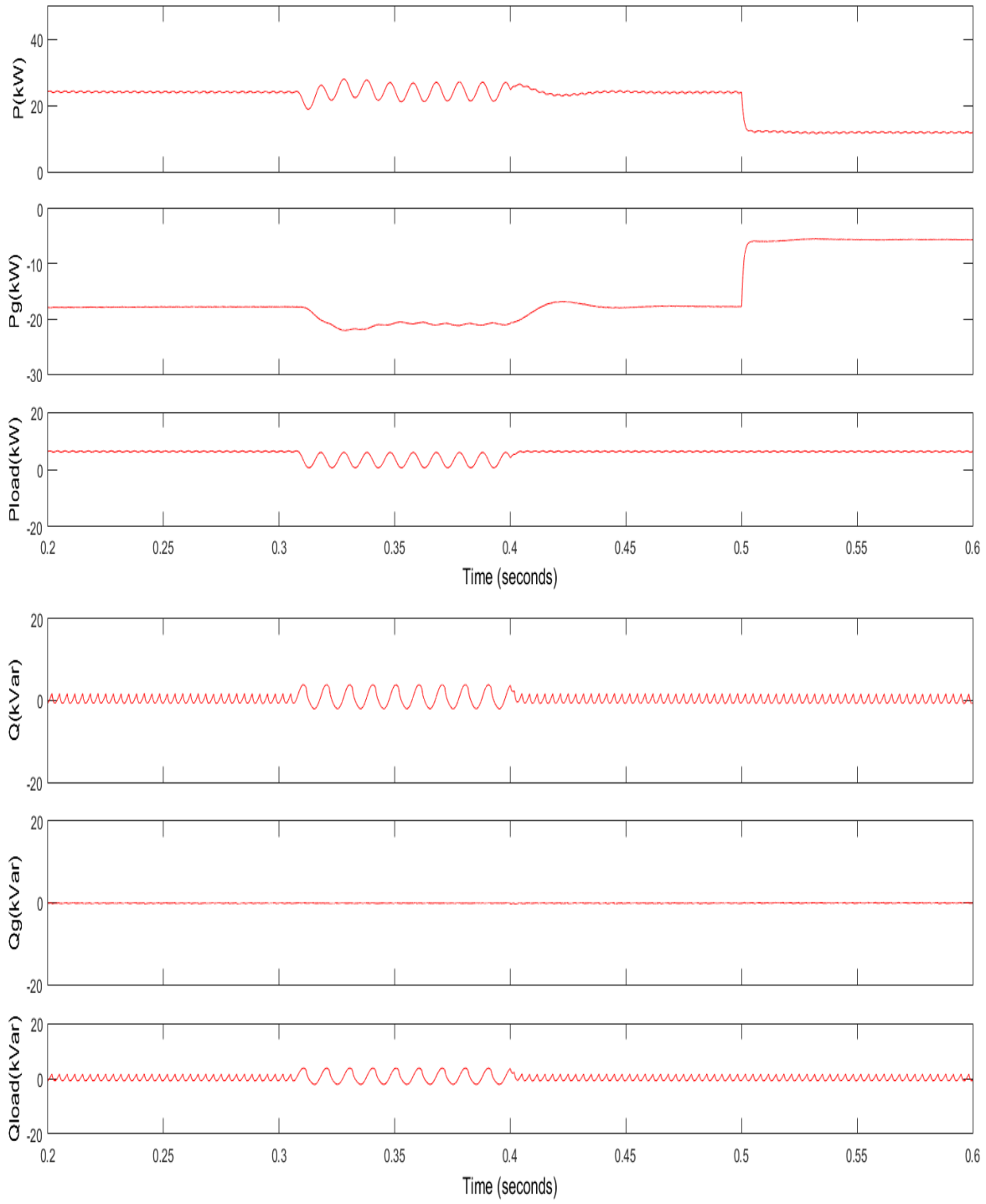

Fig. 4.31 Real and reactive power characteristics for LMS control under load imbalance and varying solar irradiance for non-linear load.

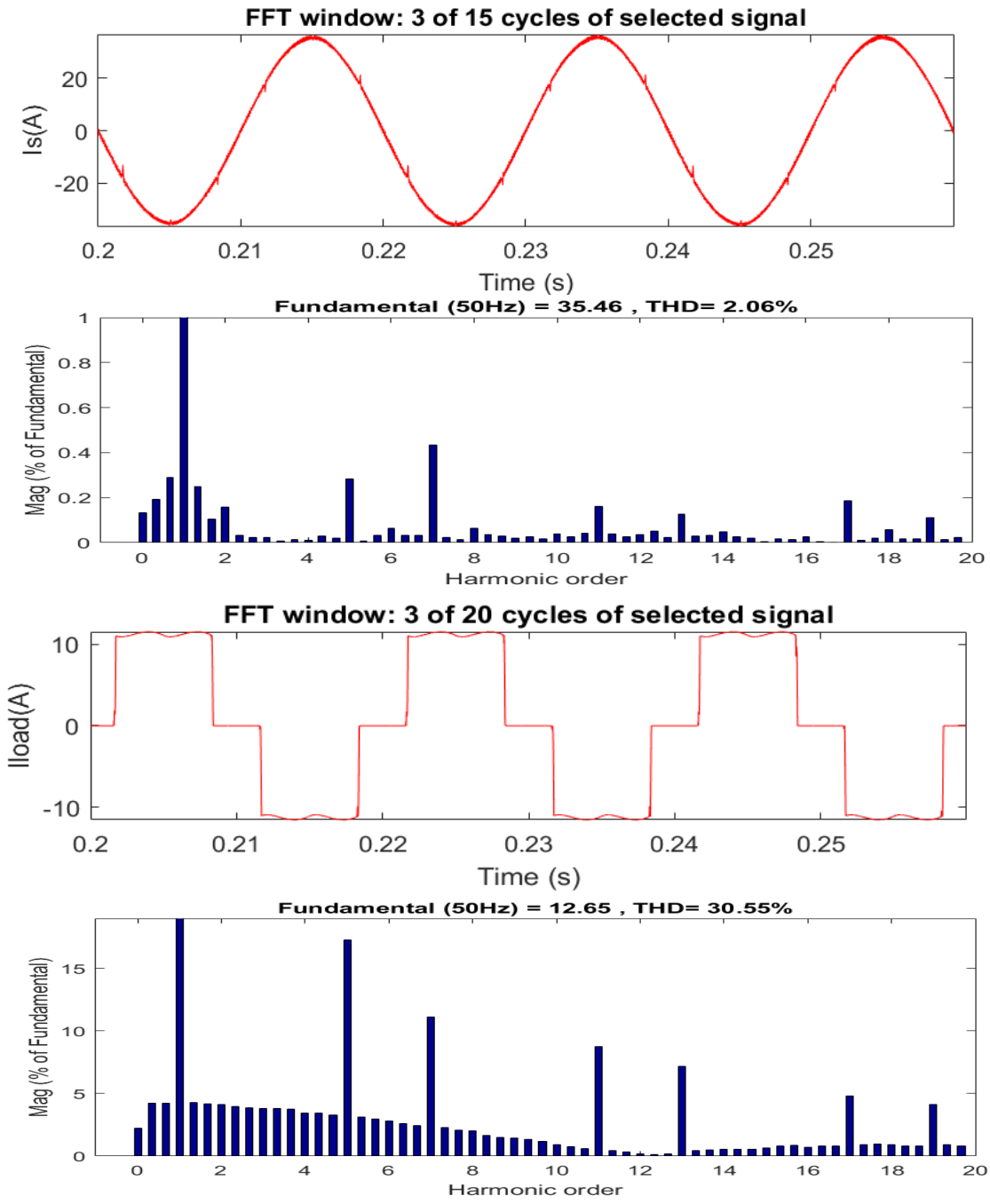

Fig. 4.32 FFT analysis of grid and load current using LMS control, respectively.

Distortion in Is during imbalance are less than those observed in SRFT in Fig 4.8. At 0.5 sec as the supply from PV reduces the P_g steps up to deliver the needful when the load is more than 25 kW. The grid current settles faster than other conventional algorithms after 0.4 s. Current converges faster than conventional algorithms.

FFT analysis is done in Fig. 4.22 and THD of I_s is 1.91% and I_{load} is 30.2%.

Table 4.4 Comparison of different parameters for linear and nonlinear loads using LMS.

PARAMETER	LINEAR LOAD		NONLINEAR LOAD	
	At 1000 W/m^2	At 500 W/m^2	At 1000 W/m^2	At 500 W/m^2
V_p (V)	505.62	501.69	505.33	500.51
I_p (A)	49.21	24.58	49.19	24.35
P_{pv} (kW)	24.91	12.44	24.91	12.44
V_{dc} (V)	800.11	794.59	800.17	793.29
V_s (V)	415.91	416.02	415.96	415.28
I_s (A)	-13.03	8.22	-29.26	-9.35
I_{inv} (A)	53.3	31.45	41.71	20.8
I_{load} (A)	39.27	39.27	11.45	11.45
P (kW)	24.29	12.2	24.29	12.2
Q (kVar)	12.2	12.2	-0.67	-0.67
P_g (kW)	-8.19	3.9	-17.93	5.64
Q_g (kVar)	-0.1	-0.1	-0.06	-0.06
P_l (kW)	16.1	16.1	6.36	6.36
Q_l (kVar)	12.1	12.1	-0.73	-0.73

2. VSS-LMS Control

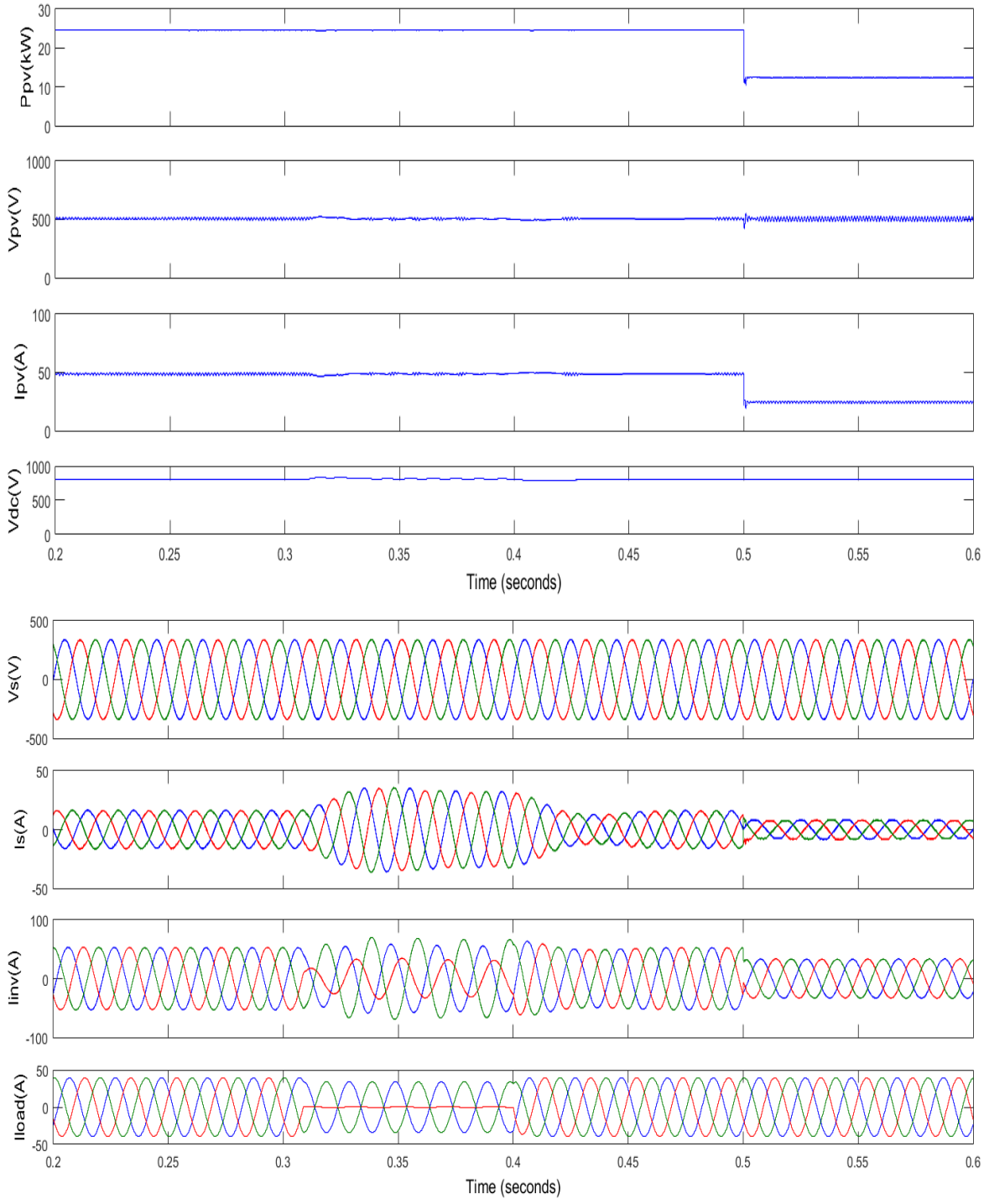

Fig. 4.33 Results for VSS-LMS control under load imbalance and varying solar irradiance for linear load.

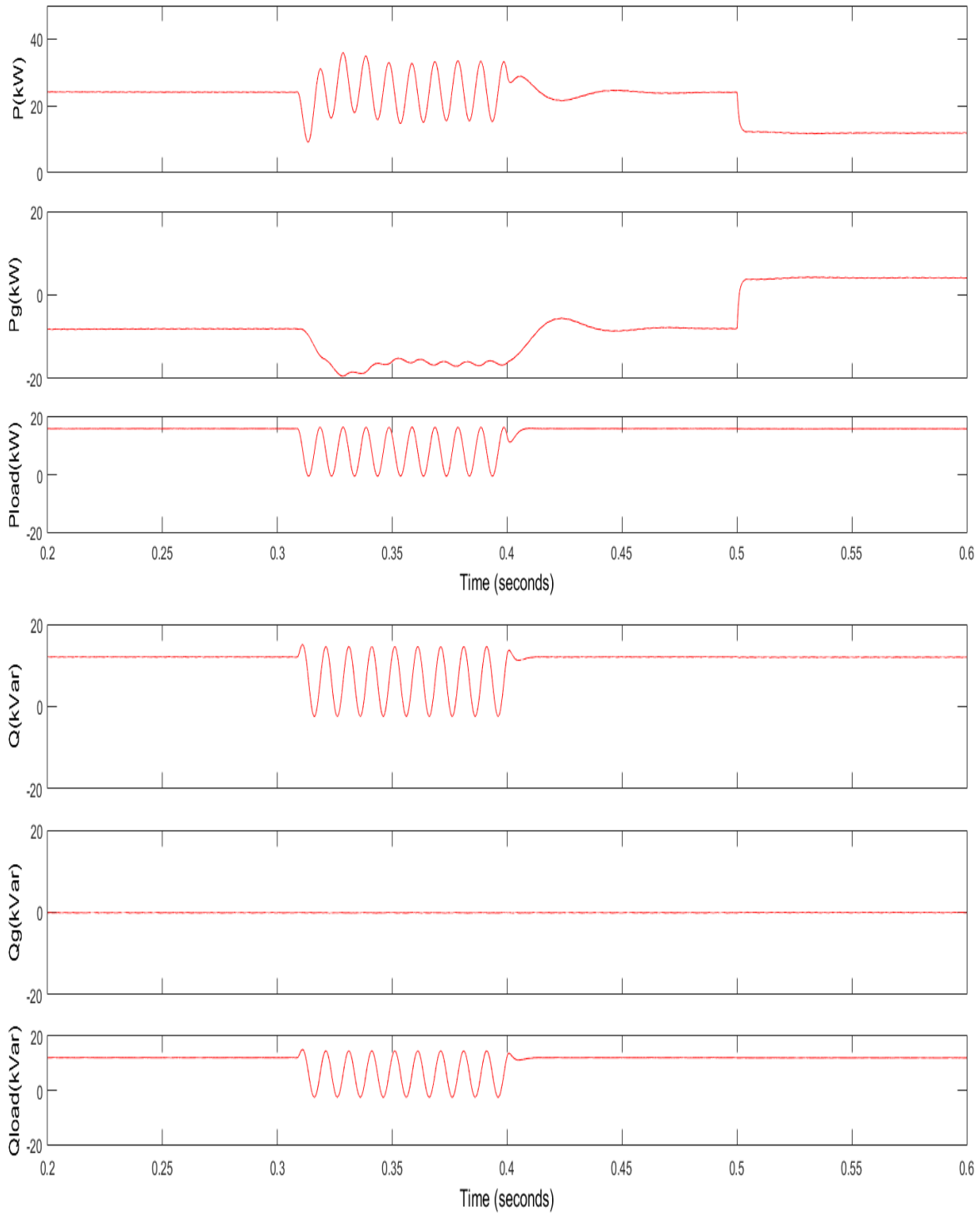

Fig. 4.34 Real and reactive power characteristics for VSS-LMS control under load imbalance and varying solar irradiance for linear load.

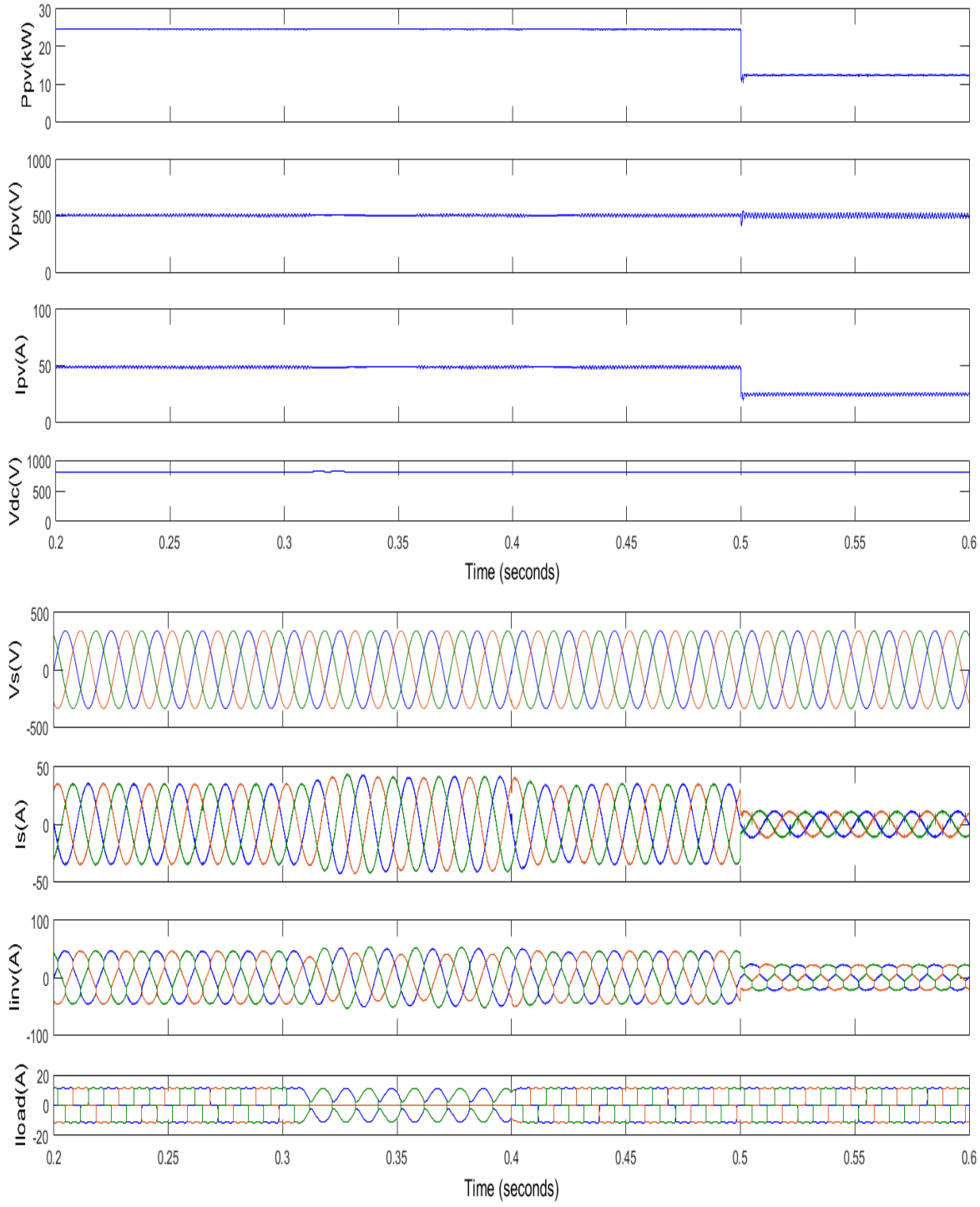

Fig. 4.35 Results for VSS-LMS control under load imbalance and varying solar irradiance for non-linear load.

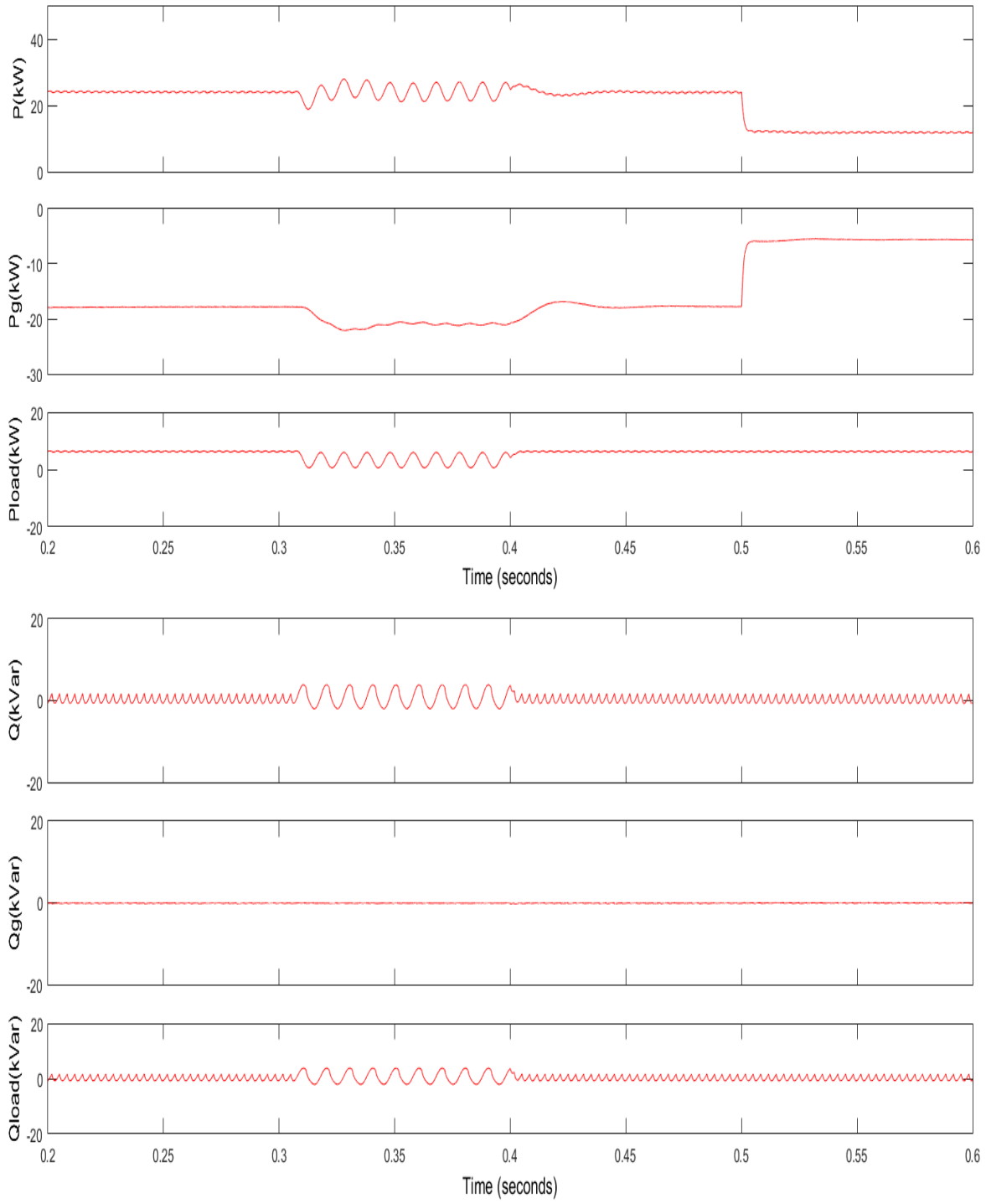

Fig. 4.36 Real and reactive power characteristics for VSS-LMS control under load imbalance and varying solar irradiance for non-linear load.

Waveforms for PV Power (P_{pv}), Current (I_{pv}), Voltage (V_{pv}), V_{dc}, V_s, I_s, I_{inv}, I_{load}, Real and Reactive Power of Grid (P_g and Q_g) , VSC (P and Q) and Load (P_{load} and Q_{load}) are plotted for load imbalance and changing irradiance for linear and non-linear load.

Rated PV power is 25 kW, but the power generated at MPP is 24.910 kW, voltage is 505 V and current is 49 A. V_{dc} is fixed at 800 V with the help of a PI controller. For a linear three phase load of 20 kVA, 0.8 lagging pf, it is noted that the PV provides 16 kW and remaining is delivered to the Grid at 1000 W/m^2. Reactive power Q is at zero which is an indicator that there is reactive power compensation in UPF (unit power factor) mode. Despite of fluctuations during load unbalancing Q returns to zero.

From 0.3 sec to 0.4 sec load unbalancing is created by disconnecting one phases (b). It is noted that the after minimal change in PV Current, Voltage and Power waveforms, they are quickly returned to normalcy. The Grid Current is almost sinusoidal all loads. Oscillations are seen in Real and Reactive Power curves which are removed as soon as load becomes balanced.

Solar irradiance is lowered from 1000 W/m^2 to 500 W/m^2 on 0.5 sec. Change in solar intensity affects the PV Current such that fall in irradiance leads to fall in PV Current along with PV Power. This can be observed in the PV Characteristics plot, where the PV Current and Power are reduced to half and Voltage remains almost undisturbed. Due to this reduction in PV system output inverter current is also reduced. Make up for the power loss Grid Current increases which causes a rise in the power provided by the Grid.

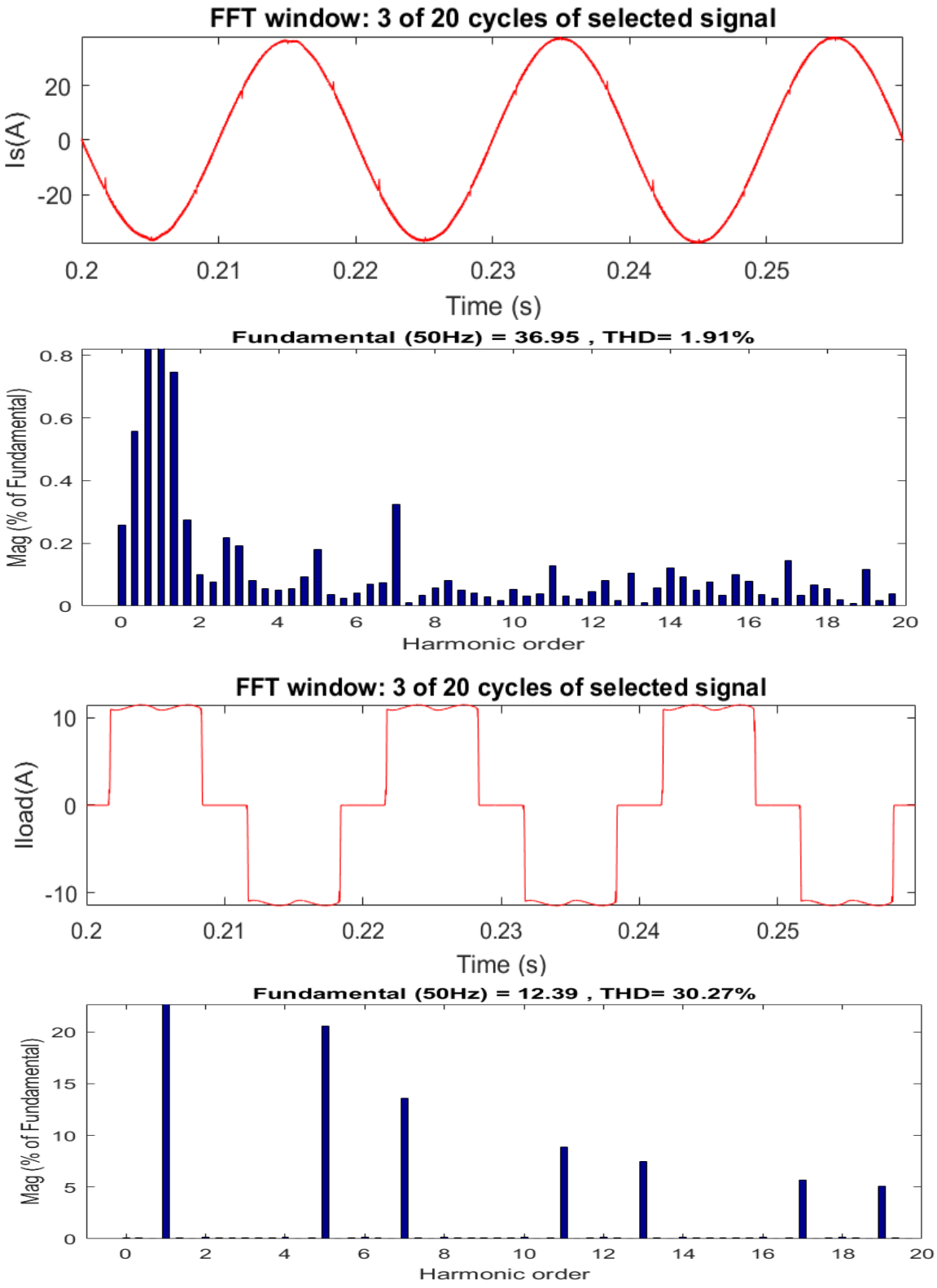

Fig. 4.37 FFT analysis of grid and load current using VSS-LMS control, respectively.

Table 4.6 Comparison of different parameters for linear and nonlinear loads using VSS-LMS.

PARAMETER	LINEAR LOAD		NONLINEAR LOAD	
	At 1000 W/m^2	At 500 W/m^2	At 1000 W/m^2	At 500 W/m^2
V_p (V)	506.71	501.12	505.89	501.23
I_p (A)	49.3	24.19	49.28	24.2
P_{pv} (kW)	24.91	12.44	24.91	12.44
V_{dc} (V)	801.61	794.82	800.98	794
V_s (V)	415.89	416.1	416.01	415.29
I_s (A)	-14.16	7.65	-30.2	-9.26
I_{inv} (A)	53.41	31.6	41.65	20.71
I_{load} (A)	39.25	39.25	11.45	11.45
P (kW)	24.38	12.32	24.38	12.32
Q (kVar)	12.2	12.2	-0.61	-0.61
P_g (kW)	-8.28	3.78	-18	3.78
Q_g (kVar)	-0.1	-0.1	-0.14	-0.14
P_l (kW)	16.1	16.1	6.36	6.36
Q_l (kVar)	12.1	12.1	-0.75	-0.75

Adaptive control techniques are better than conventional as they offer faster tracking in changing environmental conditions. They also offer faster convergence and low THD. The step size in LMS is constant, so it can either have high convergent speed or low mis adjustment error, but not both. VSS-LMS offers both but has high computational complexity.

FFT analysis is done to calculate the THD of grid and load current for all the given control techniques.

4.5 CONCLUSION

All the algorithms offer satisfactory performance under unbalancing and varying environmental conditions for both all loads. Performance of grid connected SPV system controlled by SRFT, IRPT, PBT, Unit Template, LMS and VSS-LMS control techniques are found to be adequate for load balancing, harmonics mitigation and reactive power compensation in UPF mode. Adaptive control is found to be better as it offers faster response under changing conditions. The PCC Voltage, Inverter and load current THD for all techniques are below 5% as per the requirement of IEEE 519 standards.

Table 4.7 Voltage and current THD of various control techniques.

Control Technique	**Grid Current THD (%)**	**Load Current THD (%)**
SRFT	2.16	30.47
IRPT	2.31	30.8
PBT	2.78	30.55
Unit Template	2.21	30.27
LMS	2.06	30.55
VSS-LMS	1.91	30.27

CHAPTER 5

VSS-LMS WITH SQUARED ERROR AUTOCORRELATION

5.1 INTRODUCTION

Least Mean Square is an adaptive control using a method based on gradient of steepest decent. It uses the gradient vector evaluates from the data available to make successive corrections through iteration to weight vector to eventually get minimum squared error. Though LMS offers high computational simplicity and good tracking performance, many variations of it have been proposed in literature and implemented. Sign-sign LMS reported in has a smaller number of multiplications, lower mean square error, higher convergence rate and faster dynamic response as compared to LMS. Other variations of LMS include continuous time LMS (CTLMS), tapped delay continuous time LMS (TDCTLMS) etc.

The step size in LMS is inherently constant which requires the system to balance between convergent speed and low mis adjustment properties. When the value of the chosen parameter is large, convergent speed is high, but the mis adjustment level also increases. Similarly, if the value of parameter is small the mis adjustment level is low, but so is the convergent speed. To overcome this problem a variable step size LMS algorithm which is proposed in [33] which provides fast settlement as well as small mis adjustment level. Numerous VSS-LMS methods have been given based on error observation criterion. A modified VSS-LMS algorithm was proposed in [34] which used error autocorrelation criterion. A robust VSS-LMS (RVSS-LMS) illustrated in [35] but it has high computational complexity. In [38] a VSS algorithm using squared error and error autocorrelation (VSS-SEAE) is shown. However, in abruptly changing environment, VSS-SEAE depicts weak performance. A gradient based VSS (GVSS-LMS) was presented recently in [39] with high convergent speed and low mis adjustment level, but high computational complexity.

The variation of VSS presented in this work is based on squared error autocorrelation (VSS-SEA) criterion [40]. In this algorithm the step size is smoothly adjusted such that in transient state it has a large value for fast convergent speed and in steady state it has a small value to maintain low mis adjustment levels. It proposes smoother convergence of step size under both transient and steady state. Using squared error autocorrelation-based cost function also

reduces uncorrelated noise. Also, it has computational complexity of the same level as that of MVSSLMS algorithm in [34].

5.2 PROPOSED ALGORITHM

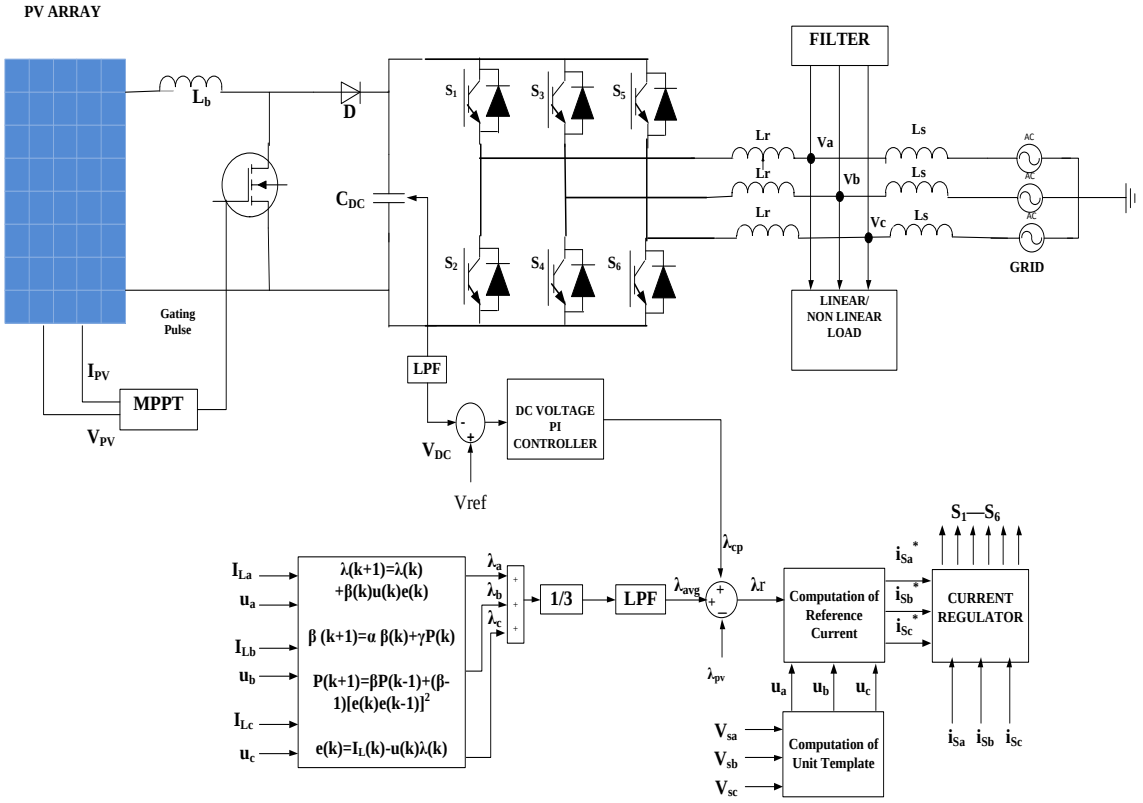

Fig. 5.1 Schematic layout of the proposed grid interfaced PV system using VSS-SEA

V_s is evaluated from v_{sab}, v_{sbc} sensed at PCC,

$$v_{sa} = \frac{2v_{sab}+v_{sbc}}{3}, v_{sb} = \frac{-v_{sab}+v_{sbc}}{3}, v_{sc} = \frac{-v_{sab}-2v_{sbc}}{3} \quad (5.1)$$

V_t is given by

$$V_t = \sqrt{\frac{2}{3}(v_{sa}^2 + v_{sb}^2 + v_{sc}^2)} \quad (5.2)$$

Unit template is estimated using,

$$u_{Pa} = \frac{v_{sa}}{V_t}, u_{Pb} = \frac{v_{sb}}{V_t}, u_{Pc} = \frac{v_{sc}}{V_t} \quad (5.3)$$

$$u_{Qa} = \frac{-u_{Pb}+u_{Pc}}{\sqrt{3}}, u_{Qb} = \frac{\sqrt{3}u_{Pa}}{2} + \frac{u_{Pb}-u_{Pc}}{2\sqrt{3}}, u_{Qc} = -\frac{\sqrt{3}u_{Pa}}{2} + \frac{u_{Pb}-u_{Pc}}{2\sqrt{3}} \quad (5.4)$$

The DC loss element, λ_{cp} obtains V_{DCref} from the MPPT and the V_{DC} sensed across the C_{dc}. V_{DCref} and V_{DC} on being equated and the gap produced is passes via a PI controller.

$$\lambda_{cp}(m+1) = \lambda_p(m) + k_p\{V_e(m+1) - V_e(m)\} + k_i V_e(m+1) \quad (5.5)$$

Where V_e(m) is error at mth instant, given by

$$V_e(m) = V_{DCref}(m) - V_{DC}(m) \quad (5.6)$$

AC loss component, λ_{cq} is given by,

$$\lambda_{cq}(m+1) = \lambda_{cq}(m) + k_p\{V_{te}(m+1) - V_{te}(m)\} + k_i V_{te}(m+1) \quad (5.7)$$

Where $V_{te}(m) = V_{tref}(m) - V_t(m)$.

To ensure the stability of this adaptive control algorithm λ_{pv} is defined by

$$\lambda_{pv} = \frac{2P_{pv}}{3V_t} \quad (5.8)$$

In VSS-SEA, evaluation of active component for phase 'a' I_L for mth instant is changed utilizing,

$$\lambda_{pa}(m+1) = \lambda_{pa}(m) + \mu_{pa}(m)u_a(m)e_{spa}(m) \quad (5.9)$$

Where λ_{pa}(m) estimated active component at mth instant, μ_{pa}(m) is used to calculate step size using,

$$\mu_{pa}(m+1) = \alpha\mu_{pa}(m) + \gamma P_{pa}(m) \quad (5.10)$$

Where the convergence time of this algorithm is dependent on $0 < \alpha < 1$ and $\gamma > 0$. They are constant parameters for controlling exponential regress and fluctuations in step size parameters, respectively. P_{pa}(k) is the squared error autocorrelation function,

$$P_{pa}(m+1) = \beta P_{pa}(m-1) + (\beta-1)[e(m)e(m-1)]^2 \quad (5.11)$$

β is a constant value which denotes an exponential weighting function responsible for smoothing the function. Its value lies between 0 and 1.

e_{spa} (m) is the prediction error estimated using,

$$e_{spa}(m) = i_{La}(m) - u_{pa}(m)\lambda_{pa}(m) \quad (5.12)$$

Similarly, weight vector, μ and squared error autocorrelation for phase 'b and c' are calculated (5.9) -(5.12).

The reactive power component, μ and squared error autocorrelation for all three phases can be calculated in the same manner using equation (5.9) -(5.12).

The average is calculated from

$$\lambda_{Pavg} = \frac{1}{3}\left(\lambda_{pa} + \lambda_{pb} + \lambda_{pc}\right) \quad (5.13)$$

The resultant weight vector is calculated by,

$$\lambda_{rp} = \lambda_{cp} + \lambda_{Pavg} - \lambda_{pv} \quad (5.14)$$

The reactive weights for all phases are obtained using,

$$\lambda_{rq} = \lambda_{cq} - \lambda_{Qavg} \quad (5.15)$$

Where $\lambda_{Qavg} = \frac{1}{3}(\lambda_{qa} + \lambda_{Qb} + \lambda_{Qc})$

The real reference grid current i_{spa}^*, i_{spb}^*, i_{spc}^* and reactive refence grid current i_{sqa}^*, i_{sqb}^*, i_{sqc}^* are calculated as

$$i_{spa}^* = \lambda_{ap}u_{pa}\ , i_{spb}^* = \lambda_{bp}u_{pb}\ , i_{spc}^* = \lambda_{cp}u_{pc} \quad (5.16)$$

$$i_{sqa}^* = \lambda_{aq}u_{qa}\ , i_{sqb}^* = \lambda_{bq}u_{qb}\ , i_{sqc}^* = \lambda_{cq}u_{qc} \quad (5.17)$$

The resultant refence grid current is given by,

$$I_{sa}^* = i_{spa}^* + i_{sqa}^* \quad (5.18)$$

$$I_{sb}^* = i_{spb}^* + i_{sqa}^* \quad (5.19)$$

$$I_{sc}^* = i_{spc}^* + i_{sqc}^* \quad (5.20)$$

I^*_s is then seen with I_s and the resultant gap is then given to a PWM controller which generates gating pulse for VSC.

5.3 RESULTS AND OBSERVATIONS

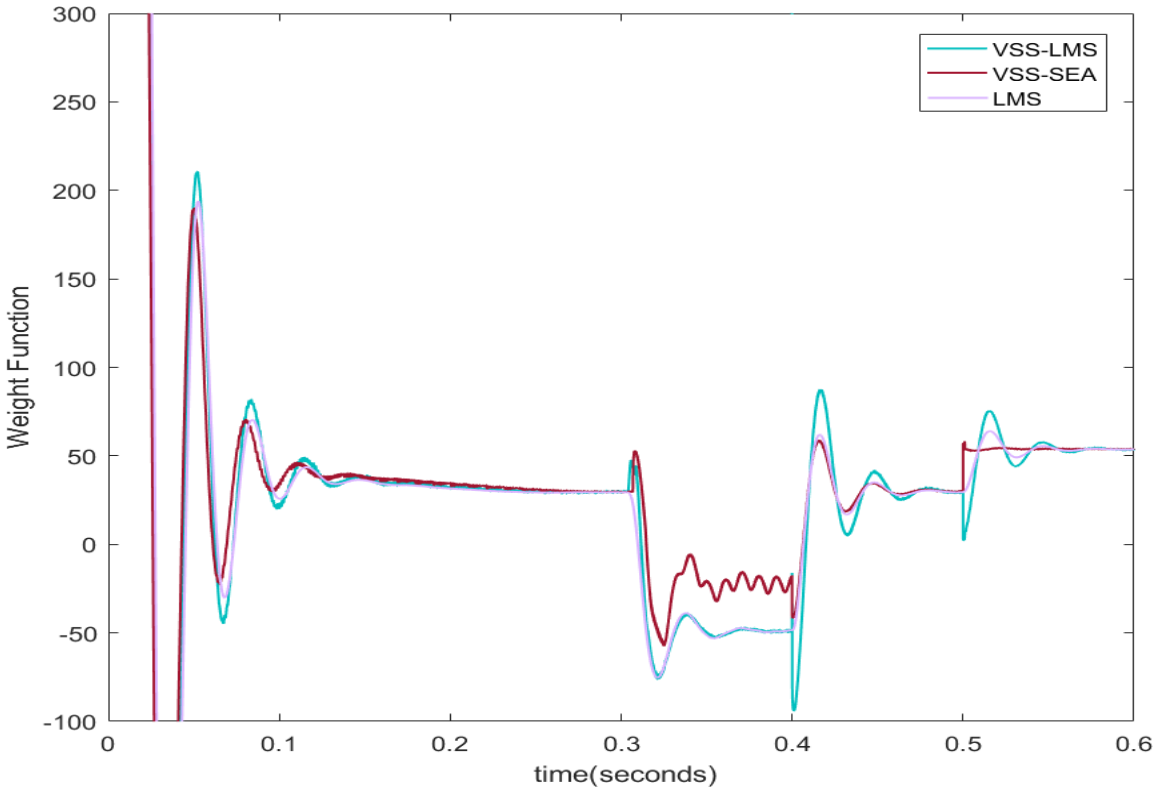

Fig. 5.2 Comparison between weights(λ) of LMS, VSS-LMS and VSS-SEA

Fig. 5.2 shows an analogy between weights of LMS, VSS-LMS and VSS-SEA control. It is observed that during imbalance VSS-SEA offers a faster response as compared to both LMS and VSS-LMS. When solar irradiance reduces at 0.5 sec it is observed that weight (λ) of VSS-LMS using SEA settles almost immediately offering a faster and better response of the system during change.

A smoother change in weight leads to a faster response during transient state and a more accurate one during steady state. This can be observed from the current waveforms which remain almost sinusoidal even during unbalancing. The proposed algorithm is also said to reduce uncorrelated noise from the system, this can be observed from the value of THD.

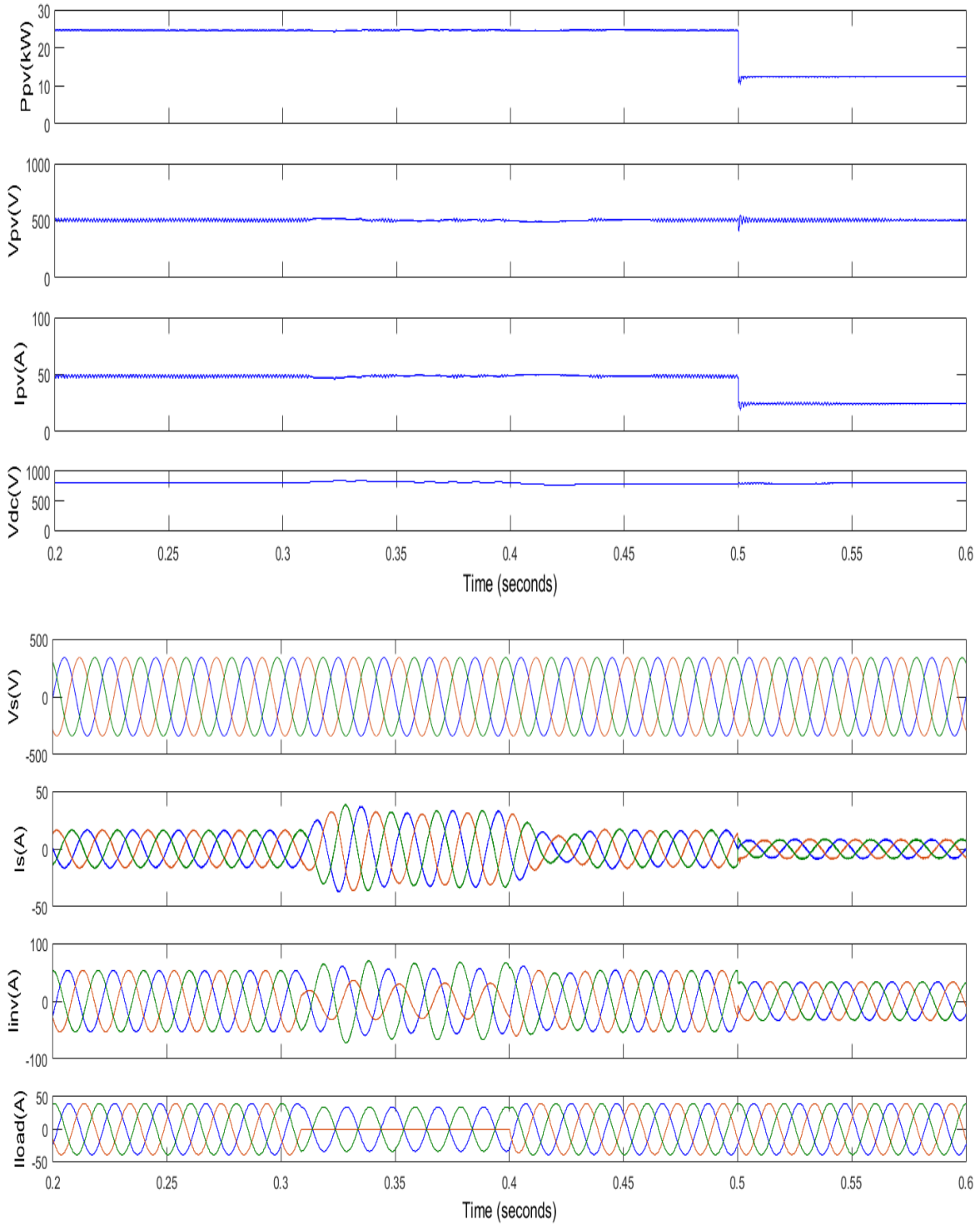

Fig. 5.3 Results for VSS-SEA control under load imbalance and varying solar irradiance for linear load.

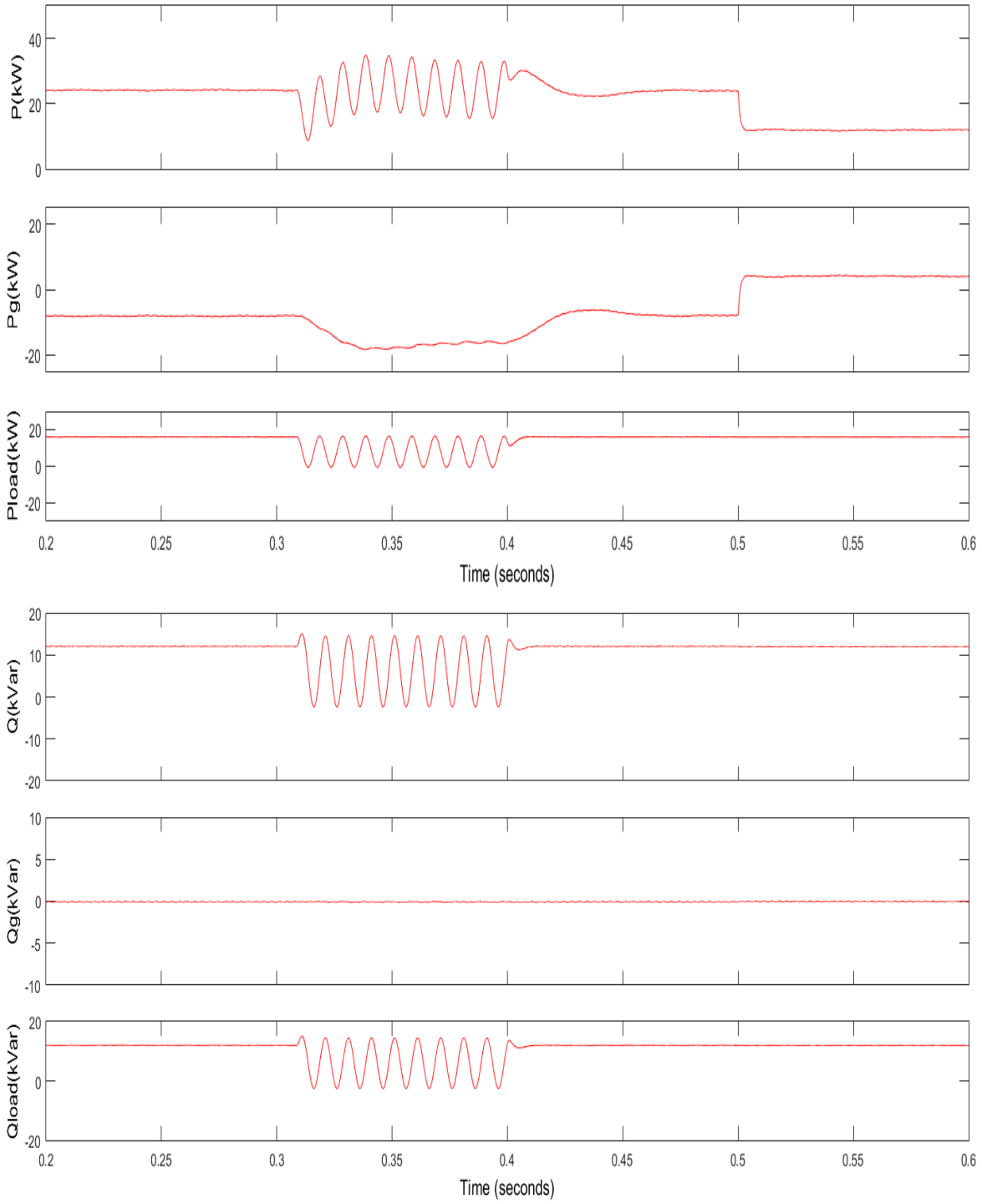

Fig. 5.4 Real and reactive power characteristics for VSSSEA control under load imbalance and varying solar irradiance for linear load.

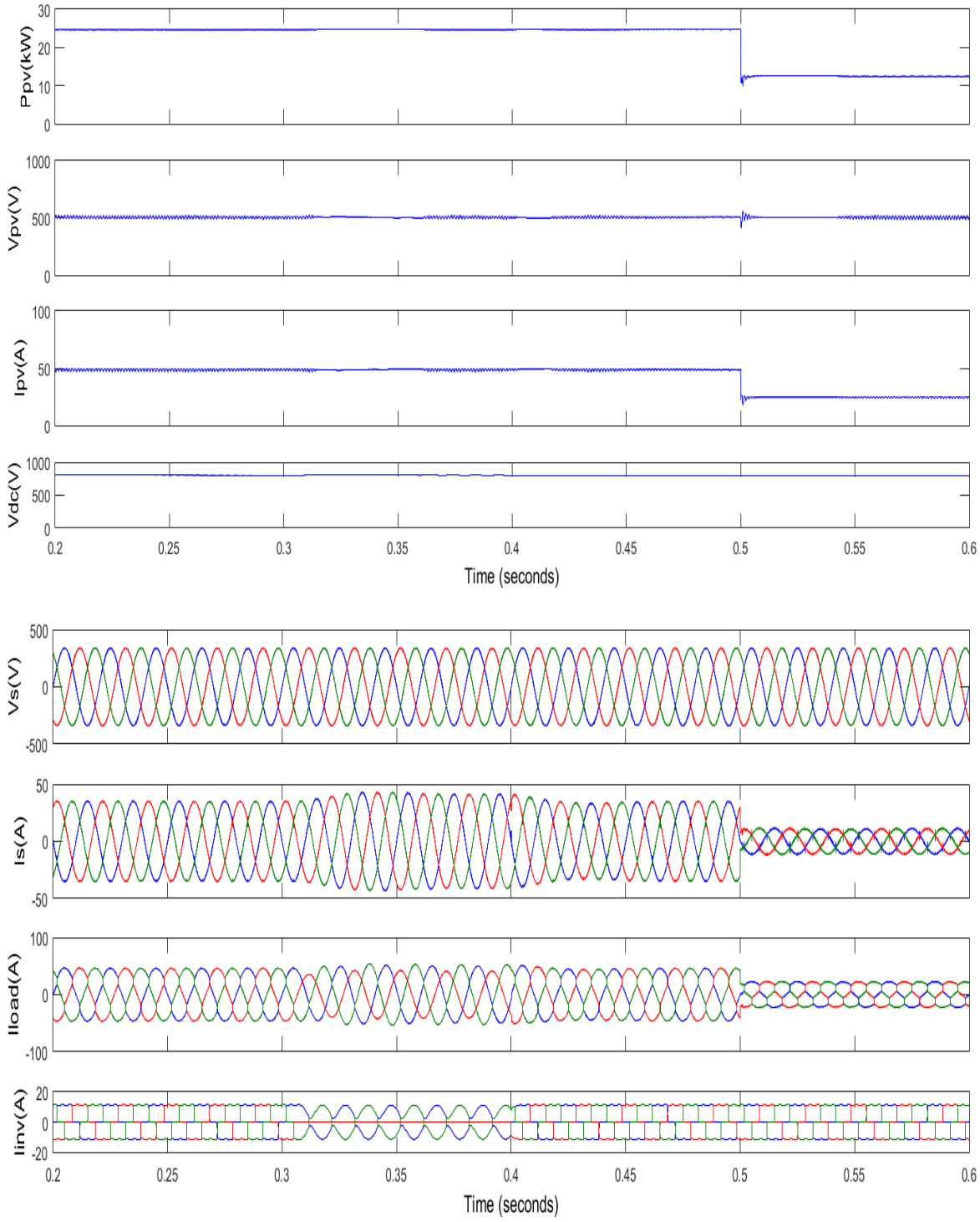

Fig. 5.5 Results for VSS-SEA control under load imbalance and varying solar irradiance for non-linear load.

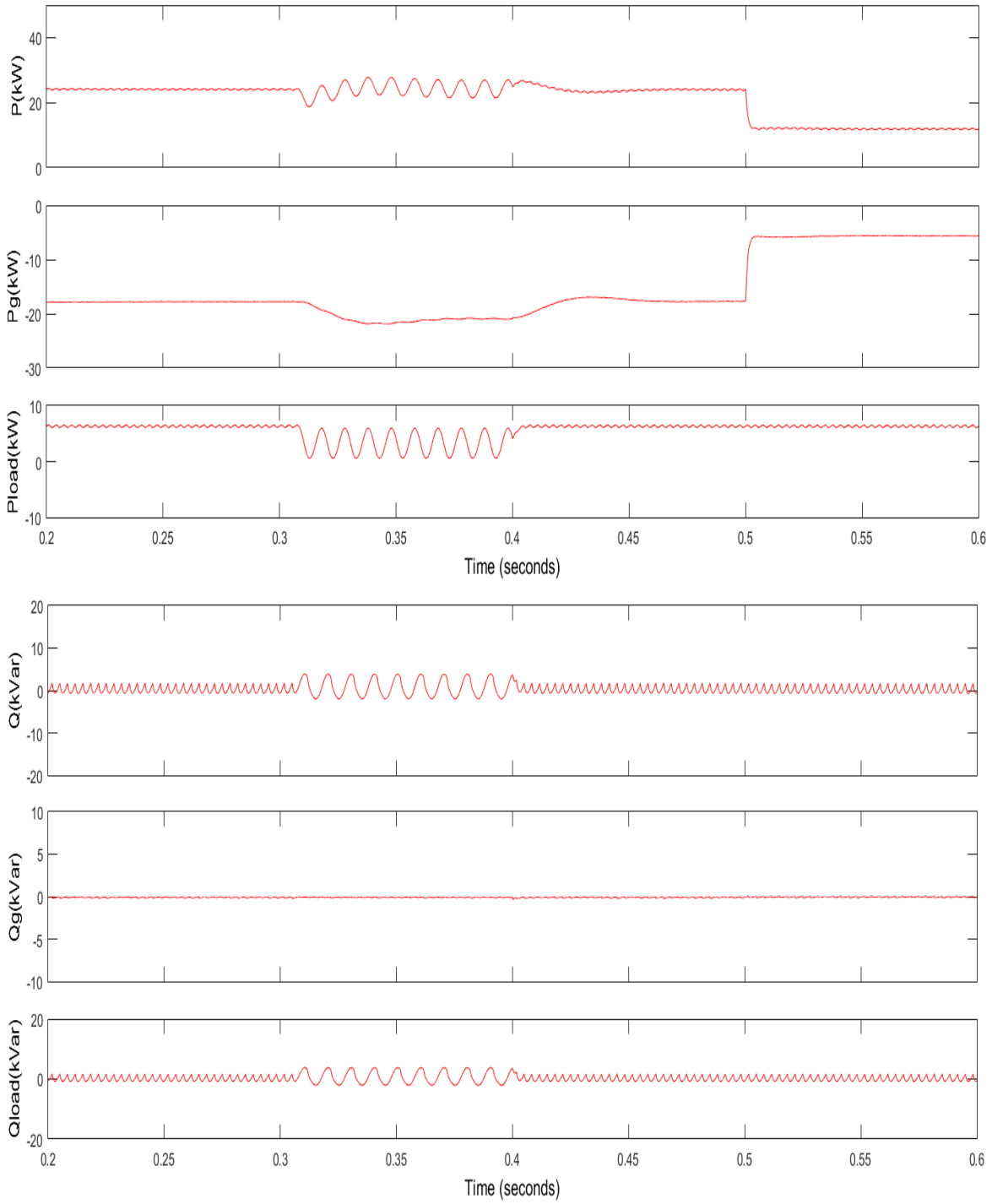

Fig. 5.6 Real and reactive power characteristics for VSS-SEA control under load imbalance and varying solar irradiance for non-linear load.

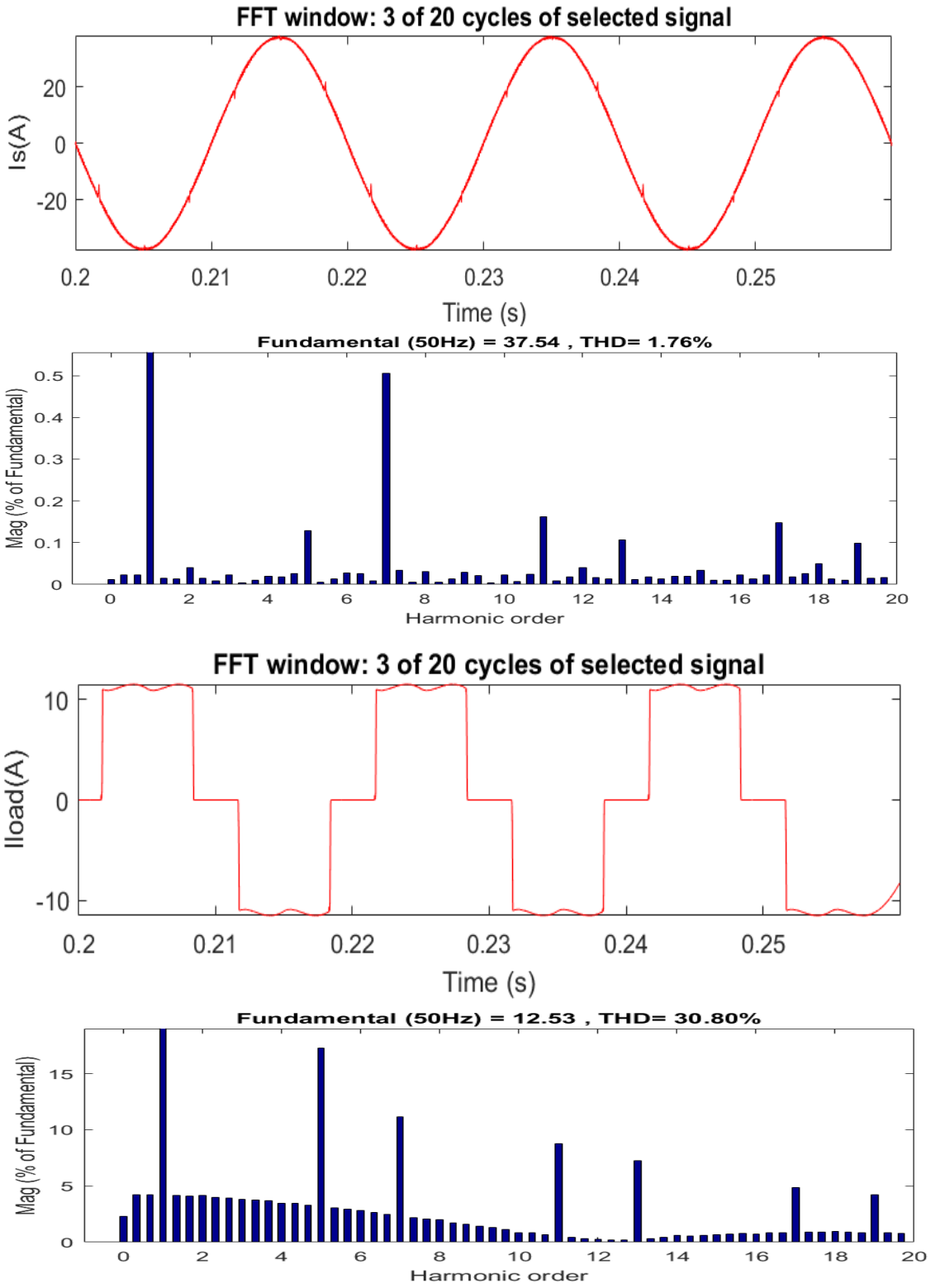

Fig. 5.13 FFT analysis of grid current and load current using VSS-SEA control, respectively.

Waveforms for PV Power (P_{pv}), Current (I_{pv}), Voltage (V_{pv}), V_{dc}, V_s, I_s, I_{inv}, I_{load}, Real and Reactive Power of Grid (P_g and Q_g) , VSC (P and Q) and Load (P_{load} and Q_{load}) are plotted for load imbalance and changing irradiance for linear and non-linear load.

Rated PV power is 25 kW, but the power generated at MPP is 24.910 kW, voltage is 505 V and current is 49 A. V_{dc} is fixed at 800 V with the help of a PI controller. For a linear three phase load of 20 kVA, 0.8 lagging pf it is noted that the PV provides 16 kW and remaining is delivered to the Grid. Reactive power Q is at zero which is an indicator that there is reactive power compensation in UPF (unit power factor) mode. Despite of fluctuations during load unbalancing Q returns to zero. Reactive power requirement of the load is fulfilled by PV.

During the unbalancing from 0.3 sec to 0.4 sec the current waveforms remain almost sinusoidal and are resorted to original stable state as soon as unbalancing is removed. Similarly, as soon as irradiance is reduced to 500 W/m^2 PV current reduces, due to which inverter current also reduced simultaneously and grid current is increased to provide the required power when load is more than PV rating. Reactive power remains constant at zero which indicates reactive power compensation in UPF mode. Dc link voltage is constant at 800 V.

The THD of AC current and load current are 1.76% and 30.8 %, respectively indicating better mitigation of harmonics and reactive power compensation in UPF mode of operation.

Table 5.1 THD of AC voltage and inverter current for various control techniques

Control Technique	**Current (%)**
LMS	2.06
VSS-LMS	1.91
VSS-SEA	1.76
SRFT	2.16

.

Table 5.1 tabulates the THD of PCC voltage and inverter current of LMS, VSS-LMS, VSS-SEA and SRFT control.

Table 5.2 Comparison of different parameters of linear and nonlinear load using VSS-SEA

PARAMETER	LINEAR		NONLINEAR	
	At 1000 W/m^2	At 500 W/m^2	At 1000 W/m^2	At 500 W/m^2
V_p (V)	505.6	501.2	505.4	500.9
I_p (A)	49.4	24.56	49.32	24.51
P_{pv} (kW)	24.91	12.44	24.91	12.44
V_{dc} (V)	800.37	794.81	800.54	793.98
V_s (V)	415.49	415.21	415.33	415.17
I_s (A)	-13.8	7.8	-30.21	-8.85
I_{inv} (A)	53.05	31.45	41.67	20.31
I_{load} (A)	39.25	39.25	11.46	11.46
P (kW)	24.78	12.18	24.78	12.18
Q (kVar)	12.2	12.2	-0.68	-0.68
P_g (kW)	-8.68	3.92	-18.42	5.82
Q_g (kVar)	-0.1	-0.1	-0.07	-0.07
P_l (kW)	16.1	16.1	6.36	6.36
Q_l (kVar)	12.1	12.1	-0.75	-0.75

Compared to the above analyzed convention control VSS-SEA shows better performance in terms of settling after disturbance and fluctuating irradiance. I_{inv} converges before the established conventional control. Its behavior when equated with adaptive control like LMS and VSS-LMS faster and smoother settling is noticed during change.

Table 5.3 Computational complexity of VSS-LMS and VSS-SEA

Control Technique	**Step-size Update Equation**	**Number of Additions**	**Number of Multiplications**
VSS-LMS	$\beta(m+1) = \alpha\beta(m) + \gamma e^2(m)$	1	3
VSS-SEA	$\mu(m+1) = \alpha\mu(m) + \gamma P(m)$ $P(m+1) = \beta P(m-1) +$ $(\beta - 1)\,[e(m)e(m-1)]^2$	2	6

5.4 CONCLUSION

The proposed algorithm is an improvement to the established LMS based control as it offers changing step size which provide fast convergence rate during transient response by increasing the step size and low mis adjustment error during steady state by reducing the step size, unlike LMS which can offer only one of these characteristics at a given time. It is also an improvement on VSS-LMS control as it offers a smoother change in weights or cost function during changing environmental conditions and unbalancing. A smoother control leads to elimination of uncorrelated noise and helps in harmonics mitigation. Computational complexity offered by VSS-SEA is high as compared to VSS-LMS as it can be seen in Table 5.3, but this does not affect the initial rate of convergence of current.

It can be deduced that the suggested VSS-SEA algorithm offers satisfactory performance when used to control a double stage Grid connected PV System. Despite of its computational complexity, it offers harmonics mitigation, reactive power compensation and load balancing under fluctuating environmental conditions and unbalancing for all loads

CHAPTER 6

CONCLUSION AND FUTURE SCOPE OF THE WORK

6.1 CONCLUSION

The main target of this work is to gain insight on working of a PV system, MPPT and integration of PV with grid. Electrical equivalent version of a PV cell is studied to acquire output characteristics of a PV array. Designing of boost converter is done for implementation of MPPT. Various MPPT techniques are studied, and IC control is utilized. The two-stage grid interconnected PV system is developed and analyzed using MATLAB/Simulink. Various conventional and adaptive inverter current control techniques are applied to the proposed system and compared. Conventional techniques studied include-

- SRFT
- IRPT
- PBT
- Unit Template

Adaptive techniques include-

- LMS
- VSS-LMS

All these techniques are implemented, and results are obtained for various loads under load unbalancing and solar irradiance variation. The system is operated in UPF mode for power factor corrections. THD of AC voltage and Current for all the algorithms are under 5%.

It is observed that even though conventional algorithms provide satisfactory performance, but adaptive algorithms settle fast after unbalance depicting the fast convergence rate of adaptive algorithms. Even after reduction in irradiance conventional algorithms take more time to reach the required value of grid current to feed the load in case of linear load as compared to adaptive algorithms.

Adaptive algorithm like LMS is faster than conventional algorithms like SRFT, IRPT, PBT and Unit template but it can either provide a fast response in a dynamically changing state of

low error in steady state, but not both due to its fixed step size. To overcome this flaw a variable step size based LMS is proposed in literature which can provide both fast convergence and low mis adjustment error.

Furthermore, a variation of VSS-LMS is proposed in the work. The proposed algorithm is called VSS-SEA which replaces the squared error cost function of VSS-LMS with squared error autocorrelation function. This improves the performance by offering a faster response during load unbalance as compared to LMS and VSS-LMS. Also, during change in solar irradiance, it settles faster and more smoothly in comparison with LMS and VSS-LMS. Whilst the computational complexity is increased, the system execution is also improved.

Table 6.1 Comparison of different parameters of all the algorithms for linear load.

PARAMETER	SRFT	IRPT	PBT	UNIT-T	LMS	VSS-LMS	VSS-SEA
V_p (V)	505.6	503.9	505.2	505.12	505.62	506.71	505.6
I_p (A)	49.04	48.91	49.11	49	49.21	49.3	49.4
P_{pv} (kW)	24.91	24.91	24.91	24.91	24.91	24.91	24.91
V_{dc} (V)	800.81	799.91	800.96	800.91	800.11	801.61	800.37
V_s (V)	414.24	415.2	416.02	416.2	415.91	415.89	415.49
I_s (A)	-13.51	-13.7	-13.95	-13	-13.03	-14.16	-13.8
I_{inv} (A)	52.76	52.97	53.21	53.27	53.3	53.41	53.05
I_{load} (A)	39.25	39.27	39.26	39.27	39.27	39.25	39.25
P (kW)	24.13	24.16	24.21	24.17	24.29	24.38	24.78
Q (kVar)	12.2	12.2	12.2	12.2	12.2	12.2	12.2
P_g (kW)	-8.03	-8.04	-8.11	-8.07	-8.19	-8.28	-8.68
Q_g (kVar)	-0.1	-0.1	-0.1	-0.1	-0.1	-0.1	-0.1
P_l (kW)	16.1	16.1	16.1	16.1	16.1	16.1	16.1
Q_l (kVar)	12.1	12.1	12.1	12.1	12.1	12.1	12.1

Table 6.1 and Table 6.2 show the comparison of different parameters of all the algorithms for linear and nonlinear loads, respectively. As observed from the table VSS-SEA extracts 24.78 kW power from the PV system which is rated to supply 24.91 kW power. This is the highest as compared to all other algorithms. Due to this it is also able to supply 8.68 kW power to the grid after fulfilling the linear load requirement. V_{dc} for VSS-SEA is also maintained at 800V.

Table 6.2 Comparison of different parameters of all the algorithms for nonlinear load.

PARAMETER	**SRFT**	**IRPT**	**PBT**	**UNIT-T**	**LMS**	**VSS-LMS**	**VSS-SEA**
V_p (V)	504.86	504.26	505.26	505.23	505.33	505.89	505.4
I_p (A)	49.31	49.01	49.21	49.01	49.19	49.28	49.32
P_{pv} (kW)	24.91	24.91	24.91	24.91	24.91	24.91	24.91
V_{dc} (V)	800.22	800.07	800.47	800.67	800.17	800.98	800.54
V_s (V)	415.29	415.56	415.68	416.16	415.96	416.01	415.33
I_s (A)	-29.45	-29.45	-29.45	-29.26	-29.26	-30.2	-30.21
I_{inv} (A)	41.21	41.21	41.21	41.71	41.71	41.65	41.67
I_{load} (A)	11.46	11.45	11.45	11.45	11.45	11.45	11.46
P (kW)	24.13	24.16	24.21	24.17	24.29	24.38	24.78
Q (kVar)	-0.61	-0.61	-0.65	-0.61	-0.67	-0.61	-0.68
P_g (kW)	-18.42	-18.45	-17.85	-18.71	-17.93	-18	-18.42
Q_g (kVar)	-0.16	-0.16	-0.11	-0.16	-0.06	-0.14	-0.07
P_{load} (kW)	6.36	6.36	6.36	6.36	6.36	6.36	6.36
Q_{load} (kVar)	-0.77	-0.77	-0.76	-0.77	-0.73	-0.75	-0.75

6.2 FUTURE SCOPE OF THE WORK

Future work is to study, understand and implement the following-

- Study and apply other adaptive and intelligent control algorithms for MPPT and VSI control.
- Integrating battery storage in grid integrated PV- Power from PV is dependent on weather and cloud movement, due to this PV can only produce power during sunshine hours. A battery along with PV can help supply power during non-sunshine hours and store excess during the day.
- Study and implement hybrid renewable energy system – Hybrid renewable energy systems integrate PV with other renewable energies like wind, biogas with grid.
- Hardware implementation of the proposed algorithm- The proposed technique can be implemented via PV simulator and other laboratory-based instruments.

PUBLICATIONS

- S. Chaudhary, R. Garg and M. Rizwan, "An Adaptive Approach for Maximum Power Extraction from Grid Integrated Solar Photovoltaic System", *1st International Conference on Energy, Material Sciences and Mechanical Engineering*, New Delhi, 2020.
- S. Chaudhary, M. Rizwan and R. Garg, "Squared Error Autocorrelation based VSS-LMS Control Algorithm for Grid Integrated Solar Photovoltaic System", *2nd International Conference on Machine Learning, Advances in Computing, Renewable Energy and Communication*, Ghaziabad, 2020.

REFERENCES

1. IEA (2020), " *India 2020,*" IEA, Paris https://www.iea.org/reports/india-2020
2. Bo Yang, Wuhua Li, Yi Zhao and Xiangning He, "Design and Analysis of a Grid-Connected Photovoltaic Power System, " IEEE Transactions on Power Electronics, vol. 25, no. 4, pp. 992-1000, 2010.
3. Marcelo Gradella Vivalla, Jonas Rafael Gazoli and Emesto Ruppert Filho, "Comprehensive Approach to Modelling and Simulation of Photovoltaic Arrays", IEEE Transactions on Power Electronics, vol 24, pp. 5-9, 2009.
4. M. E. Elnagi Mahmoud, A. A. Zaki Diab and D. A. Kotin, "Simulation and Experimental Validation of Two-Diode Model of Photovoltaic (PV) Modules," *XIV International Scientific-Technical Conference on Actual Problems of Electronics Instrument Engineering (APEIE)*, pp. 244-251, Novosibirsk, 2018.
5. T. V. Myasnikova, A. A. Kirillova, S. P. Ivanova, O. V. Sveklova and O. A. Nadezhdina, "Simulation of Solar Energy Photovoltaic Conversion," 2020 International Youth Conference on Radio Electronics, Electrical and Power Engineering (REEPE), pp. 1-4, Moscow, Russia, 2020.
6. V. M. R. Tatabhatla, A. Agarwal and T. Kanumuri, "Improving the output power of Solar PV Array under different irradiation conditions," *IEEE International Students' Conference on Electrical, Electronics and Computer Science (SCEECS)*, pp. 1-6, Bhopal, 2018.
7. TrishanEshram and Patrick L. Chapman, "Comparison of Photovoltaic Array Maximum Power Point Techniques", IEEE Transaction on Energy Conversion, vol. 22, no. 2, pp. 439-449, 2007.
8. N. Zinelaabidine, M. Karim, B. Bossoufi and M. Taoussi, "MPPT algorithm control for grid connected PV module," *International Conference on Advanced Technologies for Signal and Image Processing (ATSIP)*, pp. 1-6, 2017.
9. K. B. Sahay and A. Yadav, "Implementation of MPPT Technique in PV Array for a Varying Load by Modeling and Simulation," *International Electrical Engineering Congress (iEECON)*, pp. 1-4, Thailand, 2018.

10. H. S. Moreira, M. V. Gomes dos Reis, L. S. de Araujo, T. Perpetuo e Oliveira and M. G. Villalva, “An experimental comparative study of perturb and observe and incremental conductance MPPT techniques for two-stage photovoltaic inverter,” *Brazilian Power Electronics Conference (COBEP),* pp. 1-6, Juiz de Fora, 2017.
11. P. Motsoeneng, J. Bamukunde and S. Chowdhury, “Comparison of Perturb & Observe and Hill Climbing MPPT Schemes for PV Plant Under Cloud Cover and Varying Load,” *10th International Renewable Energy Congress (IREC),* pp. 1-6, Tunisia, 2019.
12. Xu Libin, Cheng Ruofa & Yang Jiajing, “A New MPPT Technique for Fast and Efficient Tracking under Fast Varying Solar Irradiation and Load Resistance”. *International Journal of Photoenergy*,.pp. 1-18, 2020
13. Motahhir, Saad & Abdelaziz, el ghzizal & Sebti, Souad & Derouich, Aziz. (2018). “Modeling of Photovoltaic System with Modified Incremental Conductance Algorithm for Fast Changes of Irradiance” *International Journal of Photoenerg* , pp. 1-13, 2018.
14. H. Deopare and A. Deshpande, “Modeling and simulation of Incremental conductance Maximum Power Point tracking,” *International Conference on Energy Systems and Applications,* pp. 501-505, Pune, 2015.
15. P. Sahu, D. Verma and S. Nema, “Physical design and modelling of boost converter for maximum power point tracking in solar PV systems,” *International Conference on Electrical Power and Energy Systems (ICEPES),* pp. 10-15, Bhopal, 2016.
16. M. E. Başoğlu, “Realization of a low cost and fast boost converter based MPPT for PV system,” *4th International Conference on Power Electronics and their Applications (ICPEA),* , pp. 1-6, Turkey, 2019.
17. A. Dhaneria and H. Khambhadiya, "Hardware Implementation of Grid connected Solar PV Inverter," *International Conference on Power Electronics & IoT Applications in Renewable Energy and its Control (PARC),* Mathura, Uttar Pradesh, India, pp. 28-32, 2020.

18. M. Satish, S. Santhosh and A. Yadav, "Simulation of a Dubai based 200 kW power plant using PVsyst Software," *7th International Conference on Signal Processing and Integrated Networks (SPIN)*, Noida, India, 2020, pp. 824-827.
19. S. V. S. Kumary, V. A. A. M. T. Oo, G. M. Shafiullah and A. Stojcevski, "Modelling and power quality analysis of a grid-connected solar PV system," *Australasian Universities Power Engineering Conference (AUPEC)*, pp. 1-6, Perth, WA, 2014.
20. Remus Teodorescu, Marco Liserre and Pedro Rodrıguez, "Grid Converters for photovoltaic and wind power system," John Wiley & Sons, Ltd, The Atrium, Southern Gate, Chichester, West Sussex, United Kingdom, 2011.
21. N. Gupta, R. Garg and P. Kumar, "Characterization study of PV module connected to microgrid," *2015 Annual IEEE India Conference (INDICON)*, New Delhi, 2015, pp. 1-6.
22. A. K. Verma, B. Singh and D. T. Shahani, "Grid interfaced solar photovoltaic power generating system with power quality improvement at AC mains" *2012 IEEE Third International Conference on Sustainable Energy Technologies (ICSET)*, Kathmandu, 2012, pp. 177-182.
23. R.Garg,A.Singh and S.Gupta, "Direct Current Control of Grid connected Photovoltaic Distributed Generation system,"*American International Journal of Research in Science ,Technology ,Engineering and Mathematics*, 2013.
24. Ravi Nath Tripathi and A. Singh, "SRF theory based grid interconnected Solar Photovoltaic (SPV) system with improved power quality," *International Conference on Emerging Trends in Communication, Control, Signal Processing and Computing Applications (C2SPCA*), Bangalore, 2013, pp. 1-6.
25. A. Khanna, A. Garg and A. Singh, "Maintenance of DC Link Voltage using Synchronous Reference Frame Theory," 2019 3rd International Conference on Recent Developments in Control, Automation & Power Engineering (RDCAPE), NOIDA, India, pp. 17-21, 2019.
26. A. kumar, R. Garg and P. Mahajan, "Performance Analysis of Grid Integrated PV System using SRF and IRPT Control," *1st International Conference on Signal*

Processing, VLSI and Communication Engineering (ICSPVCE), Delhi, India, 2019, pp. 1-7.

27. A. R. K P and J. P, "Comparison of SRFT and ISOGI-QSG Control Algorithm for Grid Integrated SPV System," *2nd International Conference on Intelligent Computing, Instrumentation and Control Technologies (ICICICT)*, Kannur,Kerala, India, pp. 119-124, 2019.
28. B. Singh, D. T. Shahani and A. K. Verma, "IRPT based control of a 50 kW grid interfaced solar photovoltaic power generating system with power quality improvement," *4th IEEE International Symposium on Power Electronics for Distributed Generation Systems (PEDG)*, Rogers, AR, 2013, pp. 1-8.
29. Singh, Bhim & Shahani, D & Verma, "Power Balance Theory Based Control of Grid Interfaced Solar Photovoltaic Power Generating System with Improved Power Quality" *IEEE International Conference on Power Electronics, Drives and Energy Systems(PEDES)*,Bengaluru, 2012, pp. 1-7.
30. B. N. Singh, B. Singh, A. Chandra and K. Al-Haddad, "Design and digital implementation of active filter with power balance theory," in *IEE Proceedings - Electric Power Applications*, vol. 152, pp. 1149-1160, 2005.
31. S. O. Haykin, "Adaptive Filter Theory," 3rd ed. Englewood Cliffs, NJ, USA: Prentice-Hall, 1996
32. Ahmad, Mohammad & Kirmani, Sheeraz," Performance analysis of LMS based control algorithm for power quality improvement in three phase grid connected system for linear/non-linear load", *International Journal of Power Electronics and Drive Systems (IJPEDS)*, vol. 10, pp. 1944-1950, 2019.
33. R. H. Kwong and E. W. Johnston, "A variable step size LMS algorithm," in IEEE Transactions on Signal Processing, vol. 40, no. 7, pp. 1633-1642, 1992.
34. Sandeep Kumar Sahoo, Shailendra Kumar and Bhim Singh, "VSSMLMS Based Control of Multifunctional PV-DSTATCOM in Distribution Network," *IET Generation Transmission and Distribution*, vol. 14, no. 11, pp. 2100-2110, 2020.

35. T. Aboulnasr, and K. Mayyas, “A robust variable step-size LMS-type algorithm: analysis and simulations,” IEEE Transactions on Signal Processing, vol. 45, pp. 631-639, 1997.
36. Subarni Pradhan, Ikhlaq Hussain, Bhim Singh and Bijay Ketan Panigrahi, “Performance Improvement of Grid Integrated Solar PV System using DNLMS Control Algorithm,” IEEE Transactions on Industry Applications, vol. 55, pp. 78-91, 2019.
37. A. Kumar, Seema, B. Singh and R. Jain, "Double Stage Grid-Tied Solar PV System Using HC-LMS Control," 2020 IEEE 9th Power India International Conference (PIICON), SONEPAT, India, pp. 1-6, 2020.
38. H.C.Woo, “Variable step size LMS algorithm using squared error and autocorrelation of error,” *IEEE Conf. on Industrial Electronics and Applications*, pp. 2699-2703, 2009.
39. Y. Zhang, N.Li, J.A. Chambers, and Y.Hao, “New Gradient-based variable step size LMS algorithm,” *EURASIP J. Adv. Signal Process*., vol. 105, pp. 1-9, 2008.
40. W. Loedwassana, "A Variable Step Size Algorithm of LMS Algorithm based on Squared Autocorrelation Criterion," *7th International Electrical Engineering Congress (iEECON)*, Hua Hin, Thailand, 2019, pp. 1-4.
41. M.H Rashid, “Power Electronics Circuits, Design and Applications,” Pearson Education, Third Edition, India, 2007
42. Ned Mohan, Tore M. Undeland and William P. Robbins, “Power electronics converters, applications, and design,” Wiley India Press (p.) Ltd. Third Edition, Reprint 2009.
43. IEEE Recommended Practice and Requirements for Harmonic Control in Electric Power Systems," *in IEEE Std 519-2014 (Revision of IEEE Std 519-1992)*, pp.1-29, 2014.